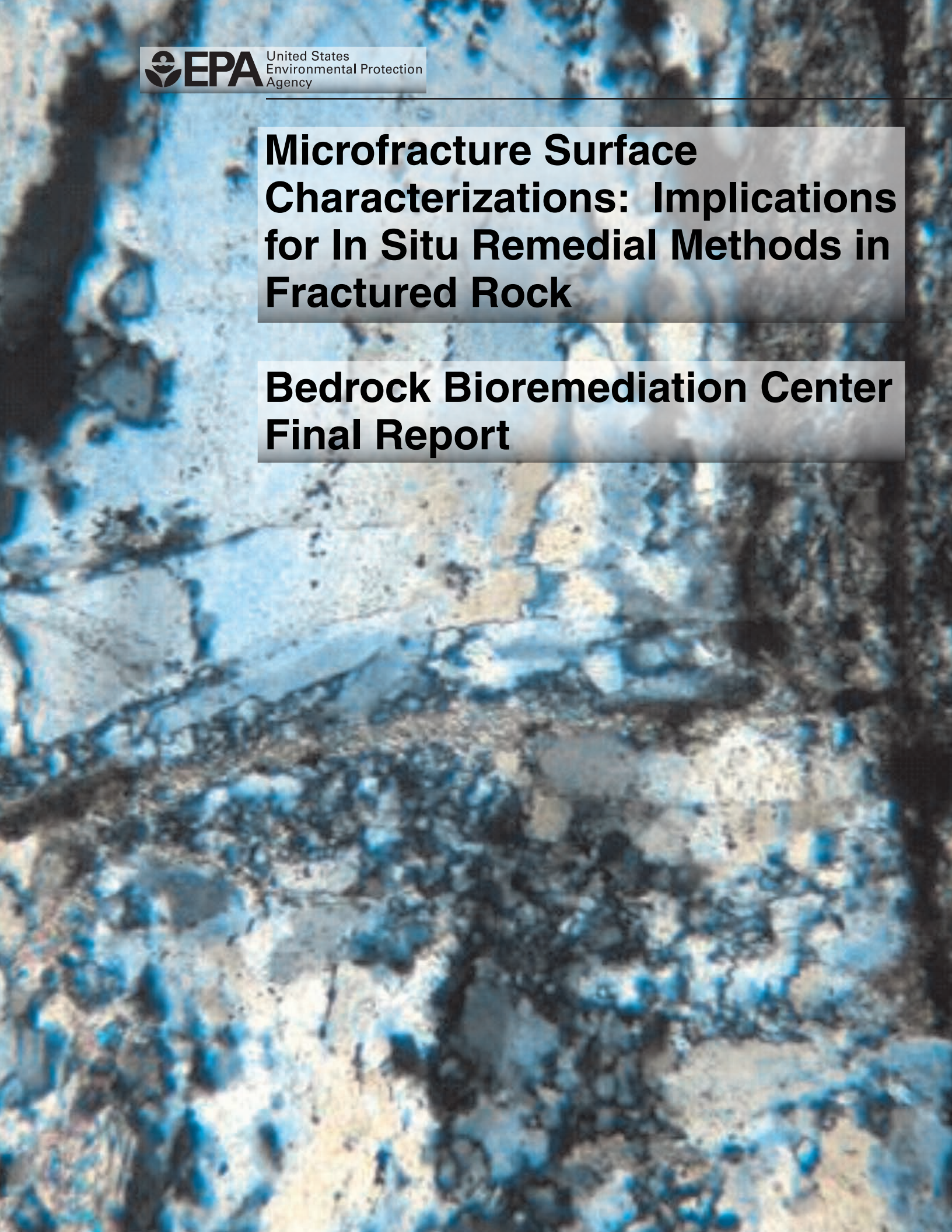

Microfracture Surface Characterizations: Implications for In Situ Remedial Methods in Fractured Rock

Bedrock Bioremediation Center Final Report

EPA/600/R-05/121
June 2006

Microfracture Surface Characterizations: Implications for In Situ Remedial Methods in Fractured Rock

Bedrock Bioremediation Center Final Report

T.T. Eighmy
J.C.M. Spear
J. Case
H. Marbet
J. Casas
W. Bothner
J. Coulburn
L.S. Tisa
M. Majko
E. Sullivan
M. Mills
K. Newman
N.E. Kinner

Cooperative Agreement No. CR-827878-01-0

Project Officer
Mary Gonsoulin
Ground Water and Ecosystems Restoration Division
National Risk Management Research Laboratory
Ada, Oklahoma 74820

National Risk Management Research Laboratory
Office of Research and Development
U.S. Environmental Protection Agency
Cincinnati, OH 45268

Notice

The U.S. Environmental Protection Agency through its Office of Research and Development funded, managed, and collaborated in the research described here under Cooperative Agreement No. CR-827878-01-0 to the USEPA. It has been subjected to the Agency's peer and administrative review and has been approved for publication as an EPA document. Mention of trade names or commercial products does not constitute endorsement or recommendation for use.

All research projects making conclusions or recommendations based on environmentally related measurements and funded by the U.S. Environmental Protection Agency are required to participate in the Agency Quality Assurance Program. This project did not involve environmentally related measurements and, as such, did not require a Quality Assurance Plan.

Foreword

The U.S. Environmental Protection Agency is charged by Congress with protecting the Nation's land, air, and water resources. Under a mandate of national environmental laws, the Agency strives to formulate and implement actions leading to a compatible balance between human activities and the ability of natural systems to support and nurture life. To meet this mandate, EPA's research program is providing data and technical support for solving environmental problems today and building a science knowledge base necessary to manage our ecological resources wisely, understand how pollutants affect our health, and prevent or reduce environmental risks in the future.

The National Risk Management Research Laboratory is the Agency's center for investigation of technological and management approaches for preventing and reducing risks from pollution that threatens human health and the environment. The focus of the Laboratory's research program is on methods and their cost-effectiveness for prevention and control of pollution to air, land, water, and subsurface resources; protection of water quality in public water systems; remediation of contaminated sites, sediments and ground water; prevention and control of indoor air pollution; and restoration of ecosystems. NRMRL collaborates with both public and private sector partners to foster technologies that reduce the cost of compliance and to anticipate emerging problems. NRMRL's research provides solutions to environmental problems by: developing and promoting technologies that protect and improve the environment; advancing scientific and engineering information to support regulatory and policy decisions; and providing the technical support and information transfer to ensure implementation of environmental regulations and strategies at the national, state, and community levels.

This publication has been produced as part of the Laboratory's strategic long-term research plan. It is published and made available by EPA's Office of Research and Development to assist the user community and to link researchers with their clients.

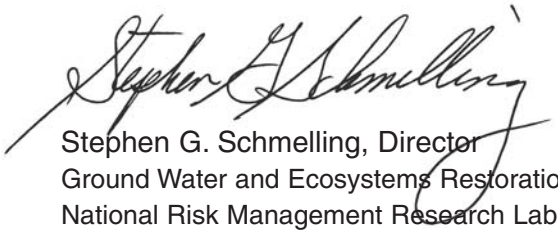

Stephen G. Schmelling, Director
Ground Water and Ecosystems Restoration Division
National Risk Management Research Laboratory

Table of Contents

Table of Contents, continued

List of Tables

List of Figures

List of Figures, continued

Abbreviations

AFCEE	Air Force Center for Environmental Excellence
BBC	Bedrock Bioremediation Center
DCA	dichloroethane
DCE	dichloroethene
DGGE	denaturing gradient gel electrophoresis
DPR	drilling parameter recorder
EDAX	energy dispersive analysis of x-rays
ESCA	electron spectroscopy for chemical analysis
FESEM	Field Emission Scanning Electron Microscopy
GC	guanine-cytosine
GC/MS	gas chromatography/mass spectrometry
ICDD	International Center for Diffraction Data
IHSS	International Humic Substances Society
MIP	mercury intrusion porosimetry
NIST	National Institute for Standards and Technology
NOM	natural organic matter
NPDOC	non-purgeable dissolved organic carbon
PCE	perchloroethene
PCR	polymerase chain reaction
SEM	scanning electron microscopy
SIMS	secondary ion mass spectrometry
TCE	trichloroethene
TEM	transmission electron microscopy
TI	Technical Impracticability
TOF	time-of-flight
UST	underground storage tank
VC	vinyl chloride
XPS	x-ray photoelectron spectroscopy
XRD	x-ray diffraction
XRPD	x-ray powder diffraction

Executive Summary

Purpose: The Bedrock Bioremediation Center (BBC) at the University of New Hampshire is a center specializing in multi-disciplinary research on bioremediation of organically-contaminated bedrock aquifers. The focus of its present work is a field research-based program conducted at Site 32 at the Pease International Tradeport (formerly Pease Air Force Base) in Portsmouth, NH. The U.S. EPA supports the overall mission of the BBC to (i) examine whether microbial communities in organically-contaminated bedrock aquifers are capable of biodegrading the contaminants, (ii) more efficiently and economically characterize the direction of groundwater flow and fracture patterns (size, direction, secondary mineralization) in contaminated bedrock aquifers, (iii) improve and develop new field technologies to control hydraulic and flow conditions in the contaminant zone, (iv) develop laboratory and field methods to estimate and accelerate *in situ* rates of bioremediation of organic contaminants in bedrock aquifers, and (v) to develop and apply innovative microbial, molecular biology and other advanced techniques to enhance *in situ* bioremediation and assess the efficacy of remediation strategies. One of the major outreach efforts of the BBC is to transfer information gained during its research to federal, state, and local regulatory agencies and environmental consultants.

Background: Site 32 contains a contaminant plume of trichloroethylene (TCE) and its transformation products dichloroethylene (DCE) and vinyl chloride (VC). These are the principal contaminants. The site is situated on a variable thickness upper sand layer overlying a marine clay layer overlying a variable thickness lower sand layer. These unconsolidated layers are situated over the Kittery Formation, a tightly folded, biotite-grade partially metamorphosed sandstone and shale crosscut by numerous porphryitic diabase dikes. The contaminant plume extends downward and laterally northeast ~0.5 km via migration through weathered and competent bedrock. The groundwater in the bedrock is predominately contaminated with *cis*-DCE (280-440 µg/L) with some *trans*-DCE (26-48 µg/L), TCE (24-59 µg/L), and VC (8-22 µg/L). Since 1997 the overburden has been managed using a sheet pile containment system coupled with pump and treat. The bedrock groundwater zone was given a technical impracticability (TI) waiver.

Research Questions: The overarching questions addressed by this portion of the project relate to possible relations between microfracture networks in the bedrock, the surface geochemistry of these microfractures, and the ecology and metabolic activity of attached microbes relative to terminal electron accepting processes and TCE biodegradation. Questions include the following: (1) How does the microfracture surface influence attachment and growth? (2) How does the geochemistry of the microfracture surface influence population ecology and metabolism? (3) What is the relationship between the relatively high specific surface area of the microfracture network and the adjacent relatively open and more voluminous open fracture system? More specifically, how does the microfracture surface influence the dominant terminal electron acceptor processes in the microfracture network? (4) Lastly, what is the precise nature of TCE biodegradative processes within the microfracture network?

As part of the overall research plan to better understand these questions, we studied 11 microfractures extracted from competent bedrock cores from two wells at Site 32 (BBC5 and BBC6) so as to characterize, with a variety of surface spectroscopic and microbial techniques, the relation, if any, between microfracture surface geochemistry and the ecology and metabolic activity of attached microbial populations relative to terminal electron accepting processes or to chlorinated solvent biodegradation.

Results are highlighted relative to host rock and microfracture mineralogy and geochemistry, groundwater geochemistry, microfracture microbiology, and terminal electron accepting processes.

Host Rock and Microfracture Mineralogy and Geochemistry: A variety of spectroscopic techniques are needed to characterize the mineralogy and chemical speciation of the host rock and the minerals coating the microfracture surfaces. Mercury intrusion porosimetry (MIP), petrography, scanning electron microscopy- energy dispersive analysis of x-rays (SEM-EDAX), x-ray powder diffraction (XRD), x-ray photoelectron spectroscopy (XPS), and secondary ion mass spectrometry (SIMS) were all used to characterize the host rock and microfracture surface precipitates. Eleven microfractures (MF 01-11) were extracted from competent rock from cores from two boreholes (BBC5 and BBC6) located at the study site. Microfracture samples were taken at depths > 21.3 m (70 ft) below ground and within the contaminant plume. Using MIP, the partially metamorphosed sandstones and shales were found to be very impermeable. The host rock had three nominal pore throat sizes (131.1, 1.136, and 0.109 µm), a porosity of 0.8%, and a permeability of < 1 µDarcy. The host rock mineralogy was typical of metasandstones and metashales (quartz, feldspar, white mica, chlorite and/or biotite). Carbonate minerals and quartz were the dominant microfracture

surface precipitates. Likely oxidized and reduced iron species were identified on the microfracture surfaces with XPS, including siderite ($FeCO_3$), pyrrhotite (FeS), wüstite (FeO), goethite (α-FeOOH), hematite (Fe_2O_3), aged hydrous ferric oxide ($Fe_2O_3 \bullet 1.57\ H_2O$), limonite ($Fe_2O_3 \bullet nH_2O$), and magnetite ($Fe_3O_4$). Carbon functional groups characteristic of humic substances and aquatic natural organic matter (NOM) were also identified with XPS. SIMS mass fragment fingerprints revealed chlorinated carbon fragments which suggested that TCE or perhaps its transformation products were partitioned to the NOM on the microfracture surfaces. The level of spatial resolution of this technique was on the order of 10s of µm. Heterogeneity in mineral abundance on the microfracture surfaces was seen at that level.

Groundwater Geochemistry: Packer sampling techniques were used to collect groundwater samples from packer intervals associated with some of the collected microfracture samples in boreholes BBC5 and BBC6. The water collected in the packer intervals (termed packer water) was characterized using various field and laboratory techniques to describe pH, alkalinity, dissolved gases (H_2, O_2), and dissolved geochemical constituents. The analyses were then used to model and interpret (subject to limitations) the geochemistry of the packer waters with the thermodynamic equilibrium model Visual MINTEQ. Given the volume of the microfracture network relative to the open fracture system, the samples were expected to reflect more from the composition of the open fractures. Packer waters were alkaline (131-190 mg/L as $CaCO_3$, pH 8.8 to 9.6), mildly reducing (Eh of -208 to 160 mV, DO of 0.4 to 2.5 mg/L), with low NPDOC values (0.8 to 1.7 mg/L), and measurable Fe(II) (0.1 mg/L) and Fe(III) (0.02 to 0.3 mg/L). H_2 was present in a number of the BBC wells at the site (2.2 – 7.3 nM). These levels are capable of supporting reductive dechlorination and are indicative of sulfate reduction as a dominant terminal electron accepting process; however, sulfate was the dominant anion in the packer sample water (110-120 mg/L), and no sulfide was detected. Additionally, no fixed nitrogen was detected. The packer waters were in apparent pseudo-equilibrium with many of the observed major mineral phases (carbonates and iron oxides) in the host rock and on the microfracture surfaces. Estimations of Eh using the Nernst equation and activities of Fe^{2+} and Fe^{3+} suggested that the dominant redox couple was Fe(II)/Fe(III). Estimated values were similar to those measured with a polished platinum inert redox probe and reference Ag/AgCl electrode.

Microfracture Microbiology: The microbiology of the microfracture surfaces was investigated using SEM, transmission electron microscopy (TEM), and a number of molecular biology techniques. SEM of microfracture surfaces revealed occasional biopatches of attached microbes. The biopatches were located in small depressions, cracks, or crevices on the microfracture surfaces. The microbes were predominantly rod-shaped (1.0 µm in diameter by 2.0 µm in length). In some instances, the bacteria had possible extracellular polymeric substances associated with them. In other cases, the microbes appeared encased in a film of organic material or surface precipitate-like material. TEM micrographs of soft calcite surface precipitate samples from one microfracture revealed more diverse prokaryotic morphologies (e.g., spirilla, stalked bacteria, filaments). In some cases, flagella and possible cell division septa may have been present. Many cells contained large, clear organelles and small dark organelles. These may have been storage bodies. Amplification with specific primer sets of microfractures from borehole BBC5 showed the presence of both bacteria and *Archaea* (which includes methanogens) in all of the borehole BBC5 microfracture samples. Positive results were also observed for dehalorespirers (*Dehalococcoides* sp.), sulfate reducing bacteria, and iron reducing bacteria (specifically the *Geobacteraceae*). Denaturing gradient gel electrophoresis community profiles of the polymerase chain reaction-amplified bacterial 16S rDNA showed between 7 and 27 band; indicating significant population diversity of the microfracture surfaces. Dendograms showed that two of seven of the microfractures tested were similar. All other samples showed significantly different banding patterns, indicating the bacterial communities on the fracture surfaces were, in most cases, compositionally unique. Microfracture porewater likely differed from packer water in composition as the microfracture network may have been more reducing than the open fracture system based on the presence of obligate anaerobes found on the microfracture surfaces.

Terminal Electron Accepting Processes: The preceding information can be used to infer about possible terminal electron accepting processes occurring in the open fracture system and the microfracture networks. The microfracture network, by virtue of its smaller volume, reduced communication with the open fracture system, and likely mass transfer limitations probably did not significantly contribute to the contaminant or biogeochemical signatures seen in the packer waters collected under fairly transmissive conditions for fractured bedrock at the site. In terms of identification of likely terminal electron accepting processes in the open fracture system, the H_2 values observed for borehole BBC6 suggested sulfate reduction. However, high levels of sulfate and the non detection of sulfide in the packer water samples suggested that sulfate reduction was not dominant, rather, Fe(III) reduction might have been the dominant terminal electron accepting process. Iron was a dominant microfracture surface element. Both Fe(II) and Fe(III) candidate minerals were observed on the microfracture surfaces. The spatial prevalence of Fe as well as its situation in the top few nm of the microfracture surface suggested that Fe(III) was available for iron-reducing bacteria. The spectroscopic characterization of the microfracture surfaces points to Fe(III) reduction as perhaps a dominant process in the microfracture network. There was generally good agreement between SEM-EDAX, XRD, and XPS about identification of C, S, and Fe within the microfracture surface precipitates and on their surfaces. However, the observed population diversity cannot be related to the speciation of any of the three elements on the MF surfaces. The spatial heterogeneity of minerals was quite high on the microfracture surfaces. Mineral grain sizes were on the order of µm. While minerals may have been common to all observed microfracture surfaces, their relative

spacing and proximity to each other and to surface topography were quite varied. It may be that the biopatches that were observed with SEM reflect more localized microbial population response to microfracture surface mineral speciation. The level of resolution of SEM, SEM-EDAX, and XPS, however, was not high enough to discern such spatial relationships though such relations are likely.

Possible TCE Biodegradative Processes: The presence of transformation products of dehalorespiration as well as H_2 concentrations supported the role of *Dehalococcoides* sp. in dehalorespiration in the microfracture networks under conditions where Fe(III) reduction was strongly correlated to the presence of oxidized iron species on the microfracture surfaces. Other means of TCE biodegradation, including abiotic as well as aerobic and anaerobic respiratory and cometabolic processes, cannot be excluded.

Significance: The bulk of the data suggested that the microfracture networks supported diverse microbial communities. The communities differed spatially and were not similar to open fracture system planktonic population compositions. The adherent populations were patchy and associated with microfracture topography. Microbes were also found within the microfracture surface precipitates themselves, suggesting a more complex mineral-microbe spatial relationship. The dominant mineralogy on the microfracture surfaces (Fe(II) and Fe(III) oxides and carbonates) was related to the microbial metabolism of some of the identified isolates, notably iron reducers. However, other types, including obligate anaerobes, suggested that the microfracture network was perhaps more reducing than the open fracture system, perhaps particularly within the microfracture surface precipitate structure. *Dehalococcoides* sp. was a predominant component of the microfracture microbial population and suggested that reductive dechlorination was one principal process whereby TCE was transformed.

A number of follow on activities are suggested. Methods to collect and characterize microfracture porewaters may help to better describe terminal electron accepting processes and may elaborate on real differences with packer sample composition. The relative absence of NOM in the system, as well as the concentration of NOM on microfracture surfaces deserves further examination. Understanding NOM bioavailability on microfracture surfaces may help to explain the phylogenetic and metabolic diversity seen on the microfracture surfaces. Studies looking at partitioning of TCE and transformation products to partitioned NOM under controlled isotherm conditions may help to better describe partitioning with respect to microfracture surface organic carbon fractions, particularly if more sensitive SIMS methods (such as time of flight SIMS) are used. Understanding the spatial proximity of adhering microbes of terminal electron accepting process activity to minerals necessary to that terminal electron accepting process may help to describe the heterogeneous nature of terminal electron accepting processes in the microfracture network and at the microscale within the formation. Determining the extent of the microfracture specific surface area relative to that of the open fracture network would help in determining the role of microfractures in terminal electron accepting processes and biodegradative processes within contaminated bedrock aquifers. The role of mass transfer between the open fracture system and the microfracture network, as well as redox zonations that might develop relative to proximity to the open fractures might be subjected to mass transfer and reaction path modeling exercises. Additional work defining the complex microbial communities, their metabolic interactions, and their possible syntrophy with respect to TCE degradation may help to explain observed accumulations of transformation products. Further, the expression of enzymatic activity relative to terminal electron accepting processes and TCE biodegradation would help determine the metabolic activity on microfracture surfaces and why these might differ from those occurring in the open fracture groundwaters.

1.0 Introduction

The Bedrock Bioremediation Center (BBC) at the University of New Hampshire is a center specializing in multi-disciplinary research on bioremediation of organically-contaminated aquifers. Field research is conducted at Site 32 at the Pease International Tradeport (formerly Pease Air Force Base) in Portsmouth, NH. Site 32 contains a contaminant plume dominated by trichloroethylene (TCE). The site is situated on a variable thickness upper sand layer overlying a marine clay layer overlying a variable thickness lower sand layer. These unconsolidated layers are situated over the Kittery Formation, a tightly folded, biotite-grade metasandstone and metashale crosscut by numerous porphryitic diabase dikes. The contaminant plume extends downward and laterally northeast ~0.5 km via migration through weathered and competent bedrock. The groundwater in the bedrock is predominately contaminated with *cis*-DCE (280-440 µg/L) with some *trans*-DCE (26-48 µg/L), TCE (24-59 µg/L), and VC (8-22 µg/L). The principal contaminant released was TCE. Since 1997, the overburden contamination is being managed using a sheet pile containment system coupled with pump and treat. The bedrock zone was given a technical impracticability (TI) waiver.

Over the last few years, a number of BBC investigatory boreholes have been installed in and around the plume at Site 32. Most of these boreholes have been used for extraction of cores from the competent bedrock as a function of depth. Our focus on microfracture characterization was limited to eleven microfractures extracted from two boreholes: BBC5 and BBC6. Eleven microfractures extracted from competent bedrock cores (comprised of Kittery Formation rock and not diabase dike rock) from boreholes BBC5 and BBC6 were characterized with a variety of surface spectroscopic and microbial techniques to determine if a relation, if any, exists between microfracture surface precipitates and the ecology and metabolic activity of attached microbial populations relative to predominant terminal electron accepting processes such as Fe(III) reduction, or sulfate reduction, or to chlorinated solvent biodegradation.

1.1 Microfractures and Their Role in Reaction and Transport

Contaminant transport and reaction in fractured bedrock are important processes, yet poorly understood and difficult to study and model. Large scale fractures with apertures from mm to many cm in size clearly play a dominant role in transport. Open microfractures with apertures less than 1 mm potentially play an important role in reaction by virtue of their extensive specific surface area.

Microfractures tend to be sub-millimeter in open width and vary in their planar or sub-planar extent (both length and depth). They are produced by a variety of deformational processes in massive host rock. Historically, in the literature, they have been referred to, somewhat interchangeably, as microcracks, cracks, or microfractures (Kranz, 1983). The term microfracture has been adopted for use in this report. Many microfractures constitute a network; such networks are situated within the more open fracture system.

Microfractures are introduced when stress exceeds strain at the local level. Local stresses are induced mechanically or thermally. Microfractures tend to locate at grain boundaries, intra-crystalline cavities, intra-crystalline cleavage planes, and internal surfaces corroded by chemically active fluids (Kranz, 1983). Microfractures can also be trans-granular and propagate along cleavage planes. Typically, microfractures propagate along paths of maximum stress.

Microfractures have one or two dimensions that are smaller than the third dimension. For reference purposes, x denotes length, y denotes depth, and z denotes open width. For flat microfractures, the width to length ratio (the microfracture aspect ratio, z/x), must be less than 10^{-2} and is frequently between 10^{-3} and 10^{-5} (Simmons and Richter, 1976).

Frequently, the surface of the microfracture is coated with secondary mineral surface precipitate (also referred to as a skin) (Kranz, 1983). This controls whether the microfracture is open relative to porewater communication with adjacent connected microfractures (and larger transmissive fractures) in a microfracture network or fracture system. Coating can be complete, wherein the microfracture is completely in filled (or healed or sealed), or partial, where the microfracture is only partially filled (or sealed or healed).

These secondary minerals are frequently deposited at higher temperatures during metamorphic intrusion (Kranz, 1983). However, more recent geologic processes associated with lower temperature hydrologic mineral weathering and precipitation of dissolved ions from porewater solutions may also be important; especially at the contact interfacial surface between porewaters and microfracture surface minerals.

The microfracture surface can also form a weathering rind: over time, elements in the host rock undergo incongruent dissolution and diffuse, via Fickian diffusion, from within the mineral out to the mineral-porewater interface, and into the porewater. This occurs on the scale of nanometers to microns and leaves a concentration profile in the host rock that decreases closer to the mineral-porewater interface. Such diffusion profiles are driven by concentration gradients between the host mineral and the porewater, the porewater behaving as an infinite sink.

A conceptual model of the mineralized microfracture interface with an open pore is provided (Figure 1.1). At the interface of the microfracture and the open pore, there are minerals deposited on the microfracture surface, and natural organic matter (NOM) present in the porewater is sorbed to these surfaces. Microbes will be adherent to the mineral surface and/or the NOM located at the surface. The microfracture surface plays an important role in the fate of contaminant solutes (both inorganic and organic) present in the groundwater moving through the microfracture network and in the framework of more open fractures that connect the microfracture networks.

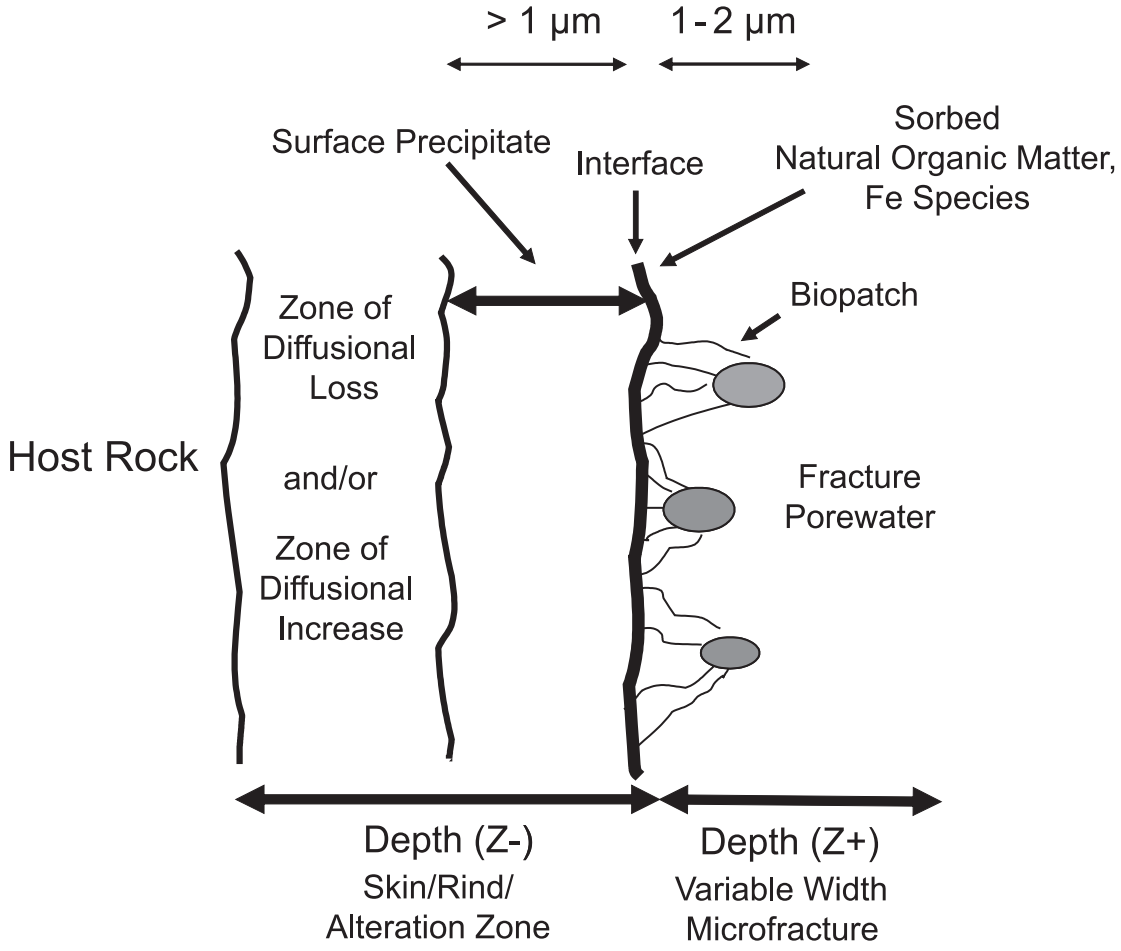

Figure 1.1. Conceptual model of adherent biopatch (in cross section) on a microfracture surface.

The reactions at the microfracture surface include: reactions between the solute and the secondary mineral directly (specific or non-specific adsorption) and reactions between the NOM and the mineral directly (specific or non-specific adsorption) which in turn can react with solutes (specific and non-specific adsorption). Further, the mineral surface can also play a role in selection or metabolism of adherent microbes in the microfracture network. These microbes, in turn, can directly react with contaminants by (i) specific or non-specific adsorption processes, (ii) contaminant metabolism, (iii) alteration of the mineral interface where the microbe resides, or (iv) secondary mineral precipitation.

Open microfractures are connected to the fracture system and therefore are in communication with larger fractures. Typically, diffusive processes are involved at a variety of scales: diffusion of components out of the host rock into microfractures (whereby solid state diffusion predominates) and diffusion within wetted microfractures where tortuous aqueous (or matrix) diffusion predominates. In the later case (Shapiro, 2001), the diffusivity of a non-absorbing ion (D, m^2/yr) is:

$$D = n_{rm} \alpha D_w = n_{rm} D_{rm} \qquad \text{[Eq. 1.1]}$$

where D_w frees diffusivity in water (m^2/yr), n_{rm} is the effective porosity of the rock matrix (unitless), α is a tortuosity factor (unitless), and D_{rm} is the effective diffusion coefficient in the tortuous rock matrix (m^2/yr). Typically, D_{rm} is one to three orders of magnitude lower than D. Recent work by Shapiro (Becker and Shapiro, 2000; Shapiro, 2001) has documented the role that matrix diffusion plays in transport processes at the large scale (km).

Robinson *et al*. (1998) developed analytical solutions for solute transport in a dual porosity (fracture-matrix) system with skins present along the fracture faces. Their results suggested that fracture skins may increase or decrease transport processes depending on their porosity relative to the host rock. This has implications relative to residence time or retardation during transport.

1.2 Microfracture Definition

A protocol (See Table 1.1.) was established to better describe the microfractures to be sampled relative to the cores extracted from the boreholes. Microfracture types are characterized by their extent for being continuous across the core, discontinuous across the core, or induced by drilling stresses. The attitude of the microfractures (relative to the horizontal ground surface) is classified as horizontal (0°), vertical (90°), or somewhere in between and therefore inclined. The aperture width or thickness of the microfracture is used to describe the opening in the microfracture. These measurements are rough estimates based on use of scales with enlarged digital micrographs. Surface mineralization is a general descriptor for the degree of secondary mineralization associated with the microfracture surface.

Table 1.1. Microfracture Description Protocol

Extent & Type	Attitude	Typical aperture width (mm)	Surface area with secondary mineralization
- Continuous	- Horizontal (0°)	> 1.0	- Little (<10%)
	- Vertical (90°)	> 0.8	- Some (10 to 30%)
- Bedding	- Steeply inclined (> 60°)	> 0.6	- Extensive (>30%)
		> 0.4	
- Cross bedding	- Moderately inclined (30-60°)	< 0.4	
	- Low angle (<30°)		
- Discontinuous	- Horizontal (0°)	> 1.0	- Little (<10%)
	- Vertical (90°)	> 0.8	- Some (10 to 30%)
- Bedding	- Steeply inclined (> 60°)	> 0.6	- Extensive (>30%)
		> 0.4	
- Cross bedding	- Moderately inclined (30-60°)	< 0.4	
	- Low angle (<30°)		
- Induced (mechanical break – likely restricted to core)	- Horizontal (0°)	> 1.0	- Little (<10%)
	- Vertical (90°)	> 0.8	- Some (10 to 30%)
	- Steeply inclined (>60°)	> 0.6	- Extensive (>30%)
- Bedding	- Moderately inclined (30-60°)	> 0.4	
		< 0.4	
- Cross bedding	- Low angle (<30°)		

1.3 Microbes in Bedrock

Microorganisms are found in many subsurface environments. Their metabolic activity affects the chemistry and physical properties of the surrounding environments. In recent years, there has been considerable interest in the microbiota of the deep subsurface including continental and oceanic crust and marine sediments. While microbes are present in the deep subsurface, they may be growing slowly and exhibit little metabolic activity. There is a dearth of information on the microbial populations that exist in crystalline bedrock aquifers (Pederson 1997; Lovley and Chapelle, 1995; Fredrickson and Onstott, 1996). Open microfractures in the bedrock in communication with larger fractures constitute a surface for microbial colonization and metabolism. Surfaces may very well confer numerous advantages to bacteria and can influence metabolic processes.

Most studies have focused on microbial communities from groundwater aquifers or sediment deposits (i.e., Ekendahl *et al*., 1994; Fredrickson & Onstott, 1996; Pedersen 1997, 2000; Fry *et al.*, 1997; Chandler *et al.*, 1998; Bekins *et al*., 1999), with only a limited number on competent bedrock, which comprises the majority of habitable subsurface environments (i.e.; Colwell *et al*., 1997; Fredrickson *et al*., 1997; Haveman *et al*., 1999; Onstott *et al*., 1998; Onstott *et al*., 2003). Composition of the microbial communities has been investigated by the use of enrichment cultures (Onstott *et al*., 1998; Lehman *et al.*, 2001a) or molecular techniques in simulated models (Lehman *et al*., 2001b).

Microbes have been characterized in extreme systems in the deep subsurface. Onstott *et al*. (1998) characterized microbes from sidewall cores of rock 2800 m below ground surface in hydrocarbon reservoirs. Bacterial phospholipids biomass indicated cell concentrations up to 4 x 10^5 cells/g of rock, a relatively low cell density by comparison to porous media.

Onstott *et al*. (2003) conducted microbial analyses on rock from a 3.2 km depth in an active gold mine in South Africa. The host rock was comprised of a carbonaceous, quartz, sulfide, uraninite, and gold- bearing layer, referred to as the Carbon Leader, sandwiched between quartzite and conglomerate deposits. The microorganisms in the Carbon Leader were mostly mesophilic, aerobic heterotrophic, nitrate reducing, and methylotrophic, and β- and γ-*Proteobacteria.* Combined phospholipid fatty acid and terminal restriction fragment length profile analyses show indigenous microorganisms were present at < 10^2 cells/g of rock. Phospholipid fatty acids, ^{35}S autoradiography, and enrichment cultures suggested that the adjacent quartzite contained ~10^3 cells/gram of rock of thermophilic sulfate reducing bacteria, including some δ-*Proteobacteria*. Porewater and rock geochemical analyses indicated that sulfate for the sulfate-reducing bacteria was made available, via diffusion, from the adjacent Carbon Leader via radiolysis of the sulfides.

Haveman *et al*. (1999) characterized the free-swimming microbes and geochemistry of groundwater samples from 200- to 950-m depths in four igneous rock sites in Finland. At these sites, fractures are partially filled with precipitated minerals such as calcite, dolomite, pyrite, epidote, or chlorite. These minerals were believed to precipitate and dissolve as a result of changing groundwater conditions over geological time. Some of the fracture-filling minerals are cycled by microorganisms, such as sulfide in pyrite, carbon dioxide in calcite, and ferric iron in iron oxyhydroxides. At these four sites, free-swimming sulfate-reducing bacteria predominated in sites where iron sulfide fracture-filling minerals were present. Free-swimming iron-reducing bacteria were dominant where iron sulfide fracture-filling minerals were not present, but iron hydroxide fracture-filling minerals were prevalent. They observed that fracture-filling minerals were a better indicator of planktonic microbial populations than was groundwater chemistry. Isotopic signatures in fracture-filling minerals seem to be reliable indicators of past and present microbial activity, especially if stable isotope ratios are analyzed.

In bench-scale fractured bedrock column studies (Lehman *et al*., 2001a), attached microbial communities were compositionally different from those in the porewater flowing through the fractures. Fracture surfaces were enriched in gram-positive bacteria and α-*Proteobacteria* and depleted in β-*Proteobacteria*. Lehman and colleagues suggested that microbial communities will be partially controlled by the surrounding geological media (Lehman *et al*., 2001b).

The ability of microbes to colonize fracture surfaces is clearly constrained by both the aperture size or pore throat width of the microfracture network, hydraulic connectivity, and advective or diffusive transport of groundwater, planktonic microbes, and entrained nutrients from near surface environs. Fredrickson *et al*. (1997) studied microbial activity in shale and sandstone cores from New Mexico relative to aperture pore width. They found that core samples dominated by pore throat widths < 0.2 µm generally did not support activity. This width is believed to be the lower limit of microbe size. Core samples with predominant pore throat widths > 0.2 µm did support significant activity as measured by ^{14}C-acetate and ^{14}C-glucose mineralization and ^{35}S-sulfate reduction assays. Colwell *et al*. (1997) studied biomass distributions in deep subsurface Late Cretaceous and Early Tertiary rock cores in the Piceance Basin in western Colorado. They found that distribution in the deep subsurface was controlled by hydrologic connection

to the surface, formation temperature, and an interconnected fracture system. Cores with higher pore throat widths (>1 μm), porosities (up to 12%) and permeabilities (0.1 to 1.0 mDarcy) correlated to higher levels of biomass. In contrast, cores with lower pore throat widths (<1 μm), porosities (< 5%) and permeabilities (<1 μDarcy) did not contain significant biomass or metabolic activity.

The deep subsurface also poses additional problems relative to availability of electron donors and acceptors for metabolism. It is important to note that carbon deposited in a geologic formation and surviving tectonic burial and partial metamorphism may provide a source of electron-rich carbon (e.g., Krumholz *et al*., 1996; Colwell *et al*., 1997; Hohnstock-Ashe *et al*., 2001) that does not require communication with the shallow subsurface.

Such studies pose intriguing questions about the role of microfracture surfaces and microfracture surface minerals: Is there an advantage to an attached rather than planktonic existence within the porewaters of the microfracture network or open fractures? What advantages do attachment and growth provide? Are microbial populations syntrophic at the surface? Does the geochemistry of the surface influence population ecology and metabolism? More specifically, how does local availability of C (organic and inorganic), Fe (and perhaps Mn), and S influence the dominant terminal electron accepting process in the microfracture network? There is a growing body of work that has examined the interactions between mineral surfaces and microbes. Reviewing this literature is useful to place into context the depth and breadth of the possible interactions between microbes and the microfracture surface.

1.4 Microbe-Mineral Interactions

There is a growing body of literature on microbe-mineral interactions. Adherent or endolithic bacteria can cause mineral weathering (Fisk *et al*., 1998). They are involved in the deposition of minerals in extracellular regions, frequently within the extracellular polymeric substance region, and on cell surfaces and appendages. Some recent examples of calcite, dolomite, and ferroan dolomite deposition have been found (Brassant *et al*., 2002; Horath *et al*., 2002; Rogers and Bennett, 2001). In deep ocean vents, microbes can also mediate the precipitation of Fe and Si (Kruber *et al*., 2002).

One question of interest is whether elements available for metabolism within crystalline or amorphous mineral phases are transformed during metabolism. *Desulfitobacterium frappieri* strain G2, is capable of using ferric and ferrous iron containing minerals for respiration. The organism is capable of reducing poorly crystalline Fe (III) oxide minerals during the redox reaction. It can also participate in reversible redox reactions of iron within the lattice of phyllosilicates (Shelobolina *et al*., 2003).

There is also a growing body of evidence that microbes seek out surfaces to adhere to that may be of nutritional benefit. Lower *et al*. (2001) report nanoscale interactions involved in "recognition" of goethite by *Shewanella*. In Fe-limited growth media, *Pseudomonas* sp. will preferentially attach to the Fe (III)-bearing minerals goethite (α-FeOOH) and hematite (Fe_3O_4) and use the Fe nutritionally (Forsythe *et al*., 1998). Dissimilatory iron-reducing bacteria will also preferentially attach to α-FeOOH (Lower *et al*., 2001).

Recent work by Kalinowski and colleagues has shown that an *Arthrobacter* species will produce a Fe-siderophore when attached to the mineral hornblende and extract the Fe from the mineral with these chelators (Kalinowski *et al*., 2000a and 2000b; Liermann *et al*., 2000b). Biofilms (or perhaps biopatches) can produce a measurable ΔpH across the biofilm that helps to enhance mineral dissolution and may be related to growth rate, production of low molecular weight organic acids, physical properties of the synthesized extracellular polymeric substances, or production of the siderophore (Liermann *et al*., 2000a). In carbon-rich anoxic groundwaters where P is scarce, microbes will colonize hornblende surfaces that have apatite ($Ca_5(PO_4)_3OH$) inclusions and solubilize the P for nutritional use (Rogers *et al*., 1998).

Dong *et al*. (2003) examined microbially mediated reduction of Fe(III) in illite. *Shewanella putrefaciens* CN32 and native illites from St. Peter Formation sandstone in Ogle County, IL, were used. The illite contained a minor component of goethite (α-FeOOH) in addition to fibrous illite. Mössbauer spectroscopy of the bioreduced material indicated that both goethite and illite were reduced, but to different degrees. Transmission electron microscopy (TEM) showed dramatic change in illite morphology upon bioreduction; the dominant morphology went from fibrous needles to plates.

At the petroleum-contaminated aquifer site in Bemidji, MN, *in situ* distribution of attached bacteria is related to the nutritional content of the host minerals (Rogers *et al*., 1998 and 1999; Bennett *et al*., 1999). Research by Bennett and colleagues (Bennett *et al*., 1996; Bennett *et al*., 2000; Bennett *et al*., 2001; Hiebert and Bennett, 1992; Rogers *et al*., 2001) has also shown that colonized mineral surfaces weather faster than uncolonized ones. Adherent microorganisms can dissolve growth-limiting nutrients from a variety of silicate minerals, which, in turn, can enhance

growth and biodegradation of the contaminants at the site (Rogers *et al*., 1999; 2001). Preference is shown for silicates containing P and Fe, rather than for those containing Al, Pb, and Ni (Rogers *et al*., 1998 and 1999).

1.5 Chlorinated Solvent Abiotic and Biotic Transformations

Chlorinated solvents such as perchloroethene (PCE) and trichloroethene (TCE) have been widely used as industrial cleaning solvents and degreasing agents and also as chemical feedstocks (ATSDR, 1999). Consequently, these solvents are prevalent groundwater contaminants at many military, industrial, and municipal landfill sites (Vogel, 1994; ATSDR, 1999).

Chlorinated solvents can undergo abiotic transformations, though at fairly slow rates when compared to most microbially-mediated processes. Substitution and elimination are the predominant reactions (Vogel, 1994; Vogel *et al*., 1987). The former involves replacement of a halogen moiety with a hydroxyl group. The latter involves the removal of a hydrogen halide from the compound with the resultant formation of an alkene. The reaction path is dependent upon the degree of halogenation. There are a number of abiotic processes that lead to dechlorination. For instance, abiotic reactions between sulfide or ferrous iron and chlorinated organics can lead to destruction of the chlorinated organics (Amonette *et al*., 2000; Butler and Hayes, 2000, 2001; Devlin and Muller, 1999; Ferrey *et al*., 2004; Kenneke and Weber, 2003; Lee and Batchelor, 2003).

Biodegradation of chlorinated solvents such as PCE and TCE can occur aerobically and anaerobically (McCarty, 1997a, 1997b; Chapelle *et al*., 2003). Under aerobic conditions, chlorinated ethenes are oxidized (Hartmans *et al*., 1985; Davis and Carpenter, 1990; Phelps *et al*., 1991; Bradley and Chapelle *et al*., 1996a, 1998a, 1998b; Bradley *et al*., 1998b) or fortuitously cometabolised (Wilson and Wilson, 1985; Semprini *et al*., 1990, 1991; McCarty and Semprini, 1994; Semprini, 1995). Under anaerobic conditions, chlorinated ethenes are oxidized (Bradley and Chapelle, 1996, 1997, 1998b; Bradley *et al*., 1998b) or reductively dechlorinated (Vogel and McCarty, 1985; Barrio-Lage *et al*., 1987, 1990; Bouwer, 1994; McCarty and Semprini, 1994; Vogel, 1994; Odum *et al*., 1995).

The propensity to aerobically oxidize chlorinated ethenes increases with decreasing chlorination (Vogel *et al*., 1987; Chapelle *et al*., 2003). The aerobic degradation of vinyl chloride (VC) to CO_2 has been seen in laboratory cultures and in aquifer sample enrichments (Hartmans *et al*., 1985; Davis and Carpenter, 1990; Phelps *et al*., 1991; Bradley and Chapelle 1996, 1998a, 1998b; Bradley *et al*., 1998b; Coleman *et al*., 2002). VC can be used as a sole carbon source for growth and metabolism (Hartmans *et al*., 1985; Hartmans and deBont, 1992; Coleman *et al*., 2002). *In vitro* mineralization of dichloroethene (DCE), as the sole carbon source, can also occur aerobically (Bradley and Chapelle 1998b; Bradley *et al*., 1998b, 1998c). Mineralization of DCE has been observed in aquifer sediments (Bradley and Chapelle, 1998b; Bradley *et al*., 1998b, 1998c) and in cultures containing DCE as the sole carbon source and oxygen as the terminal electron acceptor (Bradley and Chapelle, 2000).

Aerobic cometabolism is another transformation process (Chapelle *et al*., 2003). Cometabolic oxidation of chloroethenes does not supply energy for metabolism or cell growth, instead, microorganisms contain nonspecific oxygenases that fortuitously oxidize chloroethenes to CO_2. Identified oxygenases include methane monooxygenase, toluene monooxygenase, and toluene dioxygenase (Fox *et al*., 1990; Li and Wackett, 1992; Newman and Wackett, 1997). Consequently, aerobic cometabolism of chloroethenes requires the presence of oxygen and a primary substrate to initiate the synthesis of the oxygenase. Wilson and Wilson (1985) first showed that methanotrophic bacteria are capable of mineralizing TCE to CO_2. Aerobic propane-, ethene-, aromatic organic-, ammonium-, and isoprene-oxidizers are able to convert TCE, DCE, and VC to CO_2 (Chapelle *et al*., 2003; McCarty and Semprini, 1994).

Microorganisms can also oxidize VC to CO_2 under anaerobic conditions (Chapelle *et al*., 2003). Oxidation requires a strong oxidant to drive microbial degradation, typically Fe (III). In an experiment conducted with sediment from a Fe(III)-reducing aquifer, addition of Fe(III) to anaerobic microcosms resulted in VC mineralization rates comparable to those observed under aerobic conditions (Bradley and Chapelle 1996). Bradley *et al.* (1998a) have also conducted microcosm work where [1,2^{14}-C] VC and [1,2-^{14}C] dichloroethane (DCA) were mineralized under anaerobic conditions to $^{14}CO_2$ where humic acid was used in the terminal electron accepting process.

In the presence of a suitable electron donor and catalyst, microbes use H_2 to replace a chlorine moiety on a chlorinated ethene molecule (Chapelle *et al*., 2003). This process is called reductive dechlorination, chloridogenesis, chlororespiration, or dechlororespiration (Löffler *et al*., 1996; Löffler *et al*., 2000; McCarty, 1997a; Sanford *et al*., 1996; Chapelle *et al*., 2003). Microbial reductive dechlorination is fairly ubiquitous in anaerobic, PCE- and TCE-contaminated aquifers. The accumulation of PCE and TCE transformation products has been observed in many anaerobic groundwater systems (Barrio-Lage *et al*., 1987, 1990; Bouwer, 1994; McCarty and Semprini 1994; Vogel 1994; Odum *et al*., 1995; Vogel and McCarty, 1985). Generally, dechlorination of PCE and TCE occurs under

mildly reducing conditions such as nitrate or Fe(III) reduction; however, dechlorination of DCE to VC requires more strongly reducing conditions typical of methanogenesis (Vogel *et al*., 1987). Field studies suggest that the extent of dechlorination is highly variable from site to site (Bouwer, 1994; McCarty and Semprini, 1994; Vogel, 1994; Chapelle, 1997; Gossett and Zinder, 1997; McCarty, 1997b; Chapelle *et al*., 2003).

Generally, the propensity of individual species of microbes to reductively dechlorinate decreases with decreasing chlorine substitution (Vogel *et al*., 1987; Bouwer, 1994; McCarty and Semprini, 1994; Vogel, 1994), though it is now known that the metabolic interactions amongst consortial members in a microbial community where dechlorination takes place can be much more complex. PCE readily undergoes anaerobic reductive dechlorination to TCE. Reductive dechlorination of TCE to *cis*-DCE occurs during Fe(III)-reduction. Reductive dechlorination of *cis*-DCE to VC can occur under sulfate-reducing conditions (Vogel et al., 1987; Chapelle, 1997) and during methanogenesis. Reductive dechlorination of VC to ethene occurs during methanogenesis (Vogel and McCarty, 1985; Barrio-Lage *et al*., 1987, 1990; Freedman and Gossett, 1989; DiStefano *et al*., 1991; de Bruin *et al*., 1992; Bouwer, 1994; Maymó-Gatell *et al*., 1997 and 1999; Odum *et al*., 1995; Wu *et al*., 1995). Reductive dechlorination of PCE and TCE can be incomplete in the subsurface. The accumulation of *cis*-DCE and VC occurs unless certain dehalorespirers are present in significant numbers (Wiedemeier *et al*., 1998; Chapelle *et al*., 2003).

Several PCE-dechlorinating isolates of the *Proteobacteria*, *Desulfitobacteria*, and the *Dehalococcoides* cluster have been identified (Chang *et al*., 2000; Holliger *et al*., 1998; Krumholz *et al*., 1996; Maymó-Gatell *et al*., 1997; Miller *et al*., 1997; Scholz-Muramatsu *et al*., 1995, Sharma and McCarty, 1996; Suyama *et al*., 2002; Wild *et al*., 1996; He *et al*., 2003). Some isolates are versatile and use H_2 or organic acids as electron donors. *Dehalobacter* and *Dehalococcoides* sp. require H_2. *Desulfuromonas chloroethenica*, a member of the *Desulfuromonas* cluster in the *Geobacteraceae*, uses acetate. Complete reductive dechlorination of PCE and TCE to ethene or ethane occurs in anaerobic enrichment cultures (deBruin *et al*., 1992; DiStefano *et al*., 1991). Almost all of the dechlorinating bacteria that have been isolated reduce PCE or TCE only to *cis*-DCE (Gerritse *et al*., 1996; Scholz-Muramatsu *et al*., 1995). The anaerobe *Dehalococcoides ethenogenes*, however, completely dechlorinates PCE or TCE; in fact, it can also use *cis*-DCE, 1,1-DCE, and 1,2-DCA as electron acceptors (Maymó-Gatell *et al*., 1997; 1999).

Many dehalorespirers are gram-positive bacteria in the *Clostridium-Bacillus* subphylum or the α and γ branches of the *Proteobacteria* (Holliger *et al*., 1999). *D. ethenogenes* is more phylogenetically dissimilar to the other dehalorespiring bacteria and has an *Archaea*-like cell wall structure (Maymó-Gatell *et al*., 1997). Phylogenetically, it may be closer to the green non-sulfur bacteria (Hugenholtz *et al*., 1998).

Dehalogenation is catalyzed by reductive dehalogenases which are typically membrane-bound and use chlorinated ethenes or chloroaromatics as substrates (Christiansen and Ahring, 1996; Cole *et al*., 1995; Holliger *et al*., 1998; Löffler *et al*., 1996; Magnuson *et al*., 1998; Maymó-Gatell *et al*., 1997; Miller *et al*., 1998; Neumann *et al*., 1994 & 1998; Ni *et al*., 1995; Utkin *et al*., 1994). The reductive dehalogenase subunit molecular mass ranges from 50 to 65 kDa and contains cobalamin and iron-sulfur clusters (Holliger *et al*., 1999). The PCE reductive dehalogenase from *D. ethenogenes* accepts only PCE as a substrate. Unlike other dehalorespirers, however, *D. ethenogenes* also uses a second enzyme, TCE reductive dehalogenase that is less specific and dechlorinates TCE, DCEs, and VC to ethene (Magnuson *et al*., 1998).

The U.S. EPA and the Air Force Center for Environmental Excellence (AFCEE) have developed and evaluated a protocol and scoring system for assessing the natural attenuation potential of chlorinated aliphatics in groundwater (U.S. EPA, 1998; Wilson, 2002; Wiedemeier *et al*., 1998). The system has been applied at numerous contaminated porous media sites. Three types of chlorinated solvent natural attenuation scenarios are identified: Type 1 behavior occurs where the primary substrate is anthropogenic carbon which drives reductive dechlorination. Type 2 behavior occurs when high concentrations of biologically available NOM are present. Type 3 behavior dominates in areas that are characterized by low concentrations of NOM and/or anthropogenic carbon and by DO concentrations greater than 1.0 mg/L. Under these conditions, reductive dechlorination will not occur, but VC can be oxidized. Sites that are mixtures of these regimes also exist.

Stiber *et al*. (1999) developed an expert system to evaluate naturally-occurring reductive dechlorination for TCE-contaminated groundwater. In their study, 22 experts were queried as part of system development. Observation of biodegradation daughter and/or end products was identified as the most valuable indication of natural attenuation.

Flynn *et al*. (2000) conducted some interesting microcosm work to examine the potential role of community metabolism during *in situ* TCE dechlorination. They obtained subcultures from river sediments that reductively dechlorinated *cis*-DCE or VC; the subcultures came from three independent enrichments that completely dechlorinated PCE to

ethene. The three subcultures completely dechlorinated *cis*-DCE and VC and could be transferred indefinitely in basal salts minimal medium with H_2 as the electron donor. Dilution transfers were then used to attenuate the ability to dechlorinate. Two of the subcultures eventually failed to dechlorinate PCE, but the third subculture maintained its ability. Analysis of the 16S rRNA genes (rDNA) from these enrichments using terminal restriction fragment length polymorphism and denaturing gradient gel electrophoresis showed changes in community composition in the attenuated subcultures, but not in the subcultures that maintained the PCE-dechlorinating activity. The data suggested that at least two populations were responsible for the sequential dechlorination of PCE to ethene in these cultures and that consortia can cooperate in the complete dechlorination of PCE.

He *et al*. (2002) studied community dechlorination activity at the chloroethene-contaminated Bachman Road site in Oscoda, MI. Microcosms were established using aquifer samples from various locations and depths inside the contaminant plume. A number of electron donors were evaluated along with various chlorinated ethenes as electron acceptors. Microcosms treated with donors showed dechlorination activity. However, precise end points for dechlorination were varied and suggested spatially heterogeneous distribution of the dechlorinating potential in the plume. Acetate treatments showed complete dechlorination of PCE to ethane; microcosms rapidly converted PCE to *cis*-DCE. PCE dechlorination in H_2- treated microcosms occurred after a lag phase and after acetate had accumulated by H_2/CO_2 acetogenic activity. In their view, H_2 can be the sole electron donor for reductive dechlorination to ethene provided syntrophic acetate-oxidizing population(s) and H_2/CO_2 acetogenic population(s) are present.

Table 1.2 summarizes the known conditions for abiotic and biotic transformations of chlorinated solvents. Table 1.3 summarizes the environmental conditions required for reductive transformations of chlorinated solvents. Table 1.4 summarizes what is known about prokaryotes that engage in reductive dechlorination.

Table 1.2. Conditions for Abiotic and Biotic Transformation of Chlorinated Solvents
(Adapted from McCarty, 1997b.)

Transformation	Carbon Tetrachloride (CT)	Tetrachloroethene (PCE)	Trichloroethene (TCE)	1,1,1-Trichloroethane (TCA)
Biotic-Aerobic				
Primary substrate	No	No	No	No
Co-metabolism	No	No	Yes	Perhaps
Biotic-Anaerobic				
Primary substrate	Perhaps	Yes	Yes	Perhaps
Co-metabolism	Yes	Yes	Yes	Yes
Hazardous intermediates	Yes	Yes	Yes	Yes
Abiotic hydrolysis	Perhaps	No	No	Yes
Abiotic reduction or elimination	Yes	Yes	Yes	Yes

Table 1.3. Environmental Conditions for Biological Reductive Dechlorination Reactions
(From McCarty, 1997b.)

Chlorinated Solvent	Redox Environment			
	All environments	Denitrification	Sulfate reduction	Methanogenesis
Carbon tetrachloride (CT)	TCA → 1,1-DCE + CH_3COOH	CT → Chloroform	CT → CO_2 + Cl^-	-
1,1,1-Trichloroethane (TCA)		-	TCA → 1,1-DCA	TCA → CO_2 + Cl^-
Tetrachloroethene (PCE)		-	PCE → 1,2-DCE	PCE → Ethene
Trichloroethene (TCE)		-	TCE → 1,2-DCE	TCE → Ethene

Table 1.4. Properties of Some Direct Chlorinated Solvent Dechlorinators
(Adapted in part from Gossett and Zinder, 1997.)

Organism	Dechlorination reactions	Electron donors	Other electron acceptors	Morphology	Phylogenetic position	References
Dehalobacter restrictus	PCE, TCE → *cis*-DCE	H_2	None	Rod	Gram + *Desulfotomaculum* group	Holliger *et al.*, 1998; 1999
Dehalospirillum multivorans	PCE, TCE → *cis*-DCE	H_2, formate, pyruvate, etc.	Thiosulfate, nitrate, fumarate, etc.	Spirillum	*Proteobacteria*	Neumann *et al.*, 1994, 1998
Strain TT4B	PCE, TCE → *cis*-DCE	Acetate	None	Rod	?	Krumholz *et al.*, 1996
Enterobacter agglomerans	PCE, TCE → *cis*-DCE	Nonfermentable substrates	O_2, nitrate, etc.	Rod	γ *Proteobacteria*	Sharma and McCarty, 1996
***Desulfitobacterium* sp. strain PCE1**	PCE, TCE → (*cis*-DCE) *o*-chlorophenols	Lactate, pyruvate, butyrate, ethanol, etc.	Sulfite, thiosulfate, fumarate	Curved rod	Gram + *Desulfotomaculum* group	Gerritse *et al.*, 1996
***Desulfitobacterium frappieri* strain TCE1**	PCE, TCE → (*cis*-DCE)	H_2 formate, lactate, butyrate, crotonate ethanol, etc.	Sulfite, thiosulfate, nitrite fumarate	Curved rod	Gram + motile	Gerritse *et al.*, 1999
***Dehalococcoides ethenogenes* strain 195**	PCE, others → ethane	H_2	None	Irregular coccus	Novel eubacterium	Maymó-Gatell *et al.*, 1997
***Dehalococcoides* sp. strain BAV1**	VC, *cis*-DCE, *trans*-DCE, 1,1-DCE, others → ethene	H_2	None	Non-motile disc	?	He *et al.*, 2003
***Desulfuromonas michiganensis* sp. nov. (Strain BB1, BRS1)**	PCE → *cis*-DCE	Acetate, lactate, pyruvate, succinate, malate, fumarate	None	Short, ovoid rods (some club-shaped rods seen in early stationary phase when grown on fumarate)	*Desulfuromonas* cluster of δ *Proteobacteria*	Sung *et al.*, 2003

1.6 Determination of Likely Terminal Electron Accepting Processes

Lovley, Chapelle and colleagues (Lovley and Phillips, 1987; Lovley and Goodwin, 1988; Chapelle *et al*., 1995; 1996b; 2003) have developed and advanced a methodology for deducing the dominant terminal electron accepting process within zones in contaminant plumes or aquifers. Three components are needed: (i) the consumption of electron acceptors (e.g., $O_{2(g)}$, NO_3^-, Fe(III), SO_4^{2-}, $CO_{2(g)}$), (ii) the production of metabolic end products (e.g., $CO_{2(g)}$, $N_{2(g)}$, Fe(II), S^{2-}, $CH_{4(g)}$), and (iii) the measurement of concentrations of transient intermediate products, especially H_2, a characteristic intermediate product of anaerobic (largely fermentative) microbial metabolism. Different terminal electron accepting processes generally have characteristic H_2 steady state concentrations in solution that reflect dominant metabolic redox reaction and are relatively independent of reactant consumption or final product production (Lovley and Goodwin, 1988). Nitrate reduction maintains H_2 concentrations below 0.1 nM. Iron (III) reduction maintains H_2 concentrations between 0.2 and 0.8 nM. Sulfate reduction has a characteristic range between 1 and 4 nM. Methanogenesis typically results in H_2 concentrations in the 5 to 15 nM range. This scheme has been applied in numerous settings by Chapelle and colleagues (See Chapelle *et al*., 1996b, 2003; U.S. EPA, 1997.) though some exceptions have been observed in colder groundwater settings (Jakobsen et al., 1998).

McGuire *et al*. (2000) used the terminal electron accepting process deduction scheme to examine a plume in a shallow groundwater site contaminated with fuel and chlorinated solvents. Terminal electron accepting process parameters including methane, dissolved Fe, and H_2 were measured within the plume over a 3-year period. The terminal electron accepting process parameters changed on different time scales, in part driven by recharge events. Some terminal electron accepting process parameters changed on short time scales (months), while others had longer time scales (years). The authors believed that when interpreting terminal electron accepting process conditions in aquifers contaminated with a variety of organic chemicals, such as those with petroleum hydrocarbons and chlorinated solvents, one must consider additional hydrogen-consuming reactions such as dehalogenation. They also recommended determinations of microbial community structure and activity.

Lendvay *et al*. (2003) used the terminal electron accepting process deduction scheme to look at the impacts of adjacent surface waters of Lake Michigan on a lake-side shallow TCE contaminant plume. A spatially discretized, multilevel well array was employed for sampling in and around the plume. Samples were analyzed for TCE, DCE, VC, ethene, $O_{2(g)}$, Fe(II), SO_4^{2-}, S^{2-}, $CH_{4(g)}$, $H_{2(g)}$, and redox potential (Eh). Methane and chloroethene decreased as the groundwater became more oxidized closer to the interface between the lake water and the plume. On the other hand, *cis*-1,2- DCE remained unchanged or slightly increased at the same locations. A negative correlation was seen between the chloroethene and methane data when compared to oxygen. The authors surmise that chloroethene is co-oxidized by methane-oxidizing bacteria in the shallow region of the plume. Reductive dechlorination of the chlorinated solvents remained the predominant biotransformation process in the deeper, more anaerobic zones of the plume.

1.7 Related Field Work on Bedrock TCE Contaminated Sites

A number of excellent field studies and case histories can be found in Chapelle *et al*. (2003), U.S. EPA (1997), and U.S. EPA (2002). Some relevant studies are discussed here.

Yager *et al*. (1997) conducted hydrogeological, geochemical, and microcosm experiments to examine TCE biodegradation in a fractured dolomitic aquifer in Niagara Falls, NY. Field observations suggested that TCE is biodegraded by sequential dechlorination to ethene through reductive dechlorination under anaerobic conditions. The groundwater samples in and around the plume showed that $H_{2(g)}$ was linked to Fe(III) reduction as the terminal electron accepting process. Bacteria from the fractured dolomite were able to sequentially dechlorinate TCE in microcosms. Dechlorination was enhanced when crushed dolomite was added to the reactions. Naturally occurring petroleum hydrocarbons present in low concentrations in the formation were the source of electrons for respiration. Amplified ribosomal DNA restriction analysis of the microbial populations indicated a low diversity, sulfur-transforming community outside the plume. Inside the plume, a highly diverse community, including *D. ethenogenes*-type microorganisms, was present (Hohnstock-Ashe *et al*., 2001).

Hendrickson *et al*. (2002) looked at the environmental distribution of *Dehalococcoides* group organisms and their association with chloroethene dechlorination activity at 24 chloroethene-contaminated sites scattered throughout North America and Europe. Soil or earth matrices were tested for the presence of *Dehalococcoides* species using polymerase chain reaction assay for *Dehalococcoides* 16S rDNA sequences. Sequences were detected at 21 of the 24 sites. Complete dechlorination to ethene occurred at these sites. *Dehalococcoides* sequences were not detected in samples from three sites where only partial dechlorination to 1,2-*cis*-DCE occurred. They used phylogenetic analysis of the 16S rDNA amplicons to show *Dehalococcoides* sequences formed a unique 16S rDNA group. Three

subgroups were identified based on specific base substitution patterns. These data suggest that members of the *Dehalococcoides* sp. are widely distributed geographically and geologically.

1.8 Spectroscopic Characterization of Microfracture Surfaces

The use of surface and mineralogical analyses to characterize the x-y and the y-z planes of the microfracture surface can provide useful information about the morphology and mineral composition of secondary mineral deposits on the outer surface, the spatial relation between microorganisms and mineral deposits, the spatial distribution of elements in the x-y plane, the depth profiles of elements of interest with depth in the rind in the y-z plane, the types of crystalline minerals present, and the depth profiles of mineral phases or species.

A suite of methods is frequently needed to study surface mineralogy and bulk mineralogy relative to adherent microbes (Figure 1.2). These methods have inherent strengths and weaknesses (frequently detection limit issues), or they rely on databases not particularly suited to the poorly crystalline secondary minerals found in the environment. However, when used in a complementary fashion, they are powerful analytical tools. More detailed and exhaustive reviews of this subject can be found in Geesey *et al*. (2002), Perry *et al.*(1990), Coyne and McKeever (1990), and Calas and Hawthorne (1988). These methods are also thoroughly described in the Materials and Methods section of this report.

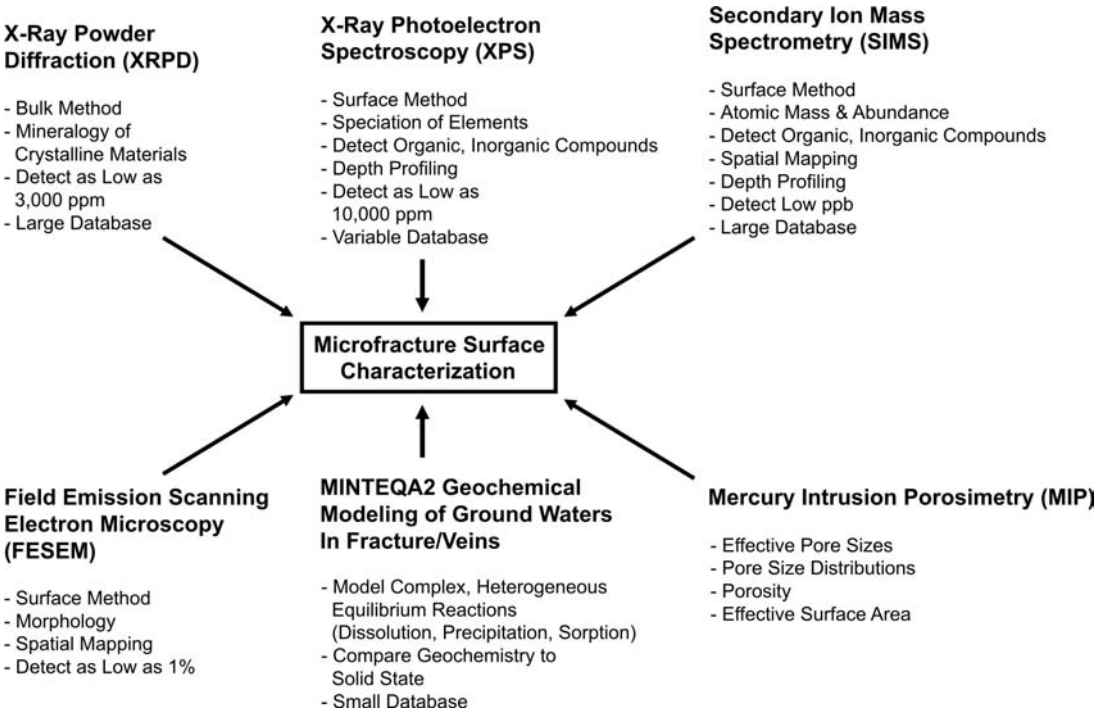

Figure 1.2. Suite of analytical methods for characterization of bulk and surface chemistry.

1.9 Objectives of This Study

In the context of the recent literature, important questions remain about the nature of the interaction between the microfracture surface and the adherent microbes. How does the surface influence attachment and growth? How does the geochemistry of the microfracture surface influence population ecology and metabolism? More specifically, how does the microfracture surface influence the dominant terminal electron accepting process in the microfracture network? What is the nature of TCE biodegradative processes? Is *Dehalococcoides*-driven dehalorespiration a dominant transformative process?

As part of the overall research plan to better understand relevant transport, retardation, and attenuation processes for TCE in competent bedrock, we studied 11 microfractures extracted from competent bedrock cores from boreholes BBC5 and BBC6 so as to characterize, with a variety of surface spectroscopic and microbial techniques, the relation, if any, between microfracture surface geochemistry and the ecology and metabolic activity of attached microbial populations relative to terminal electron accepting processes or to chlorinated solvent biodegradation.

2.0 Materials and Methods

2.1 Core/Microfracture Locations

As part of its research program, the University of New Hampshire's Bedrock Bioremediation Center (BBC) [http://www.unh.edu/civil-engineering/research/erg/bbc] has conducted research on a TCE-contaminated saturated bedrock field study site (Site 32) in southeast New Hampshire.

Site 32, which is located at the Pease International Tradeport (formally Pease Air Base) in Portsmouth, NH, is situated on a variable thickness upper sand layer overlying a marine clay layer overlying a variable thickness lower sand layer. These unconsolidated layers are situated over bedrock of the Kittery Formation (See Figure 2.1.). The groundwater in the bedrock is predominately contaminated with DCE (100 to 700 µg/L) with lesser amounts of TCE and VC. The contaminant plume extends about 0.5 km through a metasandstone (partially metamorphosed sandstone) of the Silurian and Ordovician Kittery Formation interbedded with Jurassic diabase dikes.

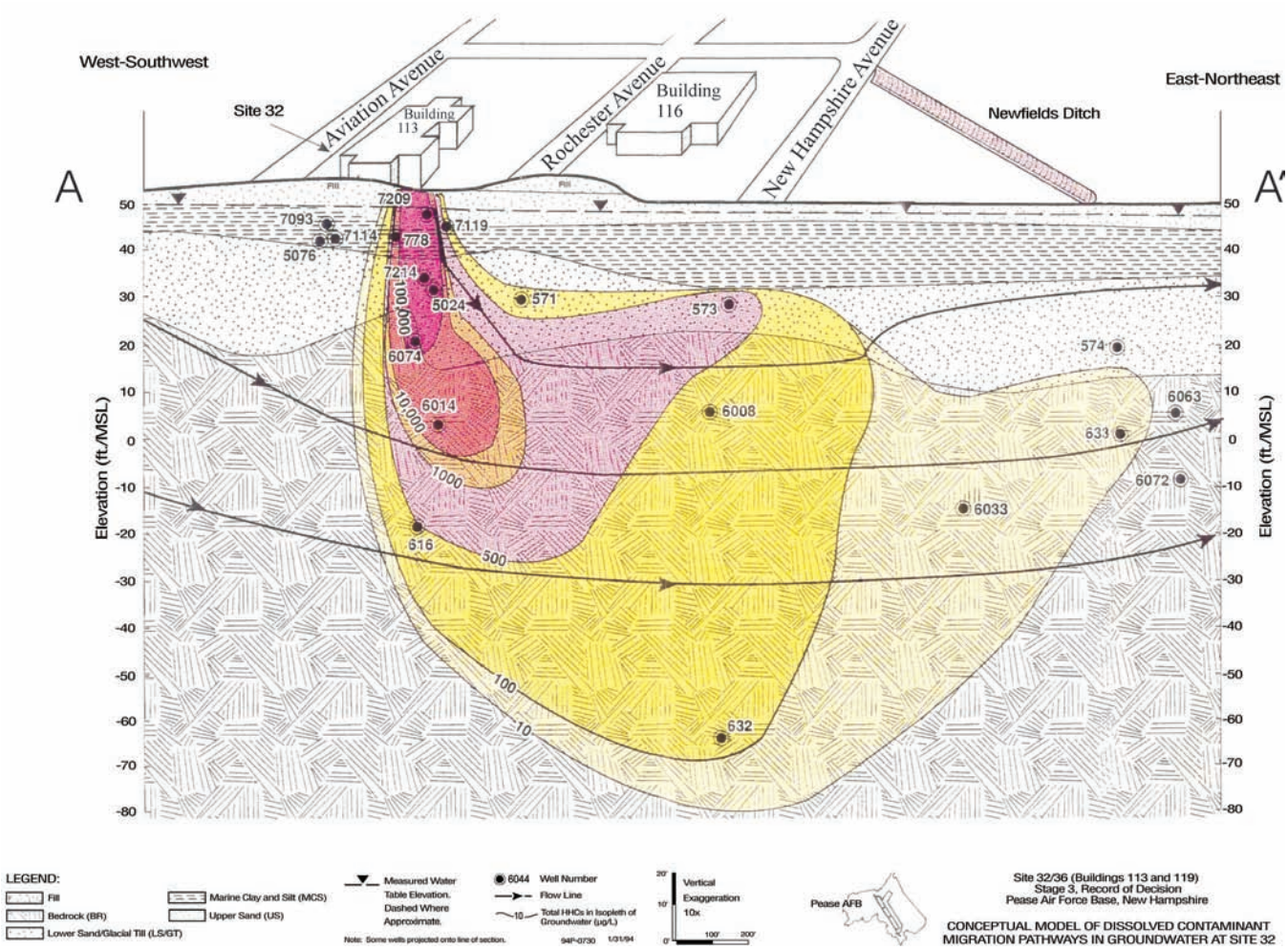

Figure 2.1. Cross section through BBC site.

The source of the TCE originated from an underground storage tank (UST) behind Building 113 where, between 1955 and 1991, aircraft munitions systems and avionics were maintained. Vapor degreasing occurred from 1956 to 1966. A 4,488 L (1,200 gal) concrete UST at the northeast corner of the building received TCE via a floor drain. In 1977, 3,740 L (1,000 gal) of waste TCE were removed, and the tank was filled with sand. In 1988, the tank was excavated and removed. At that time, an overflow discharge pipe was discovered. The pipe and 441 tons of contaminated soil were removed in 1990 (footprint and depth of excavation unknown). A pilot pump and treat system was used to treat the lower sand layer and weathered bedrock from 1991 to 1995. The site was deemed to be a TI zone, and sheet piles were installed down to competent bedrock in 1996. Groundwater pumping within the sheet pile area commenced in 1997 and has been ongoing since that time.

Over the last few years, six investigatory boreholes (termed BBC1 through BBC6) have been installed in and around the plume at Site 32 (Figure 2.2). These boreholes have served a variety of purposes. All but one of these boreholes have been used for extraction of cores from the competent bedrock as a function of depth. Our focus on microfracture characterization was limited to 11 microfractures extracted from boreholes BBC5 and BBC6. These boreholes are about 7.6 m (25 ft) from each other. The bedrock portion of borehole BBC5 was drilled between December 6, 2001, and January 9, 2002. The bedrock portion of borehole BBC6 was drilled between August 30, 2002, and October 7, 2002.

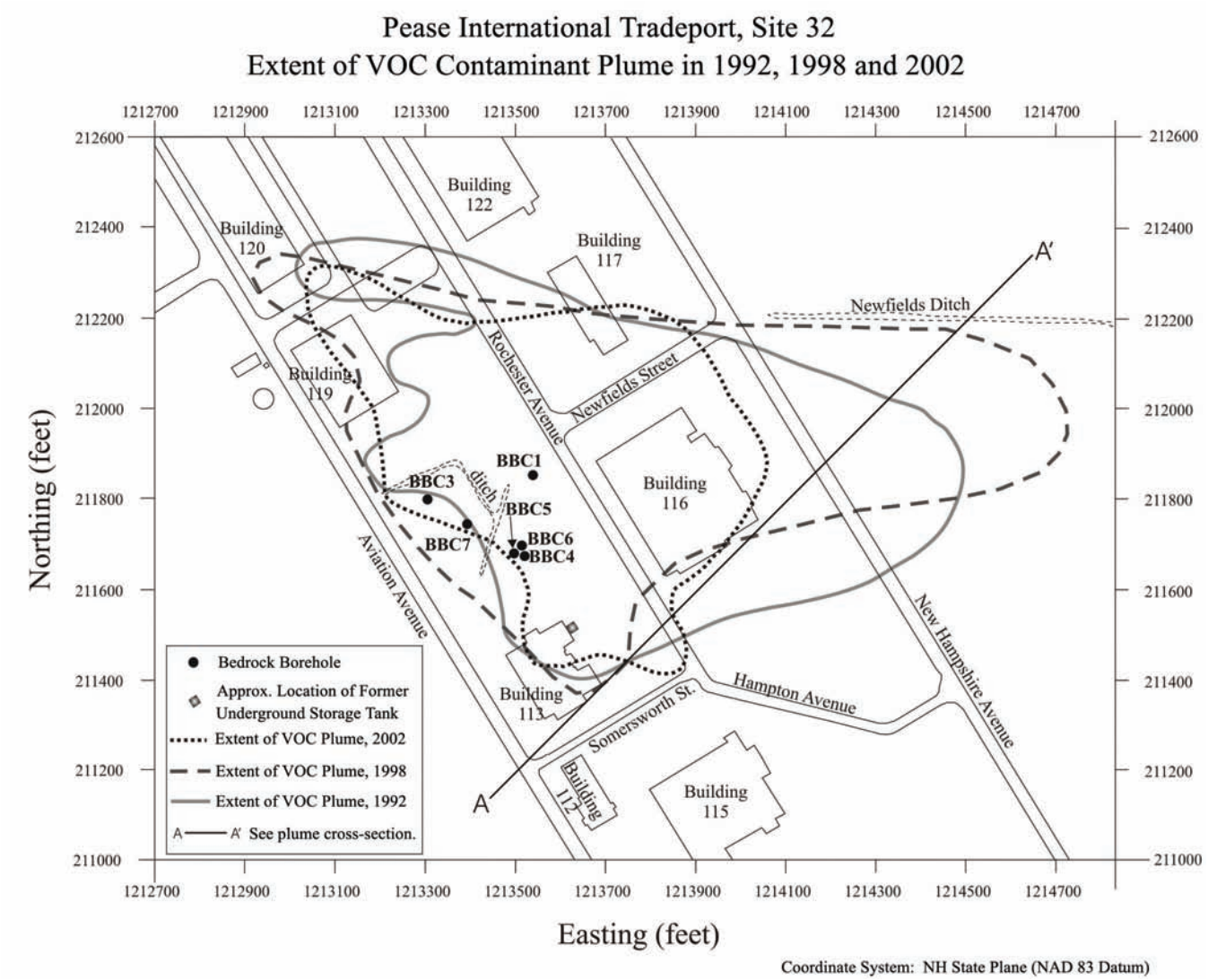

Figure 2.2. Plan view of borehole locations at Site 32.

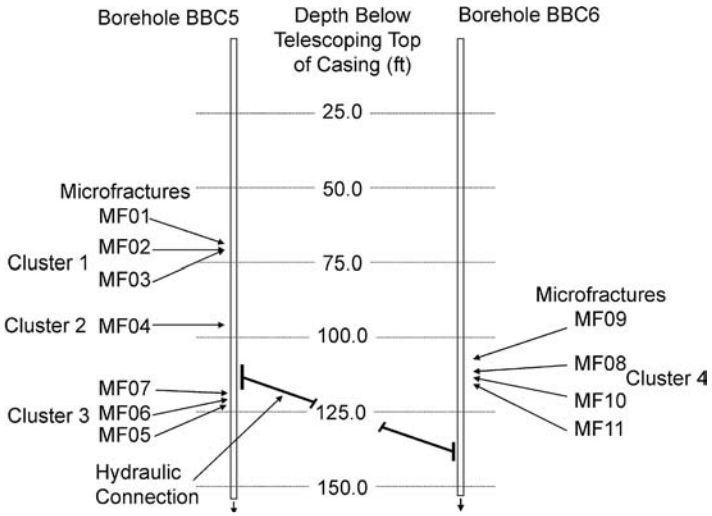

Figure 2.3. Cross section through boreholes BBC5 & BBC6 showing microfracture locations and hydrologic connections between the two boreholes.

Microfractures from borehole BBC5 were collected on December 20, 2001. Microfractures from borehole BBC6 were collected on September 24, 2002. The locations of these microfractures (designated MF01 to MF11) as a function of depth are shown in Figure 2.3. All microfracture samples that were collected from the Kittery Formation and not from the diabase dikes are reported relative to the top of the telescoping casing installed through the overburden and weathered bedrock.

Table 2.1 provides a generalized description of the 11 microfractures, their assignment into four spatial clusters, and the gross appearance of each microfracture surface as well as their gross features relative to core stratigraphy. Descriptions are based on BBC protocols identified in Table 1.1. Table 2.2 summarizes the analyses that were applied to each microfracture sample.

Table 2.1. Microfracture Location, Cluster Assignment, and Description

Micro-fracture #	Well	Core interval / fracture depth, ft	Cluster	Microfracture exposed surface visual appearance after removal from the core	Extent	Type	Attitude	Aperture width in mm (aspect ratio, z/x)	Exposed surface area with secondary mineralization
MF01	BBC5	70.5-75.5 / 71.5	1	Wetted, Olive Green Precipitate, Flakey, Homogenous, Some Pyrite	Continuous	Cross Bedding	Low Angle	> 0.4 (< 0.003)	Extensive (>30%)
MF02	BBC5	70.5-75.5 / 73.0	1	Wetted, White Precipitate, Molted/Patchy, Some Flakey (Soft), No Pyrite	Continuous	Bedding	Steeply Inclined	< 0.4 (< 0.001)	Some (10-30%)
MF03	BBC5	70.5-75.5 / 73.0	1	Wetted, Fine Grained Grey Black Surface, No Apparent Precipitate, No Pyrite	Continuous	Bedding	Steeply Inclined	< 0.4 (< 0.001)	Little (<10%)
MF04	BBC5	95.5-100.2 / 97.0	2	Wetted, Fine Grained Grey-Black Surface With White Precipitate Traces, No Pyrite	Continuous	Bedding	Low Angle	> 1 (< 0.006)	Little (<10%)
MF05	BBC5	119.9-124.7 / 122.7	3	Wetted, Chalky Slate Blue Precipitate, Some Quartz Veins, Homogenous, No Pyrite	Discontinuous	Cross Bedding	Steeply Inclined	> 0.6 (< 0.004)	Extensive (>30%)
MF06	BBC5	119.9-124.7 / 122.0	3	Wetted, Shiny Green-Yellow Precipitate, Homogenous, No Pyrite	Continuous	Bedding	Moderately Inclined	> 0.6 (< 0.004)	Extensive (>30%)
MF07	BBC5	119.9-124.7 / 121.5	3	Wetted, Olive Green-Black Precipitate, Very Fine Grained, No Pyrite	Continuous	Cross Bedding	Low Angle	> 1 (< 0.006)	Little (<10%)
MF08	BBC6	107.39-112.14 / 112	4	Wetted, White Precipitate, Homogenous, No Pyrite	Continuous	Bedding	Horizontal	> 0.4 (< 0.003)	Extensive (>30%)
MF09	BBC6	107.39-112.14 / 107.4	4	Wetted, White Precipitate, Homogenous, No Pyrite	Discontinuous	?	?	> 0.8 (< 0.005)	Extensive (>30%)
MF10	BBC6	112.14-116.94 / 113.31	4	Wetted, White Precipitate, Homogenous, No Pyrite	Continuous	?	Moderately Inclined	> 0.4 (< 0.003)	Extensive (>30%)
MF11	BBC6	112.14-116.94 / 116.72	4	Wetted, White Precipitate, Homogenous, No Pyrite	Continuous	?	Steeply Inclined	< 0.4 (< 0.001)	Extensive (>30%)

Table 2.2. Analytical Methods Applied to the Host Rock and Microfracture Samples

Micro-fracture #	Well	Cluster	MIP of HR	SEM of MF	SEM-EDAX spatial mapping of HR/MF	Petrography of HR/MF	XRD of HR/MF	TEM of MF	SIMS of MF	XPS of MF	Packer sampling in MF regions	PCR Primers/ DGGE/ gene sequencing from MF
MF01	BBC5	1	General host rock samples from BBC5	Yes	MF	HR	HR/MF	-	-	No	No	Yes
MF02	BBC5	1		Yes	MF	HR/MF	HR/MF	-	-	Yes	No	Yes
MF03	BBC5	1		Yes	MF	HR	HR	-	Yes	Yes	No	Yes
MF04	BBC5	2		Yes	MF	HR	HR/MF	-	-	Yes	Yes	Yes
MF05	BBC5	3		Yes	MF	HR	HR	-	-	Yes	Yes	Yes
MF06	BBC5	3		Yes	MF	HR/MF	HR/MF	-	-	Yes	Yes	Yes
MF07	BBC5	3		Yes	HR/MF	HR	HR/MF	-	-	Yes	Yes	Yes
MF08	BBC6	4	None	Yes	MF	HR	HR/MF	-	-	Yes	No	-
MF09	BBC6	4		Yes	HR/MF	HR	HR/MF	-	-	Yes	No	-
MF10	BBC6	4		Yes	MF	HR	HR/MF	-	-	Yes	Yes	-
MF11	BBC6	4		Yes	MF	HR/MF	HR/MF	Yes	-	No	Yes	-

Abbreviations:
DGGE – Denaturing Gradient Gel Electrophoresis
HR – Host Rock
MF – Microfracture
MIP – Mercury Intrusion Porosimetry
PCR – Polymerase Chain Reaction
SEM-EDAX – Scanning Electron Microscopy – Energy Dispersive Analysis of X-Rays
SIMS – Secondary Ion Mass Spectrometry
TEM – Transmission Electron Microscopy
XPS – X-Ray Photoelectron Spectroscopy
XRD – X-Ray Diffraction

2.2 Core/Microfracture Sample Collection

Competent bedrock cores extending into the Kittery Formation and (in some cases) sections of diabase dike, were collected for microbial analysis using a triple barrel corer as described in Volume 1: Fractured Rock Drilling. As noted in Volume 4: Fractured Rock Microbiology, the drilling fluid was from a non-contaminated pristine bedrock well and was not re-circulated so as to minimize microbial cross contamination with depth. BBC researchers have developed unique drilling procedures to obtain and process 10.16 cm (4-inch) diameter cores that contain intact, representative, microbial populations. These procedures allow for the option of maintaining and examining cores under anoxic conditions. Using these procedures, the BBC installed six bedrock boreholes (BBC1 to BBC6) . Each borehole was installed with telescoping casing through the overburdened and fractured bedrock in an effort to limit contamination by these zones.

Each completed borehole was analyzed by the following methods: videologging, omni-directional borehole radar, acoustic and optical televiewer scanning, heat pulse flowmeter, natural gamma, caliper, single-point resistivity, and fluid temperature/resistivity. In addition, BBC4 through BBC7 were monitored during completion with a drilling parameter recorder (DPR). The DPR is a computerized system that automatically collects data from a series of transducers installed on conventional drilling equipment. The data include information on the advance rate, down-thrust and pull-up pressures, rod torque, rotation time, mud/water pressure and flow, depth, and time. All cores reamed from the boreholes were examined for standard lithological features by a geologist. Data from the DPR, videologs, and geophysical logs were used to select fracture zones in each borehole for further study. These fracture zones were the focus of the groundwater sampling and hydraulic testing conducted in each borehole.

Selection of microfractures for analysis involved some initial trials. Basically, microfractures had to be exposed by breaking apart the core so that the break occurred within the microfracture surface itself, as this was the weakest portion of the rock sample. If struck correctly, the core would break apart and expose two surfaces of the microfracture. In some cases, the surface precipitates adhered to only one side of the break, in others precipitates adhered to both sides. We elected to analyze those specimens that had surface precipitates on them. Further, we had to select microfractures with steep inclination relative to the length of the core so that thin specimens could be collected

and fitted into spectroscopic instruments for analysis. Consequently, the microfractures needed to be extensive across the entire thickness of the core, with steep inclination, and have an apparent aperture width that was measurable and open in appearance. Tightly sealed microfractures frequently would not break apart after repeated hammer blows.

Subsequently, partially mineralized, partially sealed microfractures which were readily exposed by striking with a surface-sterilized geology hammer were collected from each of the boreholes. A typical microfracture and the orientation of the microfracture face relative to the core are shown in Figure 2.4. All of the microfractures were separately processed for microbiological and geological analyses.

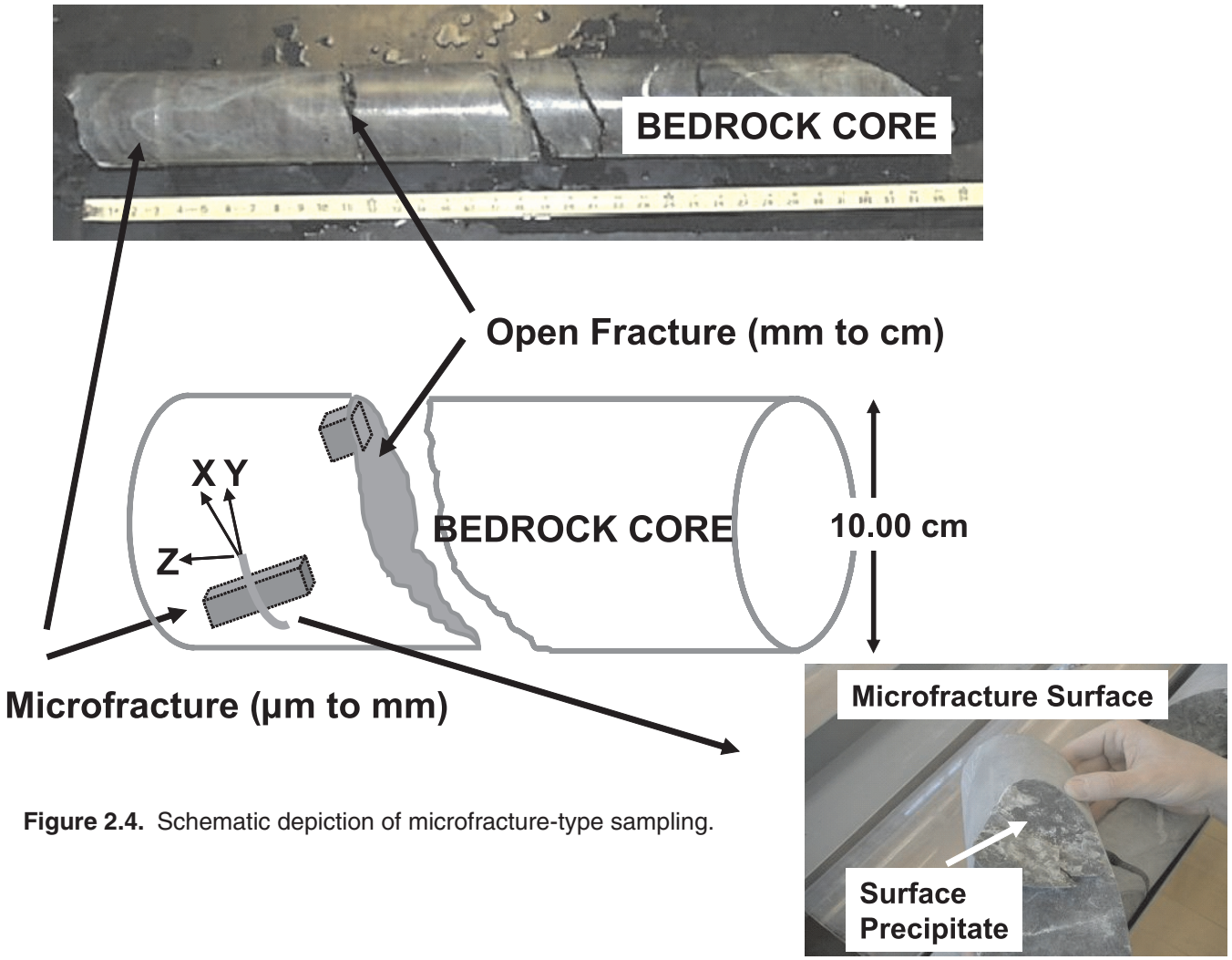

Figure 2.4. Schematic depiction of microfracture-type sampling.

2.3 Microfracture Sample Preparation

The recovered microfracture surfaces were further broken into pieces between one and 30 cm^3 using a sterilized chisel. Samples were marked on all sides except on the surface face of the microfracture with solvent-free water-soluble ink. All samples were stored in sterile 100-mL plastic specimen bottles. Further preservation required for specific analyses is described below.

2.4 Overall Analytical Sequence

The general sequence of sampling and analysis is shown in Figure 2.5. The sequence involved drilling, core extraction, core processing, microfracture sampling, extraction of the adherent microbes, borehole characterization, characterization of the microfracture surfaces, packer sampling over the interval in which the microfracture was located, characterization of the porewater, and geochemical modeling of the porewater.

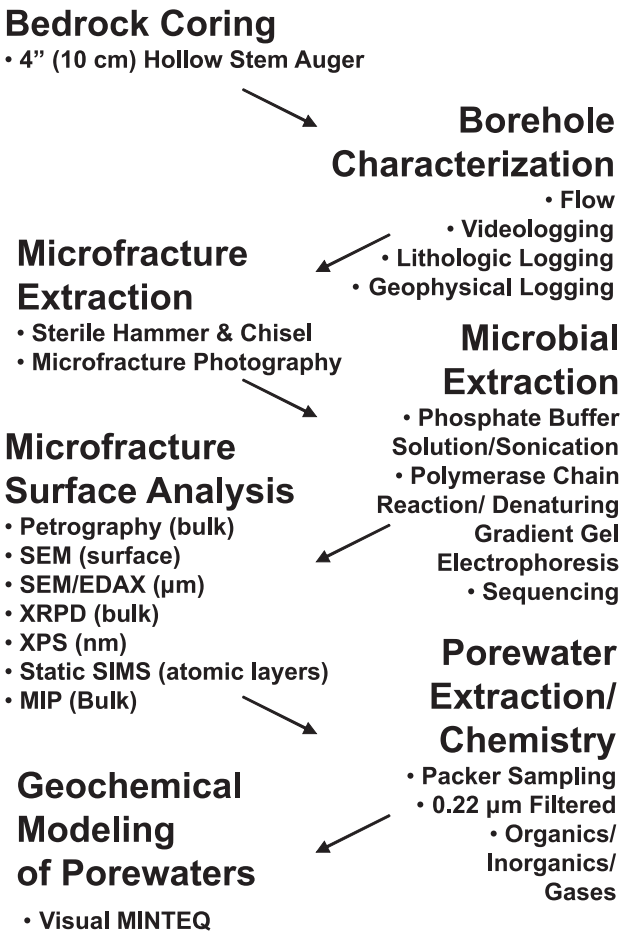

Figure 2.5. Analytical scheme.

2.5 SEM-Morphology and Biopatch Distribution

SEM is used to examine the morphology of microfracture surfaces in the x-y plane. It also is used to determine the presence of adherent microorganisms as well as examine morphology and extracellular features. SEM uses secondary and backscattered electrons from the primary interaction of an electron beam with nuclei of atoms in the near surface region of the sample. It produces a reflected energy beam picture of the sample. The sample is analyzed in a high vacuum (unless environmental SEM is used), so samples must be dehydrated prior to analysis.

The primary electron beam penetrates the sample to a depth of 2 to 3 µm. Emitted secondary or backscattered electrons originate from shallower depths. Frequently, specimens must be sputter-coated with Au or Pd to make them electron dense or reflective. Carbon paint is used to provide good contact to prevent charging (localized charge build-up). Precise detail can be observed up to magnifications of 5,000x. A review by Blake (1990) provides further details about this method.

If SEM is used to characterize the adherent microbial population, some treatments of the sample are required to stabilize the cell structure for analysis under vacuum with a high energy beam. This frequently involves cell fixation with buffered glutaraldehyde solutions (at *in vivo*, buffered pH values, 2% glutaraldehyde), followed by graded ethanol series dehydration, and then by critical point drying with liquid CO_2 under high pressure. Such treatments can induce dehydration artifacts and remove less firmly adhered microorganisms.

Samples for SEM examination of adherent biopatches were prepared by 2.5% glutaraldehyde fixation in 0.1M cacodylate buffer (CB, pH 8.0) and then graded ethanol series dehydration. Samples were critical point dried prior to storage and examination in an AMRAY 3300FE field emission SEM. The samples were sputter-coated with Au/Pd prior to analysis. The same samples were used for SEM examination of the surface precipitate morphology.

2.6 SEM- EDAX Spatial Maps

SEM's primary excitation beams cause characteristic x-rays to be emitted. As a result, SEM can be coupled with either energy dispersive analysis of x-rays (SEM-EDAX) to quantify elements with atomic numbers greater than 8 in a sample. Detection limits are on the order of 10^{-15} g (0.1 to 1 wt %). Samples can be characterized visually with spatial maps of elements in the x-y plane (or y-z plane if cross-sectional thin sections are analyzed) and then quantified using microprobe analysis. The probe is calibrated with primary standards, and elemental quantification of surface material can be accomplished by counting the number of x-rays in discrete channels over a continuum of energies. Spatial maps showing the origin of emission of the characteristic x-ray can be used to spatially locate elements at the µm to sub-µm scale. There are techniques that use standardless calibrations. Bulk quantitation must be used with caution given the depth of profiling that occurs; however, they do provide very useful analysis of element associations, particularly if it is coupled with petrography.

SEM-EDAX was performed using an AMRAY 3300Fe SEM outfitted with a PGT Imix-PC energy dispersive x-ray microanalysis system for quantitation and spatial mapping. Analysis was performed at multiple locations on the sample and at various magnifications (30x – 1000x). Elemental spatial mapping was used to identify elemental distribution in the selected view field. Elements examined included Al, Ca, Fe, K, Mg, Na, O, S, Si, and Ti. Higher elemental concentration in a given region was indicated by a more intense color display in the spatial map. The color display was user selected and not specific to each element. Color palette choices were not equivalent in intensity to concentration for a given map, so intensity may only be compared within an element map, not between maps. By comparing features on the spatial maps of each element, associations between various elements were identified.

2.7 Microfracture Surface Precipitate Fixation & Embedding for TEM

Calcite-dominated surface precipitate minerals from microfracture MF011 were readily removed from the microfracture surface with a sterile stainless steel spatula by simple scraping. The mineral material was prefixed in 2.5% glutaraldehyde in CB for 3 h (at which time the precipitate was carefully crushed into sub mm particles), rinsed with CB three times using careful decantation, followed by fixation with 1% osmium tetroxide in CB for 3 h. After fixation, the samples were rinsed in CB three times, dehydrated in a graded ethanol series (5, 10, 25, 50, 75, 100, 1000, 100%), and embedded by traditional resin techniques using either Spurr's or Epofix. After curing, the samples were thin sectioned with a diamond knife, post stained with 15 min in 0.5% uranyl acetate (in 50% methanol) and 2 min in 0.4% lead citrate. The presence of small quartz minerals in the precipitate made sectioning difficult. Epofix was found to be better than Spurr's resin. The quartz crystals damaged the diamond knife.

2.8 TEM - Microbial Ultrastructure

The JEOL 100S was used at accelerating voltages ranging from 40, 60, 80, and 100kV and at magnifications ranging from 1,000x to 100,000x.

2.9 Petrographic Thin Sections

Petrography can be used to examine phase morphology of rock minerals. Samples are embedded in epoxy resins, cut and polished to produce 30 µm thin sections. This method can be coupled with modal analysis to quantify the relative abundance of phases in a cross-section (Hutchinson, 1974). Modal analysis produces an accurate representation of the distribution and volume percent of the mineral within a petrographic thin section. Typically, a point count method is used where each mineral type occurrence along a series of traverse lines across a given thin section is documented. For a statistically valid result, > 2,000 individual points must be counted. The number of grains counted, the spacing between points, and successive traverse lines are dependant on the mean grain size of the sample and affect the percent abundance calculations.

When light is transmitted through mineral grains or mineral petrographic thin sections, a number of characteristic properties of the mineral can be ascertained depending on the behavior of the light. Light wavelengths can be shortened and slowed down. Light can be reflected, refracted, dispersed, and adsorbed. For isotropic minerals where mineral orientation is identical in all directions, polarized light will be adsorbed when the polarizing filters are cross polar. Mineral identification of isotropic materials can be made by examining grain structure and comparing this information to databases of isotropic minerals. Anisotropic minerals exhibit a characteristic uniaxial or biaxial nature using interference microscopy. Birefingence, the resolution or splitting of a light wave into two waves with mutually perpendicular vibration directions, can also be used to characterize the mineral. Such properties are characteristic of anisotropic minerals. Coupled with refractive index measurements of mineral grains, such information can be used to identify minerals (Nesse, 2003).

Petrographic thin sections to characterize host rocks (metasandstone and metashale of the Silurian-Ordovician Kittery Formation and cross-cutting Jurassic diabase dikes) were prepared by Mineral Optics Laboratory (Wilder, VT) and in-house. Sections were cut normal to layering; some were polished for subsequent analytical work, others were covered. Standard petrography was performed on all, using both plane and cross-polarized light and a range of objectives (4x, 10x, 20x, and 40x).

Primary mineral phases were identified for rock classification. Because of the fine-grained nature of these rocks, modes of primary mineral phases were determined by visual point counts along traverses across thin sections. Rock textures, contact relationships, and microfaults were noted within and between the three major rock types to evaluate metamorphic, deformation, and intrusive effects on these rock units. Careful examination was made of secondary and/or alteration minerals particularly at the boundary between host and vein and microfracture fillings.

2.10 SEM-EDAX Spatial Mapping Microfracture Surface Precipitates and Host Rock

Thin sections were also examined by EDAX, and spatial mapping was employed as described in Section 2.6. The elemental spatial mapping was focused on the intersection of the microfracture surface and the underlying host rock in order to highlight elemental differences between these two areas.

2.11 XRD Analysis of Microfracture Surfaces and Host Rock

XRD is a very important tool for characterizing the mineralogy of crystalline phases in host rock or microfracture surface precipitate samples. The detailed principles of this method are given in Bish and Post (1989) and Whan (1986).

XRD of powder samples relies on Bragg's Law and uses an x-ray from a non-monochromated or monochromated source that is rotated through a powdered sample. Diffracted x-rays, generated by crystal inter planar (d-spacing) reflections in the crystalline structure of the mineral assemblages, are collected by an x-ray detector as a function of the diffraction angle (theta) as the sample is rotated through the beam using a goniometer. The source can also rotate about a stationary sample. The diffraction pattern that is generated shows diffraction peaks of varying intensity as a function of the diffraction angle. The resulting diffractogram is compared to diffractograms of known mineral samples that contain precise locations of peaks and relative peak intensity. The International Centre for Diffraction Data (ICDD, See http://www.icdd.com/.) maintains databases of the many thousands of minerals and inorganic compounds that are used for comparison with either manual (visual comparison of diffraction patterns between candidate and experimental spectra) or computer-based search-match routines. Typically, XRD has a detection limit of about 1 to 2 % by weight. Care must be taken in selection of the target element to generate characteristic monochromatic x-rays (in this case, Kα x-rays) because of the potential for adsorption of x-rays of certain wavelengths. Cu is usually used, but Co can be used when samples contain a high percentage of Fe.

Powder preparation is very important. Hutchinson (1974) and Zussman (1976) discuss preparation methods. Particle sizes that are too large cause problems such as extinction and microabsorption. They can also interfere with the underlying assumptions of random orientation. For very coarse-grained or coarse-phased crystals in rock, particle size production will create a particle size equal to a phase size. For very fine-grained or fine-phased crystals in rock, particle size may exceed phase size. It is best if powders are ground close to 10 µm in diameter or that phase size is less than 10 µm. Larger particle sizes give qualitative information; smaller particle sizes can be used for quantification (Snyder and Bish, 1989). Snyder and Bish (1989) also discuss methods of sample mounting (smears, packed tubes, thin films), requisite sample thickness, characteristics needed for the sample surface, and procedures for optimizing intensities.

Because rock specimens contain numerous major mineral constituents, as well as numerous minor ones, the identification of mineral phases can be quite complex using typical manual search-match procedures. Computer-aided methods are available (Smith, 1989) and can be used to identify candidate minerals with some measure of likelihood or probability (termed figure of merit) based on peak location and peak intensity. However, verification of information from the computer search routines should be done using standard identification methods, such as petrography.

XRD can also be used for semi-quantitative analysis of crystalline phases in solids. This can increase sample analytical times from one to two hours to up to fifteen hours. Additional details are provided in Whan (1986).

Host rock and/or microfracture surface precipitates were analyzed by XRD. Mineral deposits were scraped from the host rock using a stainless steel spatula and ground by hand with mortar and pestle. Host rock samples were also ground by hand with a mortar and pestle. All samples were ground to a fine powder (< 100 µm) and loaded

on a glass slide. XRD was performed with a Rigaku Geigerflex rotating anode goniometer using a Cu-Kα source (45kV, 35 mA). Data were collected from 4 to 90 degrees 2-theta, with a step size of 0.05 degrees and a rate of 0.6 degrees/min. A tungsten standard was added to the sample to serve as a 2-theta reference. Mineral identification was performed using Jade 5.0, which utilizes the ICDD database. Element exclusion was used to limit the searchable database. A fairly rigorous routine was employed for searching (three lines of match, 0.1 degrees 2-theta error). During search-match, a figure of merit is assigned by Jade to each mineral identified in the sample. A smaller figure of merit indicated a high degree of certainty in mineral identification. Mineral matches with a figure of merit less than 20 were included in the candidate mineral list. Given the large number of minerals in the ICDD database, many unreasonable minerals were identified and discarded. Jade designates mineral phases as major, minor, or trace based on relative peak intensity in the sample diffractogram. This serves as an indirect measure of mineral abundance.

2.12 XPS Speciation of Microfracture Surfaces

XPS, formerly known as electron spectroscopy for chemical analysis (ESCA), is an extremely sensitive surface analysis technique. In XPS, high energy non-monochromated or monochromated x-rays are directed at a sample. The x-rays induce ionization of the surface atoms in the sample. As an atom ionizes, a photoelectron is emitted from the atom. The ejected photoelectron has an energy that is, in part, characteristic of its binding energy. Over a range of binding energies, emitted photoelectrons can be counted in discrete channels. Usually, at least one peak or doublet appears for each element (except hydrogen). Peak intensity is used for quantitative analysis. Peak shift, or chemical shift, is also an extremely valuable tool for documenting valency, nearest neighbor effects and speciation. A variety of techniques are used to quantify peak shift. Frequently, energy referencing to the adventitious carbon (binding energy of 284.80 eV) peak is used as this contaminant (from vacuum pump oil) is present on the surface of all samples, even under high vacuum. This peak can be discriminated from other types of carbon peaks in the sample. Detailed reviews are given in Hochella (1988) and Perry *et al*. (1990).

XPS can detect most elements. It has a spatial resolution of μm. Since photoelectrons are readily absorbed, only those emitted from the top ten of angstroms of a surface are detected. Thus the technique is considered to be a true surface spectroscopy. The sample must be dried and degassed in a roughing vacuum before analysis under high vacuum. Interesting applications are provided by Eggleston *et al*. (1996) and Eighmy *et al*. (1999).

XPS is usually conducted with an ion sputtering apparatus to allow for removal of adventitious carbon and oxygen. It can also allow for removal of the top atomic layers of a sample. The method is very slow, so quantitative and chemical shift analysis can take many hours. Charging can be a problem with insulated samples. The large beam size means that individual particles cannot be analyzed. Some spatial mapping can be done, but with low spatial resolution. The technique is very elegant for looking at speciation and abundance with depth if coupled with the sputtering techniques. Whan (1986) provides more detail on the method.

For the BBC work, surface species were detected using a Kratos Axis HS spectrometer. The instrument was equipped for surface analysis, surface chemical mapping, and depth profiling of metallic, semi-metallic, and nonmetallic samples. The sample is typically evacuated to 10^{-9} Torr or better, for quality measurements. The system was designed around a 127 mm mean radius hemispherical analyzer, which was equipped with a triple channeltron detection system for improved sensitivity. By using a magnetic immersion lens, high sensitivity was apparent on small analysis areas. The charge neutralization system allowed high resolution spectra to be obtained from insulating materials using either the standard Mg/Al or Al monochromatic source. The instrument was controlled by the VISION data system, on a SUN computer workstation and a Windows environment. Methods are described elsewhere (Eighmy *et al*., 1999; Meima *et al*., 2002).

The microfracture face of each sample was examined. A non-monochromated Mg Kα X-ray source was used. High-resolution scans were performed with a pass energy of 40 eV, a current of 10mA, and a step size of 0.1 eV. Duration of data collection for each element was based on the relative intensity of the peak to be characterized. The elements and lines characterized by XPS were Al2p, C1s, $Ca2p_{3/2}$, $Fe2p_{3/2}$, Mg2p, O1s, and Si2p. Peak fitting was performed using the software package CasaXPS provided by the manufacturer. For energy referencing, a binding energy correction was applied to all data based on the C 1s line for adventitious carbon at 284.80 eV (Hochella, 1988). The National Institute for Standards and Technology (NIST) XPS database, version 3.3 (See http://srdata.nist.gov/xps.), was used to identify likely candidate minerals based on the binding energy of the fitted peaks. For mineral identification, each element in the mineral had to have a binding energy characteristic of that mineral for the mineral to be a candidate. An error of ± 0.3 eV was allowed during the search routine. Given the large number of phases in the NIST database, many unreasonable phases were identified and discarded.

Additionally, binding energy values for Ca, Mg, O and C in calcite and dolomite were obtained from the literature (Baer *et al*., 1992; Gopinath *et al*., 2002; Stipp and Hochella, 1991). Binding energy values for Ca, Si, Al, and O in a synthetic zeolite similar to faujasite ($CaAl_2Si_4O_{16} \bullet 6H_2O$) were also obtained from the literature (Barr, 1983). Binding energy values for Fe and O in goethite (α-FeOOH), fresh amorphous hydrous ferric oxide (nominally $Fe(OH)_3$ but thermogravimetrically $Fe_2O_3 \bullet 3.26\ H_2O$), aged hydrous ferric oxide ($Fe_2O_3 \bullet 1.57\ H_2O$, likely some crystalline goethite present) and limonite ($Fe_2O_3 \bullet nH_2O$) were obtained from the literature (Harvey and Linton, 1981). Binding energy values for C in various chemical states in (NOM) Leonardite humic acid and soil humic acid from the International Humic Substances Society (IHSS), or from purified Aldrich humic acid were obtained from the literature (Boughriet *et al*., 1992; Monteil-Rivera *et al*., 2000) and used to assign principal peaks to C functional groups. Assigned C1s binding energy values are: aromatic C-C/C-H (284.41 to 284.66 eV), aliphatic C-C/C-H (285.00 eV), alpha C-C(O) (285.42 to 285.63 eV), ether/alcohol C-O (286.38 to 286.58 eV), ketone C=O (287.50 to 287.68 eV), amide C(O)N (288.43 to 288.47 eV), carboxylic C(O)O (289.02 to 289.26 eV), and π-π (290.88 to 291.35 eV).

2.13 SIMS Fingerprints of Microfracture Surfaces

SIMS is an excellent near-surface analytical technique. Molecular fragments from the surface can be quantified to extremely low levels (< 1 ppb). High degrees of spatial resolution are obtainable (Hochella, 1988). The method works by bombarding a specimen with an ion beam (Cs^+, O_2^+, or O^-) which sputters atomic and molecular ions from the sample into the vacuum of the instrument. The sputtered ions are then extracted into a mass spectrometer where they are quantified with magnetic and electrostatic sector analyzers. More recently, time-of-flight (TOF) SIMS has been employed that allows for greater detection of mass fragments (See for example, Briggs *et al*., 2002.). The system operates under high vacuum, and charging can be problematic in insulated samples. Topography plays a large role in both the mass fragment yield and sputter crater that are produced during ion bombardment, so very flat, planar samples are preferred for analysis. Detailed methods are provided by Metson (1990). Some applications are described by Bancroft *et al*. (1987)

A Varian VG quadrapole filter type static SIMS was used for mass fragment detection under high vacuum. This instrument is located at the University of Massachusetts at Lowell. A sample from microfracture MF03 was used for analysis. A Ga^+ ion beam was used for bombardment. Rock specimens were mounted on In foil to help minimize charging. Generally, the ion source was operated at 10keV and 10 nA. Target biases were 13 V.

2.14 MIP of Host Rock

MIP is a method used to study and characterize a material's interconnected pores (pore network) particularly as they relate to or comprise the microfracture network in the rock. The principle of MIP is that a sample of known volume is subjected to a pressure within a mercury penetrometer. As pressure increases, larger pores and microfractures are first filled with Hg. At higher pressures, smaller pores or microfractures are then filled. The change in Hg volume within the penetrometer is directly related to sample porosity. The pressure at which the pores or microfractures are filled is related to the pore diameter using the Washburn equation:

$$d = -4\gamma \cos\theta / p \qquad \text{[Eq. 2.1]}$$

where d is pore diameter (nm), γ is surface tension of the Hg (N/m), θ is the contact angle between the Hg and the rock sample (degrees), and p is the pressure applied to the penetrometer (MPa). Pore size distributions may be obtained by differentiating the change in pressure versus pressure applied plot.

Slices (1.5 - 2 cm in height) of borehole BBC5 core material were precisely cut into 1.4 x 1.4 x 2.0 cm cubes using a Buehler Isomet Precision Saw. A diamond blade was used to cut the sample. Minimal water was used for cooling the blade. These block dimensions were the maximum possible for use in the penetrometer, but small relative to the spatial distribution of microfractures. Attempts to cut blocks with intact microfractures almost always resulted in the separation of the microfracture. Sample blocks were freeze-dried for 3 days to remove water from the internal portions of the cube.

MIP was performed with a Micromeritics Autopore III. The penetrometer selected for analysis was a 15-cc bulb with a stem volume of 0.387 cc. This allowed for maximum sample size and sensitivity of mercury intrusion into the bedrock sample block. The instrument was calibrated and checked with both non-porous (steel cube) and porous (aluminosilicate powders) standards of known porosity or pore size. According to Micromeritics, at least 25% of the Hg loaded into the penetrometer stem volume must intrude to generate reliable data. Data were collected over a pressure range of 0 psia to 30,000 psia. Corrections were made for blank pen runs, compression of Hg (modified Tait Equation), and the sample compressibility at high pressures. Preliminary work indicated the BBC host rock to

be monolithic with low porosities (< 1%), making MIP difficult to use. Of the 10 samples that were analyzed, only one sample gave reasonable readings relative to the 25% intrusion requirement. Much of the host rock was found to be very impermeable to intrusion.

The method of Swanson (1981) was used to estimate host rock permeability (in Darcys) based on mercury intrusion capillary pressures (psia) and cumulative porosity (%). The method is based on the principles embodied in Thormeer capillary pressure plots. A nomograph is used to estimate permeability based on correlations between permeability and porosity for many sandstones and carbonate rocks. The method was used previously by Colwell *et al*. (1997), Fredrickson *et al*. (1997), and Onstott *et al*. (2003).

2.15 Packer Water Collection and Analytical Methods

Straddle packer interval sampling techniques were used to isolate regions in the borehole for segregation, purging, and then sampling of waters (termed packer waters). Four sampling events were conducted. Microfracture MF04 (Cluster 2) was sampled on July 20, 2002. Microfracture MF05-MF06-MF07 (Cluster 3) was sampled on April 15, 2002, and May 29, 2002, and microfractures MF10-MF11 (Cluster 4) was sampled on June 3, 2003. Cluster 1 in borehole BBC5 (microfractures MF01-MF02-MF03) was not sampled as the location was too close to the bottom of the telescoping casing.

In the field, temperature (calibrated probe, Standard Methods 2510.B), pH (calibrated probe), Eh (polished platinum inert redox electrode combined with an Ag/AgCl reference electrode checked with two reference solutions made of $K_4Fe(II)(CN)_6 \bullet 3H_2O$ and $K_3Fe(III)(CN)_6$), alkalinity (titration), soluble Fe^{2+} (Chemetrics Field Kit), and sample filtration (0.22 µm) were conducted (Eighmy *et al*., 2002a and 2002b). Samples were then preserved as needed and sent to Resource Laboratories Inc. (Hampton, NH) for analysis of soluble ions by ion chromatography, metals by flame or graphite furnace atomic absorption spectrometry, and organics by various gas chromatography/mass spectrometry (GC/MS) methods. Methane, ethane, and hydrogen were also determined. Fe^{3+} was determined by the difference between total dissolved Fe and soluble Fe^{2+}.

The following analytical methods were used: temperature (Standard Methods 2510.B), dissolved oxygen (Chemetrics Field Kit), pH (Standard Methods 4500 H^+B), alkalinity (Standard Methods 2320.B), specific conductivity (Standard Methods 2510.B), ammonium (EPA 350.1), nitrate (EPA 300.0), nitrite (EPA 300.0), bromide (EPA 300.0), chloride (EPA 300.0), sulfate (EPA 300.0), sulfide (Standard Methods 4500 SF), ferric iron (Standard Methods 3500.b), ferrous iron (Standard Methods 3500.b), ferrous iron (Chemetrics Field Kit), metals (e.g., K, Cu, Cd, Pb, Zn, EPA 6010), hydrogen (Chapelle *et al*., 1995), DOC (EPA 415.1), ethane (EPA 8015), ethene (8015), methane (EPA 8015), and volatile organics (EPA 8260 or 524). Dr. Frank Chapelle and Dr. Paul Bradley of the USGS (Columbia, SC) conducted the H_2 analyses.

2.16 Geochemical Modeling

The modeling of apparent inorganic chemical pseudo-equilibrium conditions between packer waters and the microfracture surfaces was done by using the Windows-based version of MINTEQA2, Visual MINTEQ (Meima *et al*., 2002; Apul *et al*., 2002). Model inputs included all aqueous components measured as described in Section 2.15, pH, temperature, total alkalinity (mg/L as $CaCO_3$), the redox couple $Fe^{2+}/Fe^{3+,}$ and the measured concentrations of Fe^{2+} and Fe^{3+}. No solids were allowed to precipitate. Output from the model included ion balances, aqueous phase speciation, mass distributions, log ion activity products, saturation indices for all possible controlling solids, and Eh.

The use of thermodynamic models to interpret solid phase control of dominant dissolved constituents, buffer systems, redox reactions, and related geochemical processes must be done with some caution. Such analyses may indicate pseudo-equilibrium for certain reaction types (particularly acid-base reactions), but that additional inference is complicated by the likely presence of kinetically-controlled reactions occurring simultaneously with equilibrium-controlled reactions. Further, there is no certainty that the system being modeled, a microfracture network comprised of more open microfractures connected by spatially and temporally at pseudo-equilibrium, particularly when microbial processes and diffusion limitations are likely to influence the system. At best, such analyses may shed some light on some dominant geochemical processes.

2.17 Microbe Extraction

Cores were removed from the boreholes located within the TCE contaminated plume at Site 32. Drilling protocols were developed to obtain core samples that contained intact representative microbial populations (See Volume 1: Fractured Rock Drilling.). Microfractures were identified, depths measured, and faces exposed with a sterilized geological hammer. Seven microfractures were identified for analysis from borehole BBC5 (Table 2.1).

To remove the microorganisms associated with the identified microfracture surfaces, samples were exposed to 15 minutes of treatment at a medium power setting in a small sonication bath that contained sterile phosphate-buffered saline (0.61g/L KH_2PO_4, 0.96g/L K_2HPO_4, 8.5g/L NaCl; pH 7). Before sonication treatment, the core side walls were first wiped down with ethanol (70%v/v) to reduce potential microbial contamination, particularly induced from drilling. It will not destroy adsorbed nucleic acid material. Microorganisms liberated from the fracture surfaces were concentrated by filtration through a 0.22 µm pore size GV membrane filter (Durapore, Millipore Corporation, MA). The filters were stored at -80°C until analysis. Genomic DNA was extracted from the filtered samples with UltraClean™ Water (Mo Bio Laboratories, Inc., CA), according to the manufacturer's recommendations. The extracted genomic DNA samples were concentrated and further purified using QIAEX II Kit (Qiagen, CA).

2.18 Microbial Characterization Using Molecular Biological Techniques

The use of molecular biology techniques allows for the detection of small quantities of microbial nucleic acid in environmental samples that are characteristic of the microbe, or population of microbes, from that sample. Ribosomal RNA is an informational molecule from a microbe that is frequently targeted for detection. Ribosomal RNA is single stranded, but highly structured. It can be separated into different size groups (e.g., 16s). Analyses of many 16s ribosomal RNA nucleotide sequences resulted in the understanding that microorganisms are highly related through depiction in phylogenetic trees of life.

The target for specific detection in this work was the segment of microbial DNA that contains the gene that codes for the 16s RNA segment of the bacterial ribosome. This piece of DNA, unique to each microbial genera, contains many 16srDNA genes. Small quantities of this extracted gene obtained from the sample genomic DNA extraction process were amplified using the polymerase chain reaction assay as a means to exponentially increase the quantity of 16rDNA genes from the extract. Sufficient quantities are needed for detection with electrophoresis separatory methods and gene sequencing. Polymerase chain reaction amplifies a specific DNA sequence, in this case the V3 region of the 16S rRNA gene, by the use of repeated temperature-mediated stages using specific primers targeted for the gene and a DNA polymerase to catalyze the reaction. The V3 region of the 16S rRNA gene is commonly used for molecular identification as it is a highly variable DNA sequence between microorganisms and thus characteristic of the microbes in the sample. Primers are short single-stranded segments of DNA, complementary to the 5' ends of the strands of the target DNA to be amplified. Therefore, a pair of primers are chosen to flank the target DNA to be amplified, known as forward and reverse primers, indicating which strand of the denatured double stranded DNA to which they anneal or bind. The three stages of a PCR cycle are DNA denaturation, primer annealing, and primer extension. During DNA denaturation, extracted double stranded genomic DNA is separated. The primers are then able to anneal to the target DNA using specific temperatures. The extension of the primers will then occur using the DNA polymerase enzyme, replicating the target gene. Multiple cycles are used to exponentially amplify the target gene. The presence or absence of specific prokaryotic groups was analyzed by polymerase chain reaction using primer sets for partial 16S rDNA sequences of specific groups, including bacteria, *Archaea* (a phylogenetic domain of prokaryotes, genetically distinct from bacteria, and consist of methanogens, and most extreme halophiles and hyper-thermophiles), *Dehalococcoides* sp., *Desulfuromonas* sp., *Geobacteraceae* and sulfate-reducing bacteria.

The diversity of prokaryotic bacterial communities and their phylogenetic affiliation (a system of classification of organisms that aims to show their evolutionary history/relatedness) was determined by the analysis of the denaturing gradient gel electrophoresis fingerprinting profiles and the sequencing of the 16S rDNA for the bacterial population. Denaturing gradient gel electrophoresis is an increasingly popular and powerful method of profiling complex microbial communities and inferring the phylogenetic relationships of the community members (Muyzer *et al.,* 1996). Nucleic acids were purified from extracts. Polymerase chain reaction was used to amplify a region of the 16S rDNA from the mixed microbial populations present in each extract using primers specific for that gene. One of the primers included a guanine-cytosine (GC)-rich sequence (termed a GC clamp) that imparted melting stability to the polymerase chain reaction products which means the amplified double stranded DNA can't completely denature (separate) and run completely through the DGGE gel. The products were essentially all the same size and were separated into discrete melting domains during electrophoresis through an acrylamide gel that contained an increasing linear gradient of denaturants. Individual, double stranded DNA molecules denatured along their length adjacent to the GC-clamp according to their melting characteristics (or sequences). This property resulted in a distinct banding pattern in the gel used for each sample. Each band represented essentially a different rDNA sequence, and hence, a different member within the microbial community. Each lane in the gel provides a phylogenetic profile of the microbial community in that sample. The number of samples processed can be greatly increased because denaturing gradient gel electrophoresis is much less labor intensive than traditional microbial community analysis. This increased experimental reproducibility and statistical relevance to the results. Denaturing gradient gel electrophoresis has a high degree of sensitivity because it can detect single-base pair differences between DNA molecules.

2.19 Primers and Polymerase Chain Reaction Assay

The V3 region of the 16S rDNA of bacteria was amplified by polymerase chain reaction with primers 907R (Lane *et al.*, 1985) and 338F (Amann *et al.*, 1990) using 10ng of genomic DNA template. A GC-Clamp (Muyzer and Smalla, 1998) was attached to the 5' end of the forward primer, 338F, for denaturing gradient gel electrophoresis analysis. Nested polymerase chain reaction was performed to amplify the V3 region of the archaeal 16S rDNA, V3 region. Nested polymerase chain reaction means that two pairs of polymerase chain reaction primers were used for a single gene. The first pair amplifies the gene as seen in any polymerase chain reaction experiment. The second pair of primers (nested primers) bind within the first polymerase chain reaction product and produce a second polymerase chain reaction product that will be shorter than the first one. The reasoning for this is to increase the amplification success of lower abundance of microorganisms and that if the wrong locus were amplified by mistake, the probability is very low that it would also be amplified a second time by a second pair of primers.

The primers 21F and 1492R (Giovannoni *et al.*, 1988 and Lane, 1991) were used to amplify the entire 16S rDNA with 25ng of genomic DNA template, and the primers 340F and 915R (Øvreas *et al.*, 1997; Amann *et al.*, 1995) were used to amplify the V3 region using 1 µL of purified 16S polymerase chain reaction product. The following primer sets, presumptive for the presence of these microbial groups, were used to amplify partial sequences of the 16S rDNA for prokaryotic groups: sulfate-reducing bacteria with the 385F and 907R primers (Lane *et al.*, 1985; Amann *et al.*, 1990), dehalorespirers including *D. ethenogenes* and *Dehalococcoides* sp. (strain FL2) with 728F and 1172R primers, *Desulfuromonas* group, including *Desulfuromonas* sp. (strain BB1) and *D. chloroethenica* with 205F and 1033R primers (Löffler *et al.*, 2000), and Fe (III) reducing *Geobacteraceae* with 338F and Geo825R primers (Snoeyenbos-West *et al.*, 2000).

The polymerase chain reaction was performed using a PTC-200 Peltier Thermal Cycler (MJ Research, Cambridge, MA) in triplicate 25 µL reaction volumes, using 0.5 µM of each primer and Qiagen HotstarTaq Master Mix (1.25 Units HotstarTaq DNA polymerase/reaction) (Qiagen, CA). The following thermal cycling parameters were used for bacterial 16S rDNA, V3 region and archaeal 16S rDNA amplification. An initial activation step of 15 min at 95°C was performed to activate HotstarTaq DNA Polymerase, followed by an initial DNA denaturation step at 94°C for 2.5 min. Eleven cycles followed of denaturation at 94°C for 30 s, primer annealing at 56°C for 45 s, and primer extension at 72°C for 1 min. This step was followed by 11 cycles of denaturation at 94°C for 30 s, primer annealing at 56°C for 1 min and primer extension at 72°C for 1 min 30 s. This stage was followed by 14 cycles of 30 s denaturation at 94°C, primer annealing at 56°C for 1 min 15 s, primer extension at 72°C for 2 min 15 s and a final extension step of 7 min 30 s. For all other amplifications, an annealing temperature of 58°C was used. Polymerase chain reaction products were pooled and purified using QIAquick Polymerase Chain Reaction Purification Kit (Qiagen, CA). Products were run on an agarose gel (1%), and visualized using a GelDoc 2000 system (Bio-Rad).

2.20 Denaturing Gradient Gel Electrophoresis

Denaturing gradient gel electrophoresis was performed on the amplified bacterial 16S rDNA with a GC-clamp with the Bio-Rad Dcode™ Universal Detection System. Samples were loaded on an 8% (w/v) polyacrylamide gel with a denaturing gradient ranging from 40% to 60% denaturant gradient, starting at 40% and running to 60%, created with formamide and urea within an acrylamide gel. Gels were run in Tris-acetate-EDTA buffer (20 mM Tris, 10 mM acetate, 0.5 mM EDTA, pH 7.4) for 16 h at 70 V and were stained for 20 min in Tris-acetate-EDTA buffer containing ethidium bromide (50 µg/ml). Gel was destained for 30 min in Tris-acetate-EDTA buffer and photographed on an UV transilluminator (FVSTI-88). The resulting banding patterns were analyzed by the use of Quantity One program (Bio-Rad Laboratories, CA). A dendrogram spatially depicting similarities between phylogenetic trees was created from the cluster analysis by using an unweighted paired group method with arithmetic averages. A similarity coefficient of >0.70 indicates that the samples are similar while those values < 0.70 indicate the samples are very different (Röling *et al.*, 2001). A lower value indicates a greater difference between the samples.

2.21 DNA Sequencing & Analysis

DNA was eluted from excised denaturing gradient gel electrophoresis bands and re-amplified using the primers cited in Section 2.19. Denaturing gradient gel electrophoresis was re-performed on individual bands, to check band purity. These bands were removed and DNA eluted and re-amplified using the above primer set without a GC-Clamp. These polymerase chain reaction products were used as a template for sequencing reactions with a DYEnamic ET Terminator Cycle Kit (Amersham Pharmacia, NJ) and an ABI 377A automated sequencer (Applied Biosystems, CA). The 338F primer was used for these sequencing reactions. The sequences were compared with the 16S rDNA available from GeneBank and EMBL database by the use of the BLAST program (http://www.ncbi.nlm.nih.gov/BLAST; Altschul *et al.*, 1997).

2.22 Data Quality

A quality assurance project plan was prepared for the entire BBC research project (Kinner et al., 2001). The plan details data quality assurance objectives, training, documentations and records, sampling, chain of custody, analytical methods requirements, quality control, instrumentation, calibration and frequency, inspection, data management, assessment and oversight, and data validation and usability.

This portion of the BBC project was considered exploratory in nature. The study of microbial populations and mineralogy on the surface of competent bedrock microfractures is a new field with many of the methods requiring development of protocols that could enable samples to be collected and characterized. Consequently, data quality objectives are more qualitative in nature with a focus on the description of the nature of the microfracture surfaces.

Table 2.2 provides an overview of the methods that were applied to each of the microfracture samples (host rock or microfracture surface precipitate). Where applicable, qualitative assessments of data quality are offered. When appropriate, specific discussions of data quality measures such as precision, accuracy, completeness, representativeness (a measure of the degree to which data accurately and precisely represent characteristics of the population) and comparability (the confidence with which one data set or method can be compared to another) are offered for each method used in this report.

Cores were obtained in 1.5 meters maximum lengths. Special handling procedures were used to retrieve the cores in order to minimize microbial contamination and alteration. These procedures included handling the cores in a specially constructed, on-site anaerobic glove chamber. The chamber was housed in a “laboratory” trailer, located at Site 32 for the duration of this study.

The drill rig and all support equipment were brought on site and were decontaminated by steam cleaning within a decontamination pad. The steam cleaning was followed by a 30 minute soak in a dilute chlorine bleach solution for drill rod, drill bits, roller bits, wrenches, and other support equipment for drilling. The support equipment was allowed to sit for 30 minutes to give the bleach solution adequate contact time to kill the bacteria. After 30 minutes, the equipment was rinsed with clean water from a well in the deep bedrock formation that was confirmed uncontaminated. Decontamination wastes were captured by a plastic liner, collected, and containerized for ultimate disposal at the Pease Site 8 groundwater treatment facility.

All pumps and hose lines used during drilling procedures were decontaminated using a dilute chlorine bleach solution. The pump and hose lines were either completely filled and left to soak for 30 minutes (contact time required to kill bacteria spores), or the water was pumped through the system and continuously recirculated for at least 30 minutes. This was followed by a flushing rinse with the clean rinse water. Decontamination wastes were containerized and stored for ultimate disposal at the Pease Site 8 water treatment facility.

Microfracture sampling protocols were developed to collect microfractures as a function of depth with the correct altitude so that, upon removal, aseptic samples could be produced that (i) were representative of the microfracture surface, (ii) could be sub-sampled for all spectroscopic analyses, and then (iii) were sufficiently thin and of correct area to allow for insertion in various analytical instrumentation. As such, sampling was somewhat a trial and error process. Nevertheless, 11 microfractures were collected for analysis from the two boreholes.

SEM, as a descriptive tool to visually examine the microbial and mineral morphology of microfracture surfaces, was really only dependent upon sample geometry. All 11 microfracture subsamples were examined using SEM at various magnifications and examining hundreds of images. Magnifications were used to provide low magnification depictions of larger areas (mm by mm) to much higher magnifications of cells. Detection limits were not applicable. No standards were run. No replicates were run. Precision and accuracy are not applicable. The images were typical of the 11 sampled microfractures and thus comparable amongst the collected samples. It is not known how representative they may be of the microfracture surfaces generally at the site within the Kittery Formation, though based on well logs, the types of microfractures and their densities were relatively uniform through the drilled regions.

SEM-EDAX can detect elements with atomic numbers greater than 8 with detection limits typically of 0.1 to 1.0 % with spatial resolutions on the order of 10-100 nm (Geesey *et al*., 2002). The EDAX detector was calibrated routinely with primary standard thin sections of known composition. The optics of the electron gun were optimized before analysis. The EDAX detector was operated so as to provide optimum counts within energy channels. All 11 microfracture subsamples were examined using SEM-EDAX at various magnifications and mapping hundreds of images. No replicates were run. Precision and accuracy are not applicable. The spectra and spatial maps were typical of the 11 sampled microfractures and thus comparable amongst the collected samples. It is not known how representative they may be of the microfracture

surfaces generally at the site within the Kittery Formation, though based on well logs, the types of microfractures and their densities were relatively uniform through the drilled regions. TEM, as a descriptive tool to visually examine the microbial morphology of cells within the microfracture surface precipitates, was very exploratory and was conducted on only one microfracture surface precipitate sample sufficiently soft, (containing low levels of quartz and high levels of carbonates) amenable to fixation, embedding, and thin sectioning with a diamond knife. Approximately 100 thin sections were generated from the various embedded samples. These were all carefully examined for cell structures and features. No standards were run. No replicates were run. Precision and accuracy are not applicable. Hundreds of micrographs were taken at various magnifications. It is difficult to ascertain how comparable and representative these data are.

Petrographic thin sections can detect minerals that are 1.0 to 2.0 mm in size within a petrographic thin section. This represents the lower limit for optical microscopic characterization and modal analysis. All 11 host rock samples were analyzed. However, only three of the 11 attendant adherent microfracture surface precipitates were sufficiently thick to characterize minerals within the surface precipitates. During point counts along transects, hundreds of digital photographs were taken under various optical systems to allow for mineral identification. No standards were run. No replicates were run. Precision and accuracy are not applicable. It is difficult to ascertain how comparable and representative these data are.

XRD can detect crystalline minerals when they constitute about 1 to 2% of the bulk sample. As described earlier, complex statistics are used to match diffraction patterns to known patterns from mineral libraries. All 11 host rock specimens were analyzed. However, only nine of the 11 samples had surface precipitates that were sufficiently thick to produce the necessary quantities for XRD. No standards were run. No replicates were run. Precision and accuracy are not applicable. The diffractograms and mineral identifications were typical of the 11 sampled microfractures and thus comparable amongst the collected samples. It is not known how representative they may be of the microfracture surfaces generally at the site within the Kittery Formation, though based on well logs, the types of microfractures and their densities were relatively uniform through the drilled regions. Also, similar petrographic data were obtained in an earlier study.

XPS can detect elements with atomic numbers >3 with detection limits typically of 1.0% with spatial resolutions on the order of 10s of µm (Geesey *et al.*, 2002). The XPS is calibrated using Au and Pd standards to examine accuracy over the linear energy scale. The detectors are controlled to obtain statistically significant counts above background. During analysis, internal charge referencing is done with adventitious carbon at 284.80 eV. Mineral identification is done using NIST protocols and databases. Nine of the 11 microfracture samples were examined with XPS. No replicates were run. Precision and accuracy are not applicable. The spectra were typical of the nine analyzed microfractures and thus comparable amongst the collected samples. It is not known how representative they may be of the microfracture surfaces generally at the site within the Kittery Formation, though based on well logs, the types of microfractures and their densities were relatively uniform through the drilled regions.

SIMS can detect mass fragments with atomic mass units >1 with detection limits typically of 0.001 to 1.0% (depending on surface roughness, geometry, charging) with spatial resolutions on the order of 10s of µm (Geesey *et al.*, 2002). Only one sample was subjected to SIMS analysis. No standards were run. No replicates were run. Precision and accuracy are not applicable. It is difficult to ascertain how comparable and representative these data are.

MIP can detect pore widths of 0.01 µm provided that the rock sample has porosities >1%. Many host rock samples were run, but had very low porosities (<1%), making MIP analyses difficult. The MIP was calibrated using standard protocols for pen operation. Standard reference samples of known porosity were run and were always within 95% of the certified value. Eventually, only one sample of the 40 that were attempted had proper porosity and pore size data. No replicates were run. Precision and accuracy are not applicable. It is difficult to ascertain how comparable and representative these data are.

Groundwater sampling/monitoring occurred at several stages throughout the BBC research. Prior to drilling activities, initial sampling of isolated fractures using well packers in select deep bedrock wells (32-631, 32-632, 32-633, 32-6012, 32-6027, and 32-6031) was conducted. The objective of the initial sampling was to obtain more detailed information about the contamination flowing into each well from particular fracture zones. Groundwater samples were also collected from the discrete fractures within each of the preliminary and test boreholes once drilling was complete. Initially, the identified fracture locations were based on the analyses of the borehole geophysical testing and video logs of existing deep bedrock wells. This information was used to plan sampling depths and intervals for each well. Packers were used to isolate the fractures during pre-drilling groundwater sampling. Groundwater samples from specific fracture zones in the preliminary and test boreholes were also collected using a straddle-packer. Groundwater samples collected, as part of this research, from preliminary and/or test boreholes were considered critical samples (required to meet the BBC research objectives).

The straddle-packer method consisted of a pneumatic sampling pump (does not generate hydrogen) that was set between two inflatable packers. The straddle-packer was lowered so that the pump intake was at the elevation of the fracture to be sampled. The packers were inflated above and below the sampling interval (using compressed N_2 gas) to hydraulically isolate the fracture from the rest of the well. A series of samples were collected during any given sampling event. When sampling was completed, the packers were deflated and raised or lowered to the next fracture. This sampling process continued until all the selected fractures were sampled.

The sampling of each fracture was meant to obtain representative water samples (and attendant water quality) from the individual fracture. pH, conductivity (Ω), and temperature (T) were monitored and the values recorded once pumping of a given fracture was initiated. This procedure was continued until the monitoring indicated that the real time parameters (pH, Ω, and T) had stabilized. After collecting the groundwater samples in the appropriate sample containers, the sample containers were placed on ice in a cooler and transported to the laboratory.

Purge water removed from the wells was collected, stored in carboys at the Site 32 treatment plant, and finally disposed of at the Pease Site 8 groundwater treatment plant when a sufficient volume had been collected.

The packer and pump assembly consisted of as much Teflon and stainless steel materials, along the water sample pathway to the surface, as practical, in order to minimize adsorption of groundwater constituents to sampling equipment during pumping and to eliminate the need for decontaminating the packer apparatus between sampling intervals within the same borehole. All sampling equipment was decontaminated between wells to prevent cross-contamination. This included successive rinses with laboratory soap, and either bottled spring water or water from a nearby bedrock well that had been confirmed clean. All decontamination fluids were containerized, stored as above, and disposed of at the Pease Site 8 groundwater treatment plant. Each well was capped and secured following completion of the sampling.

The analyses conducted on the packer water samples included volume, collection time, temperature, pH, conductivity, DO, Eh, TCE, trans-1,2-DCE, cis-1,2-DCE, 1,2 DCE, VC, acetone, methane, ethane, ethene, NPDOC, NH_4^+, alkalinity (as $CaCO_3$), Cl^-, SO_4^{2-}, NO_3^-, S^{2-}, Fe^{2+}, Al, As, Ba, B, Ca, Cr, Cu, Fe, Pb, Mg, Mn, L, Si, Na, and Zn. Kinner *et al*. (2001) discusses the methods. Table 3.16 (page 60) shows detection limits. The groundwater characterization program was subject to extensive QA/QC as described by Kinner *et al*. (2001). The methods of collection and subsequent analyses were typical of the entire sampling campaign associated with the project and thus comparable amongst all the collected samples. The analyses for these samples were also typical of the entire sampling campaign and thus representative.

Hydrogen analyses were performed as a small side study. Hydrogen analyses were performed on water samples following the methods developed by Dr. Francis H. Chapelle (USGS; Columbia, SC). Dr. Chapelle and Paul M. Bradley (USGS; Columbia, SC) traveled to New Hampshire to sample and analyze groundwater for hydrogen, as an indicator of microbial activity. Sampling was performed using a piston-type pump (e.g., pneumatic positive displacement pump) powered by compressed air to avoid problems with generation of hydrogen typical of electrically driven pumps. The sampling and analytical methods for hydrogen are outlined in Chapelle *et al*. (1995). It is difficult to ascertain how comparable and representative these data are.

Polymerase chain reaction (PCR) was used to amplify a region of the 16S rRNA gene from the DNA extracted from mixed microbial populations using primers specific for that gene. Detection limits are around 0.1 µg of DNA. This was performed to determine the diversity of prokaryotic microbial communities found associated with the fracture surfaces of BBC5 microfractures with various mineral deposits. Seven of the 11 microfracture samples were run (as intended). All of the samples were from BBC5. PCR reactions were performed in triplicate with ≤1 µg template DNA, with a positive DNA control (certified DNA strands from *E. coli* or *B. subtillus*), to show assay specificity and a negative water control to test for user contamination. In cases where the positive or negative controls indicated problems, samples were rerun. The triplicates were then pooled for denaturing gradient gel electrophoresis analysis. No replicates were run. Precision and accuracy are not applicable. It is difficult to ascertain how representative and comparable the analyses were.

Denaturing gradient gel electrophoresis (DGGE) is a molecular fingerprinting method which enables visualization of PCR amplified genes as a distinct banding pattern. DGGE has a high degree of sensitivity because it can detect single base pair differences in the amplified gene, creating a different band and hence a different microorganism within the community (Muyzer & Smalla, 1998). Band definition depends on the amount of DNA in the sample. Volumes of extract to be denatured on the gel are modified to produce clear, bright bands that are neither too dim nor too bright. The bands are quantified by computer analysis of scanned images that uses statistical protocols for identifying band pixel brightness and band area extent definition compared to background. During runs, controls are run in the two perimeter lanes. If the behavior of the controls (band patterns and migration) were incorrect, gels were re-run. The large number of bands indicates a higher level of microbial diversity both on and between the microfracture surfaces. Banding patterns for each sample were analyzed and compared to give similarity coefficients (Röling *et al*., 2001). Only two fractures were shown

to be similar, indicating bacterial communities were independent of each other. No replicates were run. Precision and accuracy are not applicable. Given the focus on comparing patterns between microfractures, the data are considered to be highly representative. It is difficult to ascertain how comparable the analyses were.

DNA sequencing was performed on DNA eluted from excised DGGE bands and re-amplified to identify specific bacteria. Sequencing was done only on DGGE bands from MF4. Sequences were compared with the 16S rRNA genes available from the GeneBank library and EMBL database by the use of the BLAST program (http://www.ncbi.nlm.nih.gov/BLAST Altschul *et al*., 1997). The method requires 0.1 to 10 picomoles of DNA. Standards are run with pure phage DNA (M13) to ensure proper protocols and sequencer performance. Chromatograms of the sequenced product were examined for purity. In the case that the chromatograms were diffused, the original samples were re-purified and run again. No replicates were run. Precision and accuracy are not applicable. Given the focus on matching sequences to library data, the data are considered to be highly representative. These sequences are considered highly comparable as the microbes in the library have been recovered from similar ecosystems.

3.0 Results & Discussion

3.1 Microfracture Locations

The microfractures collected from borehole BBC5 were distributed in three clusters (Figure 2.3): Cluster 1 [those at around 21.79 to 22.25 m (71.5 to 73.0 ft) below top of telescoping casing (microfractures MF01, MF02, MF03)], Cluster 2 [those at 29.56 m (97 ft) below top of telescoping casing (microfracture MF04)], and Cluster 3 [those at around 37.03 to 37.39 m (121.5 to 122.7 ft) below top of telescoping casing (microfractures MF05, MF06, MF07)]. The microfractures collected from borehole BBC6 were distributed in a fourth cluster [those at around 32.73 to 35.57 m (107.4 to 116.72 ft) below top of telescoping casing (microfractures MF08, MF09, MF10, and MF11)]. Further, microfractures MF02 and MF03 in Cluster 1 from borehole BBC5 were adjacent to each other, but were not connected, at least within the volume of the core.

Two of the four cluster regions were subjected to hydraulic testing to ascertain transmissivity. The region around Cluster 3 (borehole BBC5) had a borehole transmissivity of 0.139 m^2/d (1.5 ft^2/d). The region around Cluster 4 (borehole BBC6) had a borehole transmissivity of 0.185 m^2/d (2 ft^2/d).

Three of the four clusters were from one well (borehole BBC5) and were separated by at most 15.24 m (50 ft) of bedrock vertical depth. The fourth cluster (borehole BBC6) is at a similar depth, but over 7.6 m (25 ft) of lateral distance away. The hydraulic connection between boreholes BBC5 and BBC6, based on hydraulic tests, is in a major fracture that runs from a depth of about 33.52 to 35.35 m (110 to 116 ft) below top of telescoping casing in BB5 to a depth of about 39.62 to 40.84 m (130 to 134 ft) below top of telescoping casing in borehole BBC6. Transmissivities in these regions were relatively high, 0.836 to 1.393 m^2/d (9 to 15 ft^2/d). This major fracture(s) was just 1.67 m (5.5 ft) above microfracture MF7 and 4.04 m (13.28 ft) below microfracture MF11. The exact point of planar intersection, if any, between the microfracture and the open fracture is not known. Consequently, the exact fluid flow line (or diffusion path) distance between any of the microfractures that were sampled and open fractures cannot be estimated. Further discussions about site hydraulics are given in Volume 3: Fractured Rock Hydraulics.

3.2 Microfracture Surface Precipitate Morphology

The microfracture surface morphology, revealed through SEM, had four general characteristics (Figure 3.1). A smooth surface, which seemed to be the host rock, was apparent on some samples. At higher magnifications (data not shown), the host rock microfracture face appeared chonchoidal. The surface was etched in some regions, an indication of weathering and incongruent dissolution of the rock. On other microfractures, the surface appeared smooth at low magnification, but at high magnification, was clearly a distinct, flaky texture (e.g., microfracture MF06, Figure 3.1c). A third surface feature was small diameter (< 1.0 µm to 100 µm) granular precipitates (e.g., microfracture MF08, Figure 3.1d). Typically angular in nature, these granules were found upon the smoother surface of the underlying host rock. Finally, some areas had a fine structured web-like material (e.g., microfracture MF01, Figure 3.1a; microfracture MF05, Figure 3.1b) . The expanse of this morphology varied between samples. More than one morphology could be observed on a single microfracture sample. Table 3.1 summarizes the surface precipitate morphologies observed on the microfractures.

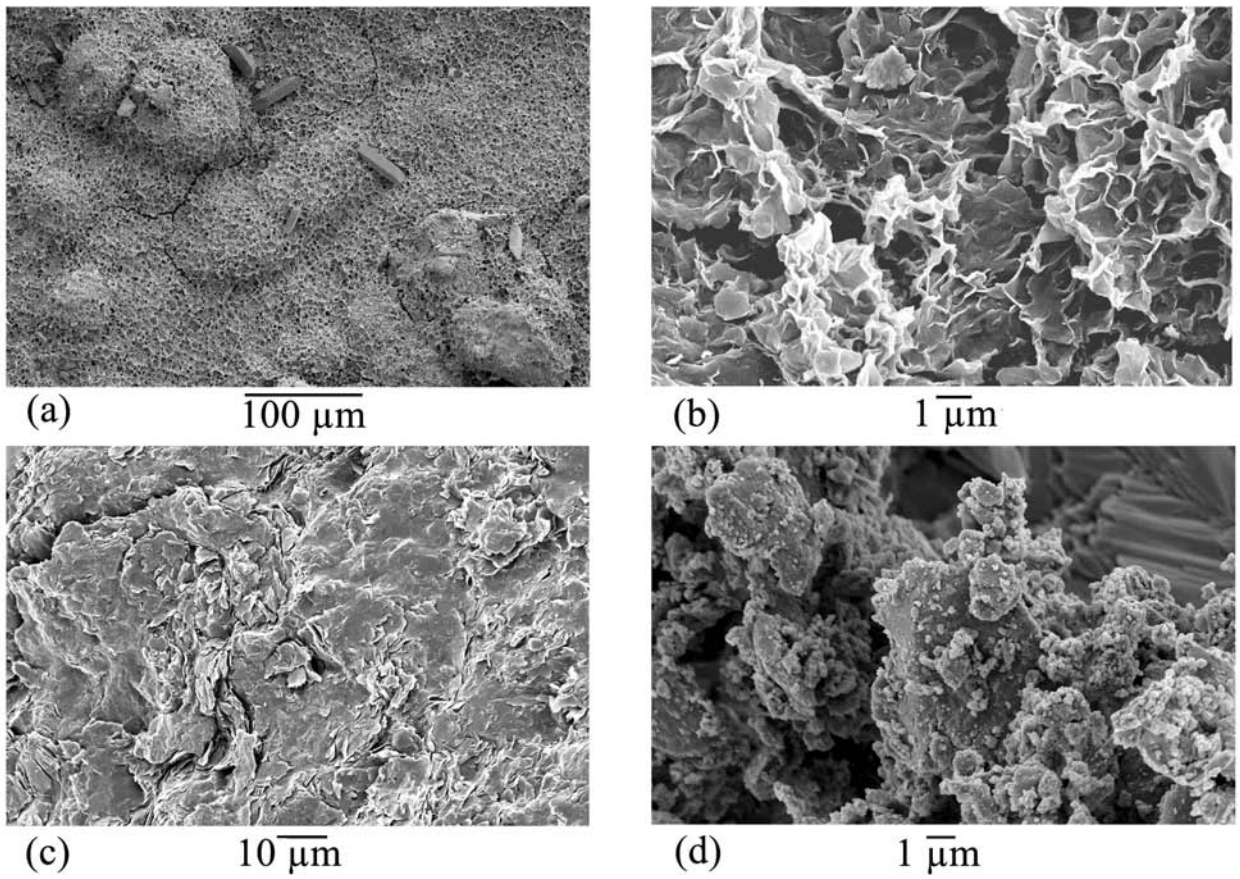

Figure 3.1. SEM micrographs of typical microfracture morphology: (a) web formation with prismatic mineral grains on microfracture MF01 (250x), (b) web formation on microfracture MF07 (7,250x), (c) flakey appearance to surface minerals on microfracture MF06 (1,000x), and (d) granular mineral precipitate on microfracture MF08 (6,100x).

Table 3.1. Summary Description of Surface Precipitate Morphologies

Microfracture #	Surface Description
MF01	Fine structured web-like precipitation with large quartz grains distributed throughout.
MF02	Host rock visible with angular granular materials dispersed over surface. Grains had a size range of 100 µm to less than 1 µm.
MF03	At low magnification, the surface appeared smooth with intermittent cracks. At high magnification, there was a consistent flakey appearance, which was visible throughout the microfracture surface.
MF04	Significant coverage of surface with angular mineral grains similar to microfracture MF02. Much of host rock was obscured. Some areas with flakey appearance as in microfracture MF03.
MF05	Smooth coverage, almost blanket like. In areas where the coverage appeared worn away, a web-like formation with high surface area and significant structure was visible.
MF06	Flakey appearance similar to precipitate on microfracture MF03.
MF07	Similar to microfracture MF05.
MF08	Similar to microfracture MF02.
MF09	Areas of flakey formations and angular granules resting on a smoother base.
MF10	Similar to microfracture MF05.
MF11	Host rock exposed with both angular granules and web-like formations visible.

3.3 Microfracture Element Spatial Maps

Figure 3.2 shows a typical EDS element spatial map of microfracture MF03 showing spatial distribution of Al, Ca, Fe, K, Mg, Na, O, S, Si, and Ti. The spatial heterogeneity of minerals is high; the surface is quite diverse at the ten's of μm scale. Table 3.2 shows dominant and minor elemental phases revealed by SEM-EDAX in microfracture MF01–MF11. Samples were sputter coated with carbon to prevent charging; therefore, carbon occurring naturally in the sample could not be characterized. Typical dominant elemental phases in microfracture MF01- MF11 were Si-Al-O, with K and/or Mg enrichment, and Ca-O. Fe enrichment in either a calcium phase or an aluminosilicate phase occurred in seven of the 11 microfractures. Sulfur-bearing iron compounds (Fe-S), nominally pyrite (FeS_2), occurred as minor phases in four of the 11 samples.

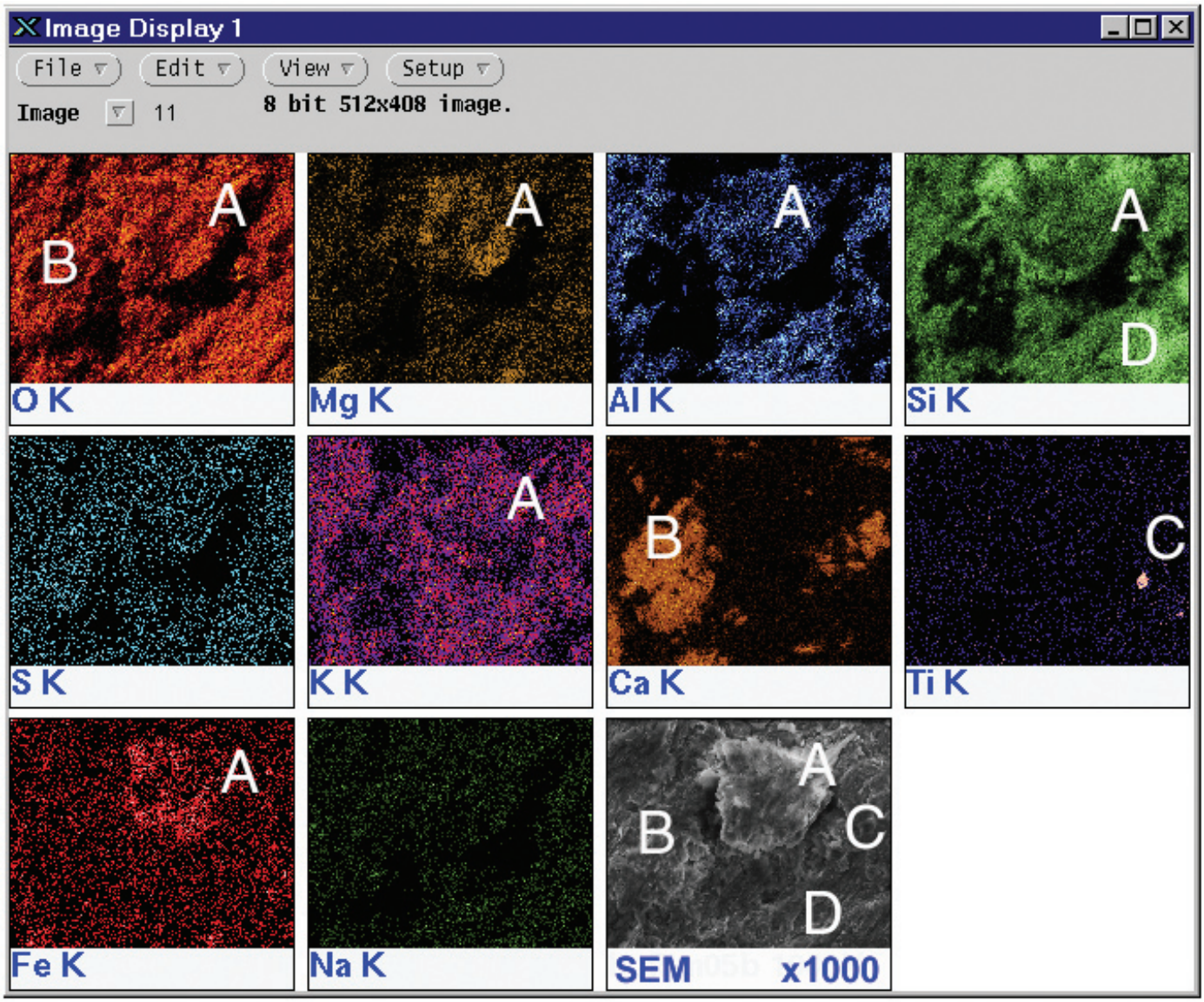

Figure 3.2. Typical EDS elemental spatial map in X-Y plane for microfracture MF03. Each window is 250 by 200 μm. (a) Si-Al-Mg-K-Fe-O, (b) Ca-O, (c) Ti, (d) Si-O.

Table 3.2. Summary Description of Element Association in Spatial Maps

Microfracture #	Dominant Phases	Minor Phases
MF01	Si-Al-Mg-O	Si-O Si-Mg-Al-K-O Ca-O
MF02	Si-Al-K-O Si-Al-K-Mg-O Ca-O	Si-O Fe-S
MF03	Si-Al-K-O Si-Al-K-Mg-O Ca-O	Si-Al-K-Mg-Fe-O Ti
MF04	Si-Al-K-O Si-Al-K-Mg-O Al-Mg-Fe-O	Si-O Ca-O Fe-S Ti
MF05	Si-Al-Fe-O Si-Fe-O Fe-S	Si-O Al-K-O Al-K-Na-O Ca-O Ca-Mg-O Fe-S Ti
MF06	Si-O Si-Al-K-O Si-Al-K-Na-O Ca-Mg-Fe-O	Si-O Fe-O Ti
MF07	Si-Al-Fe-O	Si-O Si-Al-K-O Si-Al-Na-O Ca-O
MF08	Si-O Si-Al-K-O Ca-O	Si-Al-O Fe-O
MF09	Si-Al-K-O Si-K-O Ca-Mg-Fe-O	Si-Al-Na-O Fe-S
MF10	Si-Al-K-O Si-Al-K-Fe-O Si-Al-K-Fe-Ca-O	Si-O Ti
MF11	Si-Al-Mg-Fe-O Si-Al-K-Mg-Fe-O Ca-O	Si-O Si-Al-K-O Si-Al-Na-O Si-Al-Fe-O

3.4 Microfracture Biopatch Distribution and Morphology

The extent and distribution of prokaryotic populations on microfracture surfaces were characterized with SEM (Figures 3.3, 3.4, and 3.5). The ability to view microbes on the surface of the microfracture seemed to be limited by the morphology or topography of the surface precipitates. Smooth, exposed host rock revealed greater numbers of microbes than the fine structure web-like surfaces typical of the surface precipitates (See Figure 3.5.). The flakey surface morphology required careful examination to discern microbial forms from the precipitates.

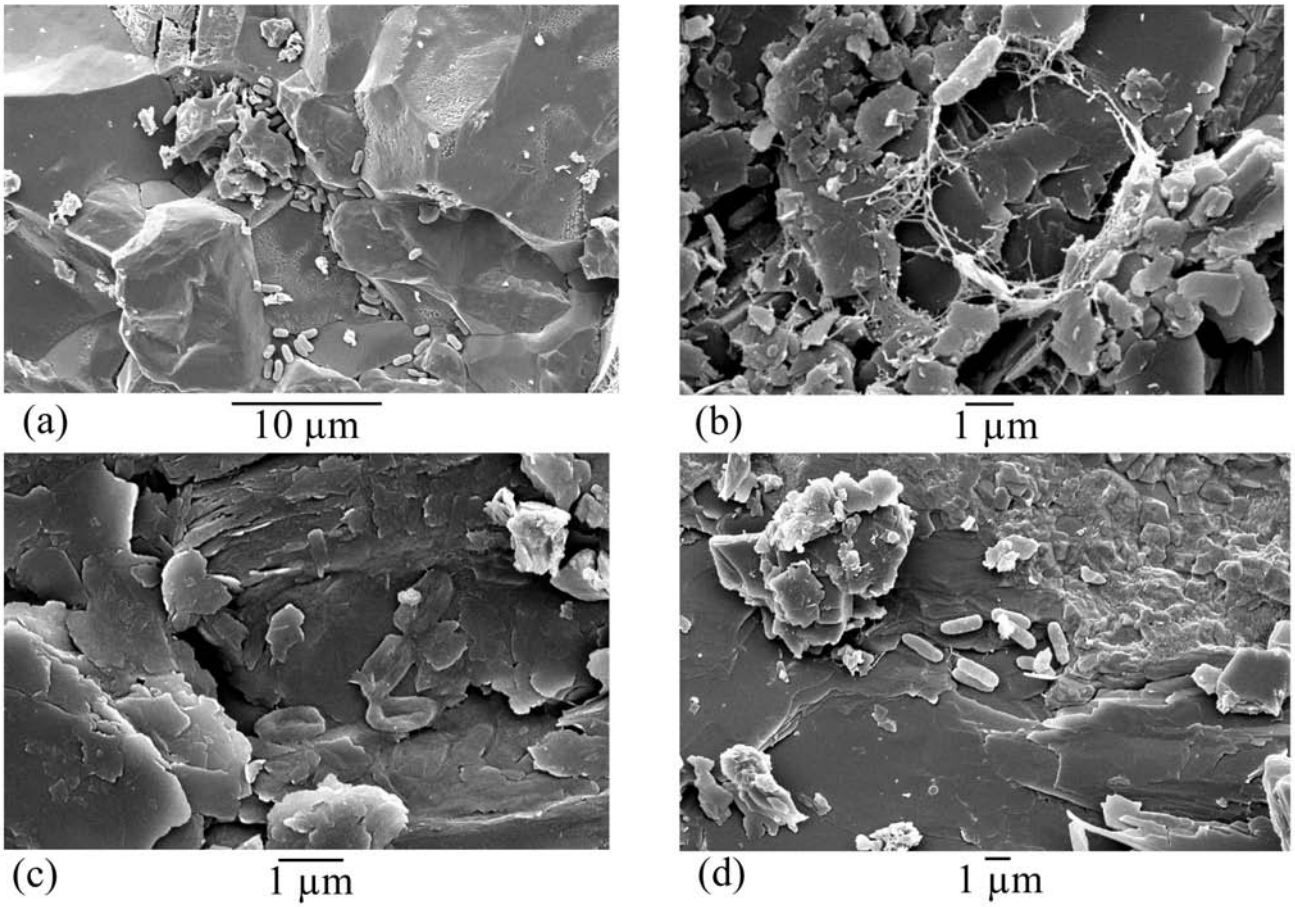

Figure 3.3. Biopatch SEM micrographs. (a) Biopatch on microfracture MF04. The microbes are situated in a crevice. (b) Microbe with extensive extracellular material on microfracture MF04. (c) Microbial populations on microfracture MF03 embedded in possible organic matrix. (d) Biopatch on microfracture MF04. The microbes are again in a crevice.

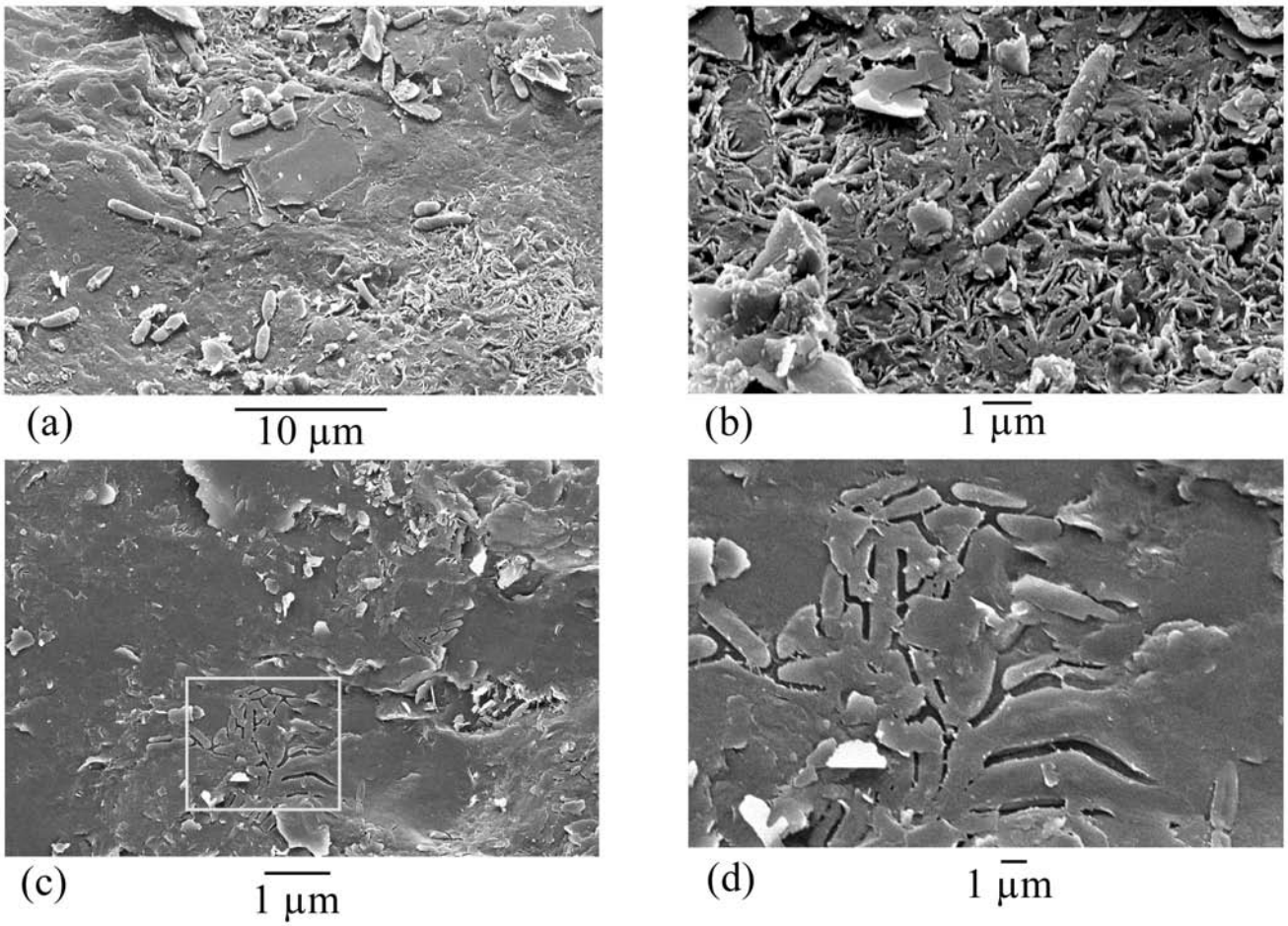

Figure 3.4. Biopatch SEM micrographs. (a) Biopatch on a smoother surface coated with possible organic material on microfracture MF07. Note the dividing cells with division septa. (b) Microbes on rough surface on microfracture MF07. Note the small grains on the surface of the microbes. (c) Coated biopatch on microfracture MF06. (d) Coated biopatch (close-up of box in image C on microfracture MF06).

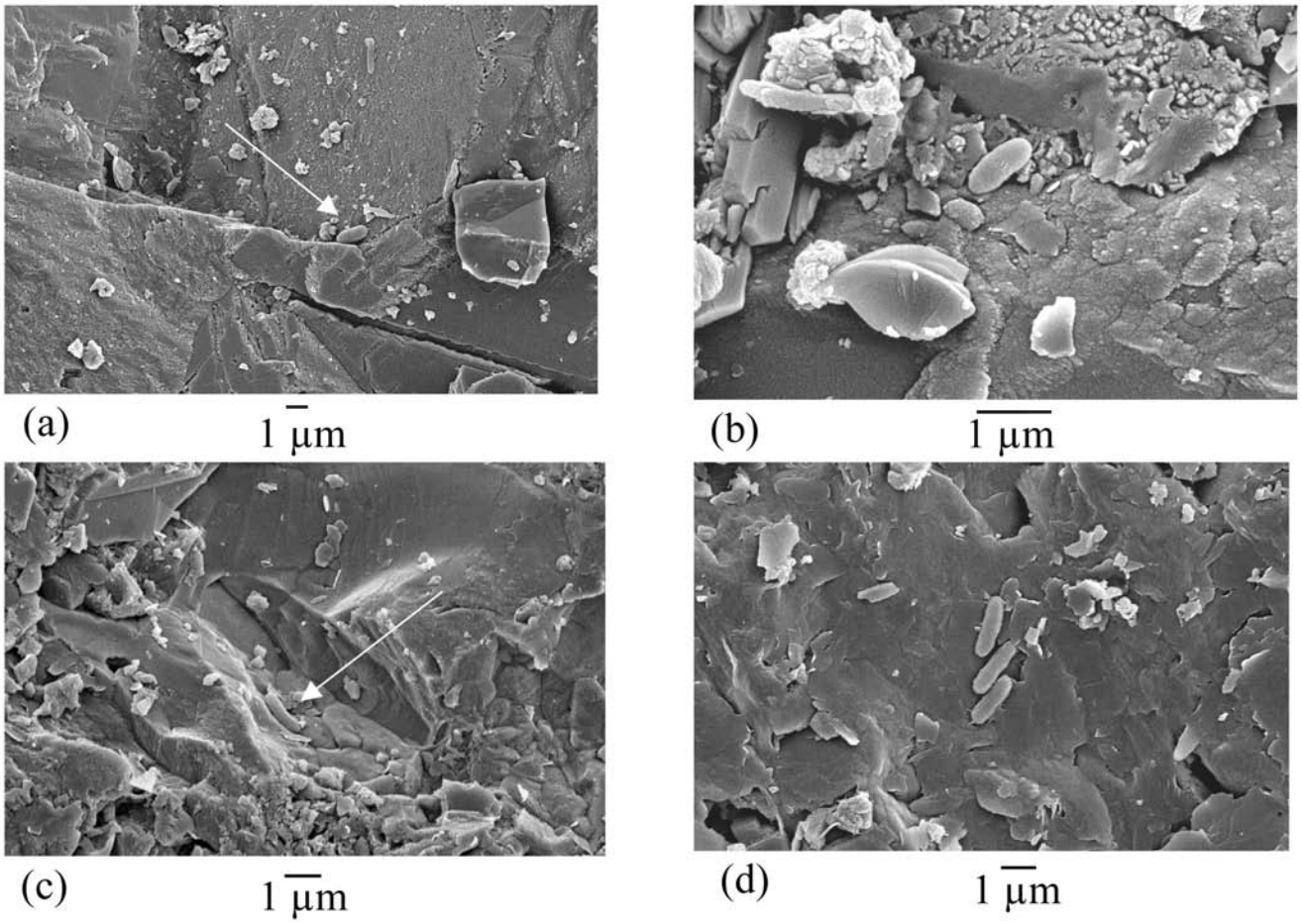

Figure 3.5. Biopatch SEM micrographs. (a) Microbe in a crevice on microfracture MF09. (b) Microbe among angular material on microfracture MF09. (c) Microbe on smooth surface on microfracture MF11. (d) Biopatch on flakey material on microfracture MF11.

Microbes were often found in crevices or topographical features. Once a single microbe was sighted, a more thorough examination of the surrounding area typically revealed other microbes in a biopatch. In some cases, evidence of cell division was seen. The typical microbial morphology found in the SEM investigation was a rod of 1.0 – 2.0 μm in length and 0.5 –1.0 μm in width. This suggests that a low diversity of morphologies may be present on the samples.

Microfracture MF04 had the largest apparent microbial population (Figure 3.3 a and b). The other microfracture samples had sparse to moderate microbial numbers, relative to microfracture MF04. Approximate cell densities (based on cell counts just in lower magnification micrographs) were relatively low (e.g., $< 10^4/cm^2$). These cell densities are only indirectly comparable to other measures of numbers of cells or biomass reported in the literature. For instance, Onstott *et al*. (2003) used phospholipid fatty acid and terminal restriction fragment length profile analyses to show that indigenous microorganisms were present at $< 10^2$ cells/g of rock in deep bedrock in South Africa. Microfracture MF06, which had a flakey surface, had microbial populations that appeared to be coated by an organic surface material. The semi-exposed cell features were often accompanied by outlines of more cell features under a blanket-like surface (See Figure 3.4 c and d.).

It is surprising that only one morphological type (rod) was observed with SEM. Related work with epifluoresence microscopy on porewater microbes reveals a variety of morphologies (e.g., rod, coccoid, filamentous, stalked). (See Volume 4: Fractured Rock Microbiology.) Further, this morphology differs from some of those seen within the surface precipitate with TEM (See Section 3.5.). It is not clear if the surface selects for one morphology, if an artifact has been introduced by fixation and critical point drying, or if the three dimensional structure of the surface precipitates prevents observation of other morphologies with SEM. The later hypothesis, given the observations with TEM, may be most relevant. There is little data from the literature on microfracture adherent microbial populations with which to compare.

3.5 Microfracture Microbial Populations Situated Within Surface Precipitates

The TEM work revealed that a diverse population was present in the calcite and quartz surface precipitates that were prevalent on microfracture MF11 from borehole BBC6. A number of stalked morphologies were seen (Figure 3.6). The cell sizes were large (0.7 µm in diameter, 1.5 to 2.0 µm in length). In some cases, the stalk was very apparent. Figure 3.7 shows some spirillum morphologies which were also prevalent. The cells were generally larger than the rod shaped cells seen with SEM. Both 0.1 µm diameter electron-opaque and 0.3 µm diameter electron transparent inclusion bodies were present in the cells (Figure 3.8). Most of the cells observed with these organelles appeared to be filamentous. At this time, the elemental composition of these organelles is unknown. Additional filamentous morphologies, some with pronounced inclusion bodies, were observed (Figure 3.9). The filaments, in some instances, were over 8 µm in length.

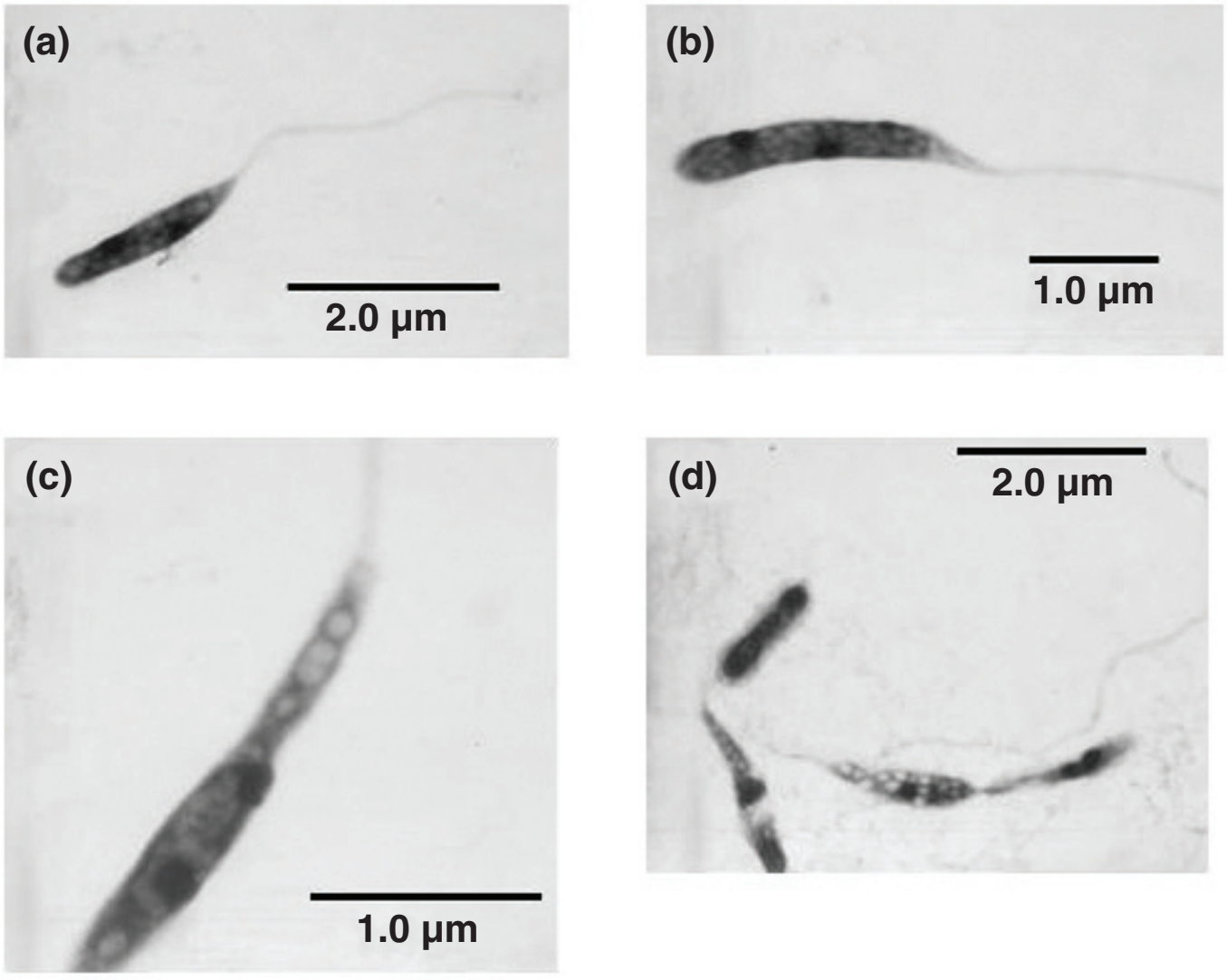

Figure 3.6. TEM micrographs of stalked morphologies present in calcite precipitates on microfracture MF11. The cells appear to have inclusion bodies.

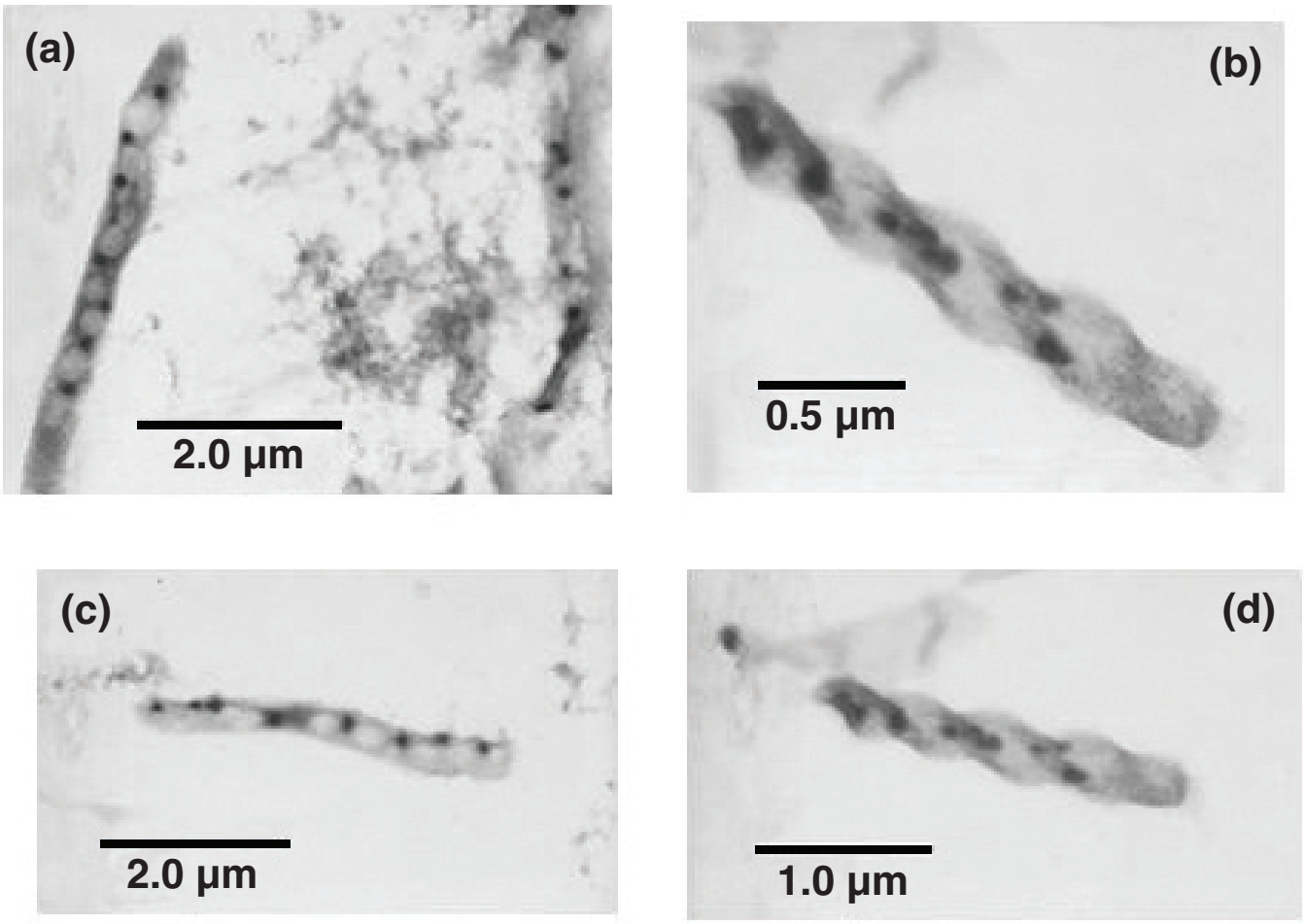

Figure 3.7. TEM micrographs of spirillum morphologies in calcite precipitates in microfracture MF11. The cells appear to have inclusion bodies.

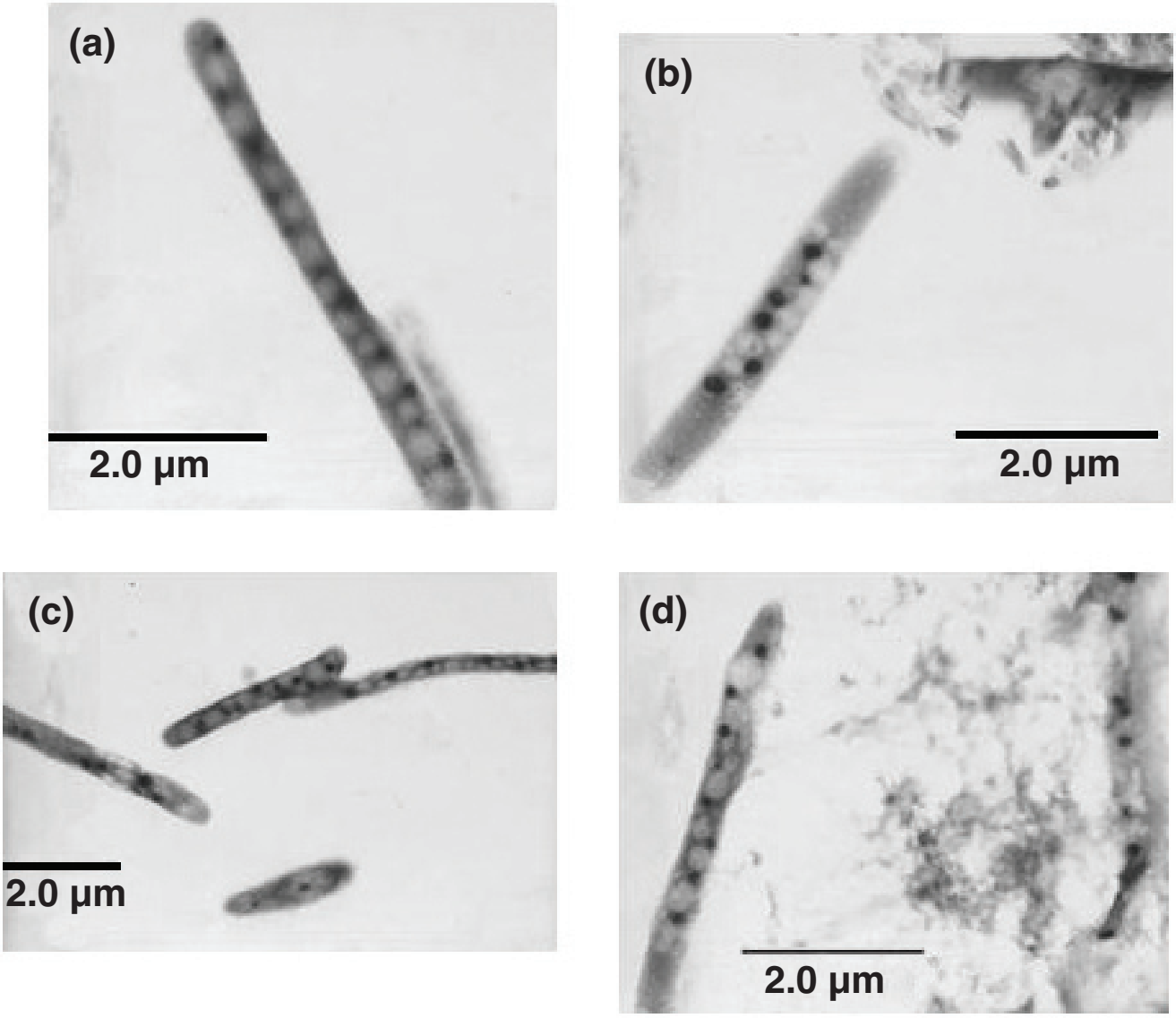

Figure 3.8. TEM micrographs of filamentous morphologies in calcite precipitates in microfracture MF11. The cells appear to have inclusion bodies.

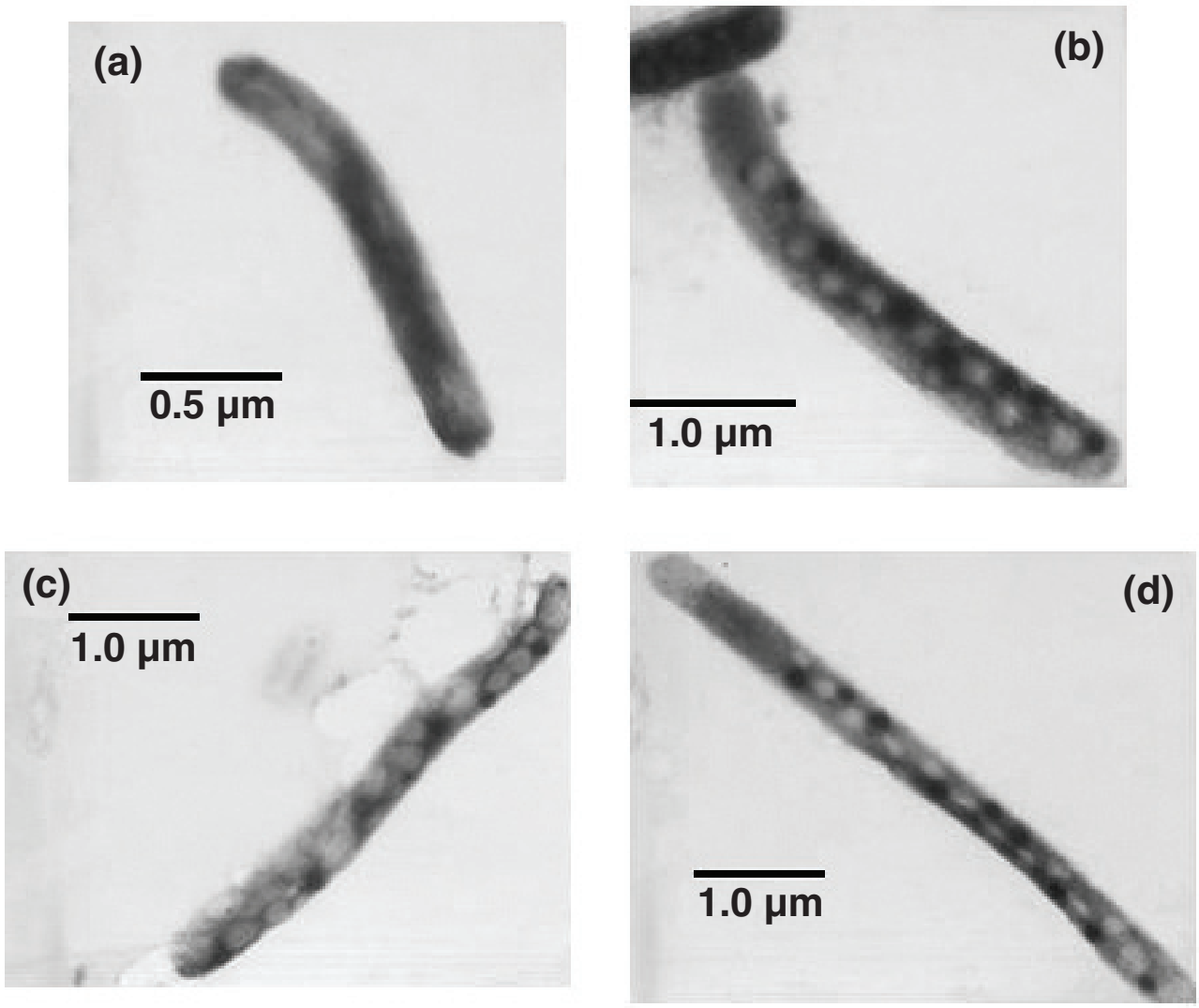

Figure 3.9. TEM micrographs of inclusion bodies within cell structures in calcite precipitates in microfracture MF11. Note that some bodies are electron dense (dark) while others are electron opaque (grey).

3.6 Petrographic Characterization of Host Rock and Microfracture Surfaces

Lithological observations involved examination of core material during well logging as well as petrographic analysis of thin sections. From a thin section perspective, the microfracture surfaces were independent of rock type. Fracture-fill material, dominated by carbonate mineral(s), crossed lithologic boundaries (bedding surfaces, minor faults, and fractures of varying types). Figure 3.10 illustrates three fracture filling types. Figure 3.11 illustrates layering and textural relations of the metasandstone and metashale in the Kittery Formation.

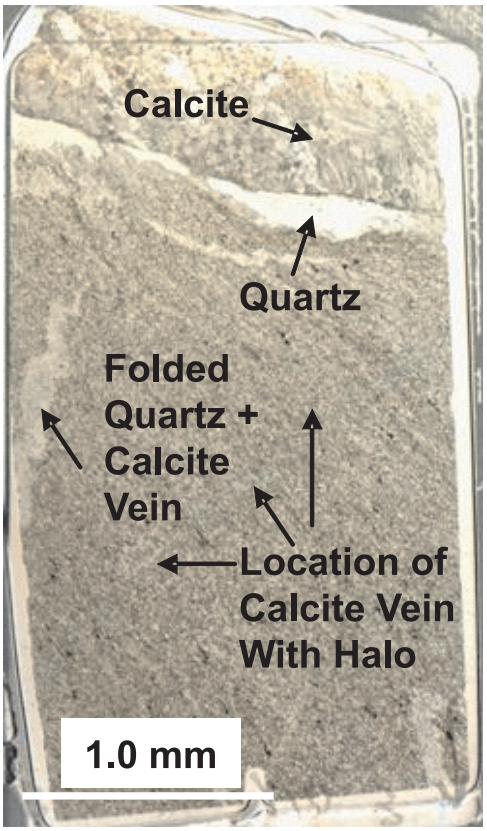

Figure 3.10 Petrographic thin section of Kittery metasandstone. The image shows three generations of fracture fillings, all crosscutting weakly foliated host rock. The quartz plus calcite vein shows folding. A very thin vein of calcite traverses the thin section. There is an alteration halo on either side of the vein when viewed at higher magnification.

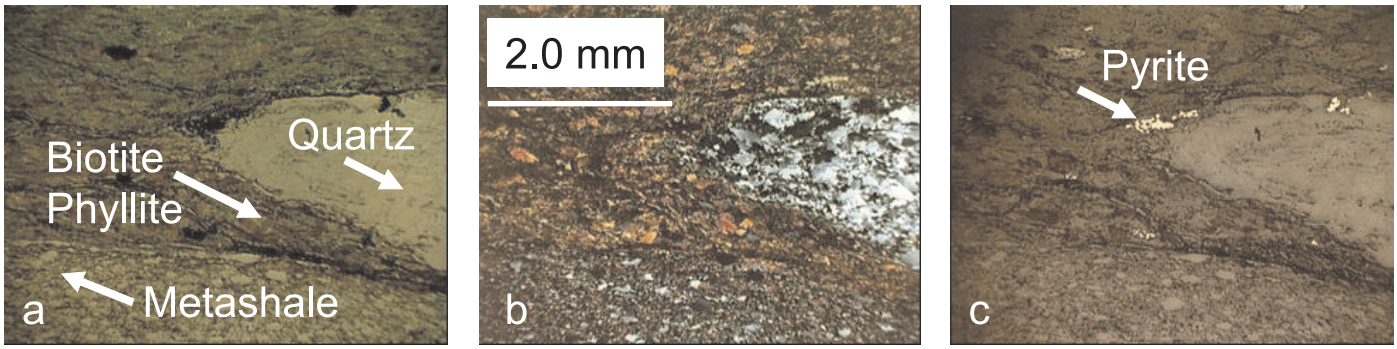

Figure 3.11 Photomicrographs of the same region of a petrographic thin section in (a) plane, (b) cross-polarized, and (c) reflected light. The images illustrate mineralogy, texture, "bedding parallel" fracture, discontinuous "early" quartz lens, and the presence of sulfides within the matrix and along boundaries of the vein and host rock. The dominant fine-grained calcareous metasandstone and biotite phyllite and a deformed quartz vein with pyrite within and at the terminus of the quartz lens is best seen in (c). Boundaries between the metasedimentary layers and between lens and phyllite are sharp. The bar scale is applicable for (a), (b) and (c).

Metasandstone was the dominant lithology (80-90%) of the host assemblage. It is composed of fine grained (< 0.5 mm) quartz, feldspar, white mica, chlorite, and/or biotite depending on its metamorphic grade. Interstitial carbonate varied from a few percent to as much as 30% exclusive of vein or fracture fillings. Pyrite (best seen in reflected light) and apatite occurred as accessory minerals. Iron hydroxides typical of limonite ($Fe_2O_3 \bullet nH_2O$) and probable clays dominated as alteration minerals. Much of the quartz and feldspar (mostly albite) grains were recrystallized, but the larger sized polycrystalline quartz grains may have reflected original sedimentary grains. Phyllosilicates showed preferred orientation as a function of recrystallization and reorientation. For the metasandstones, the preferred orientation remained parallel to the original layering.

Field observations revealed that the thin metashale layers (10-20%) were intercalated with dominant metasandstone. Some layers were as thick as a few 10's cm, but many were only 2 - 10 cm thick. They contained the same mineral assemblage, but with less quartz and feldspar and more phyllosilicate. Preferred orientation was strong throughout. The phyllosilicates showed a second preferred orientation that cross cut an earlier "bed" parallel foliation.

Porphryitic diabase dikes were encountered in all BBC boreholes. Thin sections across contacts with the Kittery Formation showed a typical chill margin containing microphenocrysts of plagioclase and microxenoliths from the host rock (Figure 3.12). No attempts to assess intrusive direction, based on preferred orientation of microphenocrysts, were made in this study. After olivine, phenocrysts of zoned plagioclase, clinopyroxene, and chlorite pseudomorphous were set in fine grained diabasic texture in the more central parts of the dikes here and throughout the Great Bay area. The dikes were generally massive, with fewer fractures and veins than the Kittery host rock. Figure 3.12 illustrates the contact relations between dike and Kittery host and cross-cutting mineralized vein and amygdular fillings.

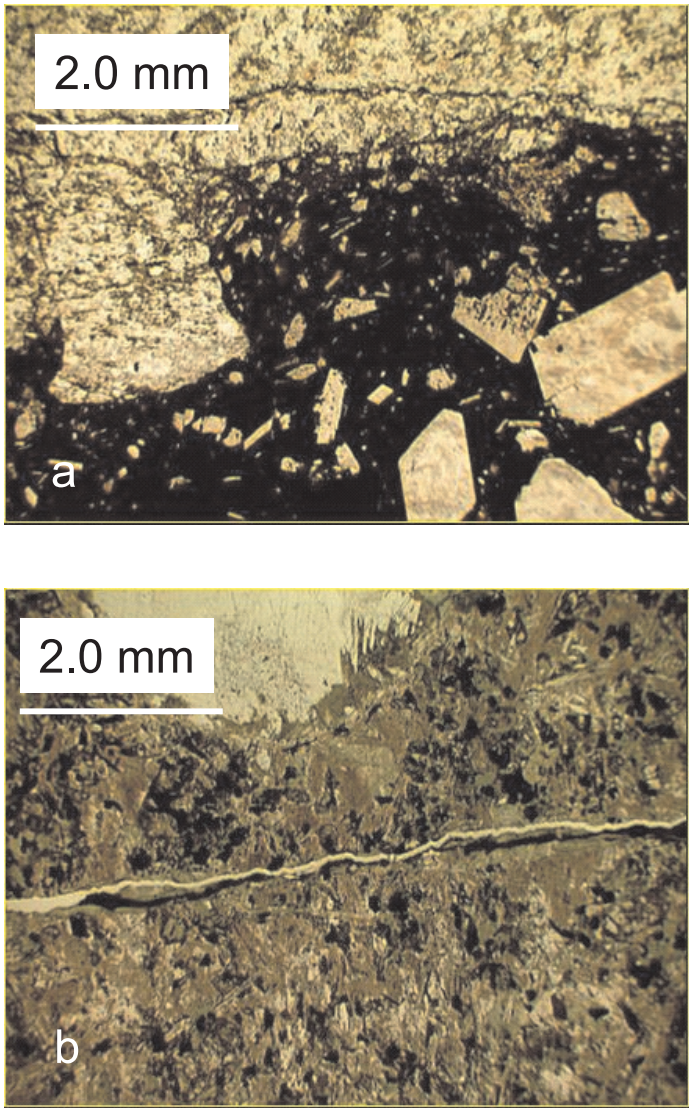

Figure 3.12 Diabase dike textures and microfracture fillings. (a) Photomicrograph of contact between Kittery (top) and chill margin of porphryitic diabase. Note that the microfractures are roughly parallel to contact, rip-ups (microxenoliths), and weakly aligned phenocrysts of plagioclase and pyroxene. Sub-horizontal fractures are filled with chlorite. The micrograph was produced with plane polarized light. (b) Photomicrograph from the center of diabase dike. The felty matrix is a coarse-grained plagioclase and pyroxene, magnetite and sulfide, and chlorite. Note the large (3 mm) amygdule filled with calcite (top) and a 0.2 mm partially sealed fracture composed of calcite, chlorite, and opaques. The micrograph was produced with plane polarized light.

Several generations of veins and fracture fillings were recognized in the metasandstone and metashale of the Kittery Formation (Figure 3.10). Early carbonate and quartz veins were separated from later veins by cross-cutting relationships and the degree of deformation (microfolding, gradational boundaries with host versus sharp discordant boundaries and planar character, Figure 3.10). Strongly strained quartz grains (identified by undulatory extinction and strong preferred orientation, Figures 3.11 and 3.12) and calcite (bent twins and curved cleavage traces) were common in earlier veins and fractures. Apparently, younger veins and fracture fillings were characterized by an absence of preferred orientation, open and/or discontinuous precipitation of calcite, quartz, and minor zeolite (Figure 3.13).

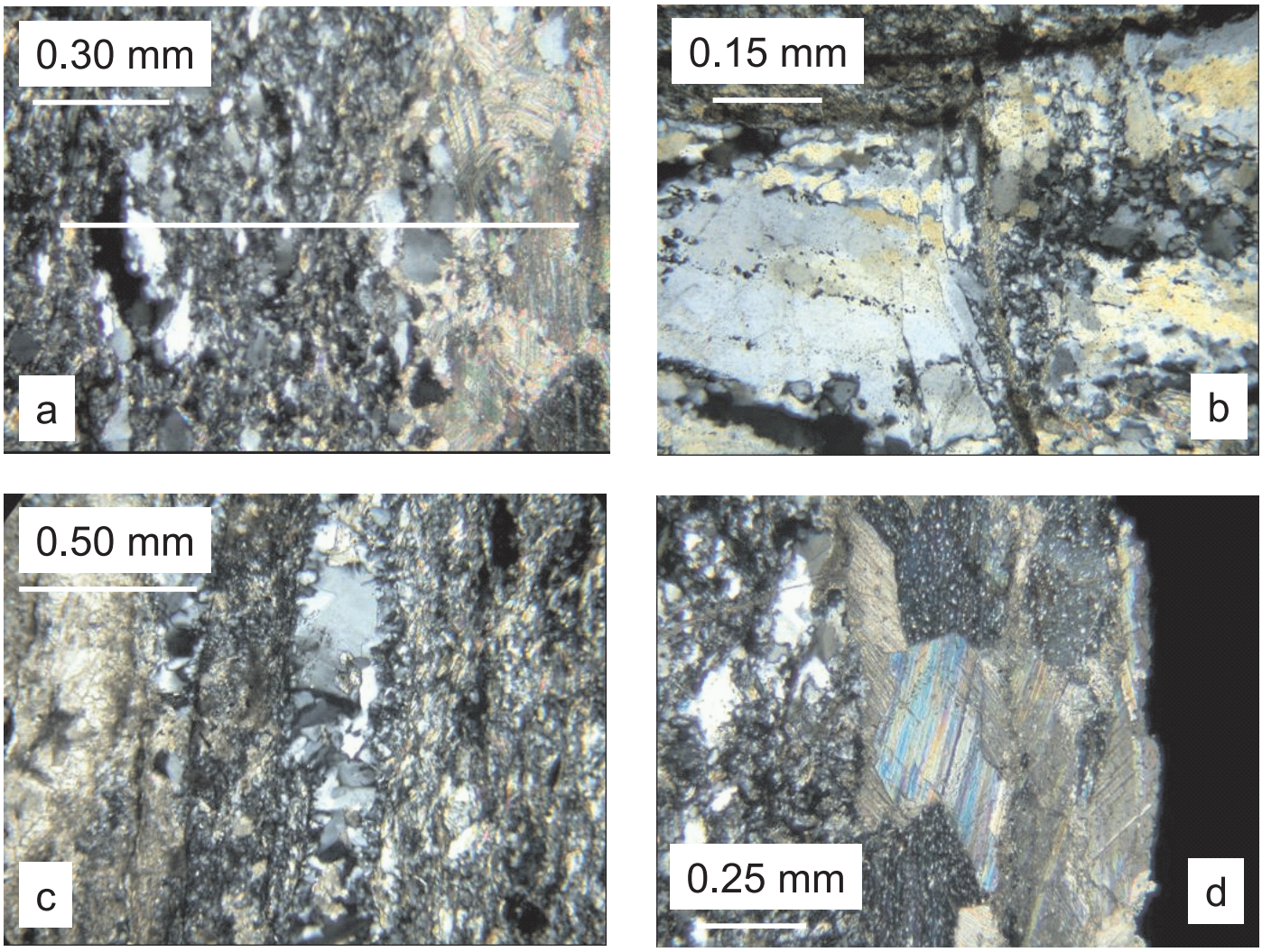

Figure 3.13 Photomicrographs of microfracture textures and morphology. The images were taken with cross polarized light. (a) A general view of the host rock displaying a strong foliation and micro-fault with larger re-crystallized grains of quartz and carbonate (right). The main foliation is parallel to the lateral edges of the photomicrograph and defined by shape-preferred orientation of quartz. The trace of the traverse for the analysis crosscuts the structures as shown. (b) Ductile deformation of quartz vein in metashale crosscut by microfaults. Calcite often shows the same degree of ductile deformation by bent cleavage and twins. (c) Multiple parallel fractures alternated with filled calcite (left) and quartz (right middle) veins. The foliation in the host rock is approximately parallel to the veins. The veins lack significant deformation. (d) Thick, un-deformed quartz plus calcite vein approximately parallel to the foliation in metasandstone host rock. There is no apparent reaction between the host rock and vein material. The irregular right edge is hammer induced fracturing.

Table 3.3 reports the specific mineralogy of the host rock associated with the 11 microfractures as determined by petrographic analysis of thin sections cross cutting the microfracture surface minerals and underlying host rock. The host rock contained the following minerals and relative abundances (based on modal analysis) generally distributed among all 11 samples: quartz (SiO_2, 10-40%); feldspar (mostly albite $NaAlSi_3O_8$ with minor $KAlSi_3O_8$, 0-25%); carbonates ($CaCO_3$, $CaMg(CO_3)_2$, $FeMgCO_3$, 0-32%); biotite ($K_2(Mg,Fe)_6Al_2Si_6O_{20}(OH,F)_4$, 0-45%) and/or chlorite ($(Mg,Al,Fe)_3(Si,Al)_4O_{10}(OH)_2 \bullet (Mg,Al,Fe)_3(OH)_6$), 0-30%); white mica ($KAl_2(AlSi_3O_{10})(OH)_2$), 0-15%); and accessory apatite ($Ca_5(PO_4)_3OH$), zircon ($ZrSiO_4$), and opaques dominated by pyrite (FeS_2).

Table 3.3. Mineral Phases Identified by Petrography in Host Rock

Micro-fracture #	Apatite (% area)	Biotite (% area)	Carbonate (% area)	Chlorite (% area)	Feldspar (% area)	Opaques (% area)	Quartz (% area)	White Mica (% area)	Zircon (% area)
MF01	Trace	15	10	5	20	5	40	5	Trace
MF02		15	20	10	10	5	35		Trace
MF03	Trace	25			15	5	40	15	Trace
MF04	Trace		20		15	1-2	45	15	
MF05	Trace		20		15	1-2	45	15	
MF06	Trace		20		25	1-2	35	20	
MF07		45	15	25		1-2	13		
MF08			10	40	10	<5	15	15	Trace
MF09			25		25	<5	45		
MF10	Trace		10	35	10	<5	20	15	
MF11		5		30	15	1-2	40	10	

Mineral Formulas (Nesse, 2003):

Apatite – $Ca_5(PO_4)_3(F,Cl,OH)$
Biotite – $K_2(Mg,Fe)_6Al_2Si_6O_{20}(OH,F)_4$
Carbonate – primarily $CaCO_3$, others include $CaMg(CO_3)_2$, $FeMg(CO_3)_2$
Chlorite – $(Mg,Al,Fe)_3(Si,Al)_4O_{10}(OH)_2*(Mg,Al,Fe)_3(OH)_6$
Feldspar – $(Na,Ca)(Al,Si)_2Si_2O_8$; may include minor $KAlSi_3O_8$
Opaques – FeS_x
Quartz – SiO_2
White Mica – $KAl_2(AlSi_3O_{10})(OH)_2$
Zircon – $ZrSiO_4$
Trace = trace amount; accessory mineral

Identification of the minerals in the microfracture surface precipitates was limited to three of the 11 samples. The optical mineral determination used a point counting method to estimate mineral composition and for the majority of microfracture samples, the mineral surface coating was not sufficiently abundant to make such estimates. Figure 3.14 shows photomicrographs of these three samples at the intersection of the mineral coating on the microfracture face and the host rock. The mineral identification results of the three characterized microfracture faces are found in Table 3.4. The microfracture surface precipitates contained the following minerals and relative abundances (based on modal analysis) generally distributed among all three microfractures: carbonates ($CaCO_3$, $CaMg(CO_3)_2$, $FeMgCO_3$, 5-50%), chlorites ($(Mg,Al,Fe)_3(Si,Al)_4O_{10}(OH)_2 \bullet (Mg,Al,Fe)_3(OH)_6$), 0-15%), and quartz ($SiO_2$, 35-95%). No pyrites were found in the surface precipitates.

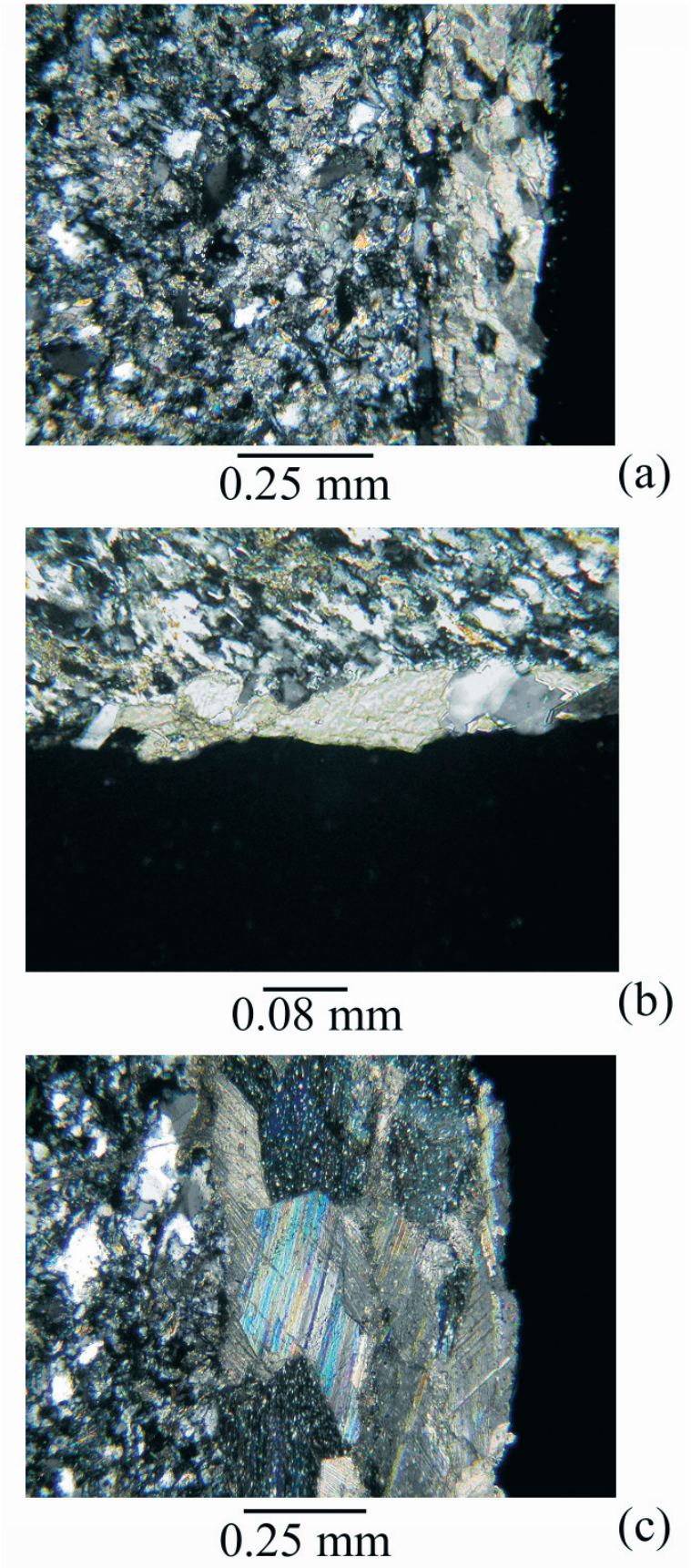

Figure 3.14 Petrographic micrographs of host rock and microfracture surfaces. The images were taken with cross polarized light. (a) Microfracture MF02 - a general view of the host rock in contact with the calcite-quartz microfracture surface. (b) Microfracture MF06 - a view showing the crosscutting relation between the microfracture with crystalline carbonate and quartz and the foliation in the host rock. The foliation makes an angle of about 35 degrees with the top margin of the photo. (c) Microfracture MF11 - the emplacement of the thick quartz-calcite microfracture is interpreted as the latest petrogenic event as there is no sign of deformation as it crosscuts the host rock.

Table 3.4. Mineral Phases Identified by Petrography in Microfracture Surface Precipitates

Micro-fracture #	Carbonate (% area)	Chlorite (% area)	Quartz (% area)	Opaque (% area)
MF02	50	15	35	Trace
MF06	35		65	
MF11	5		95	

Mineral Formulas (Nesse, 2003):

Carbonate – primarily $CaCO_3$, others include $CaMg(CO_3)_2$, $FeMg(CO_3)_2$
Chlorite – $(Mg,Al,Fe)_3(Si,Al)_4O_{10}(OH)_2*(Mg,Al,Fe)_3(OH)_6$
Quartz – SiO_2
Opaque – FeS_x
Trace = trace amount; accessory mineral

EDS investigation of the microfracture face and host rock in the y-z plane, as found on the thin section slides, was conducted on two samples, microfractures MF07 and MF09. Microfracture MF07 showed a distinct elemental difference at the microfracture surface of higher Fe content and lower Si content than in the underlying host rock. In Figure 3.15, this is seen as the more intense red at the center-right region of the Fe map and a less intense green area in the coordinating location on the Si map. The fracture face was composed of Al, Mg, and O accompanying the Fe and Si concentrations. The underlying host rock was composed of Si-Al-K-Mg-Fe-O phases, as well as interspersed Ca-O and Ti phases. The fracture surface of microfracture MF09 was composed of a Ca-Mg-Fe-O phase, distinct from the immediate underlying Si-Al-K-O phases.

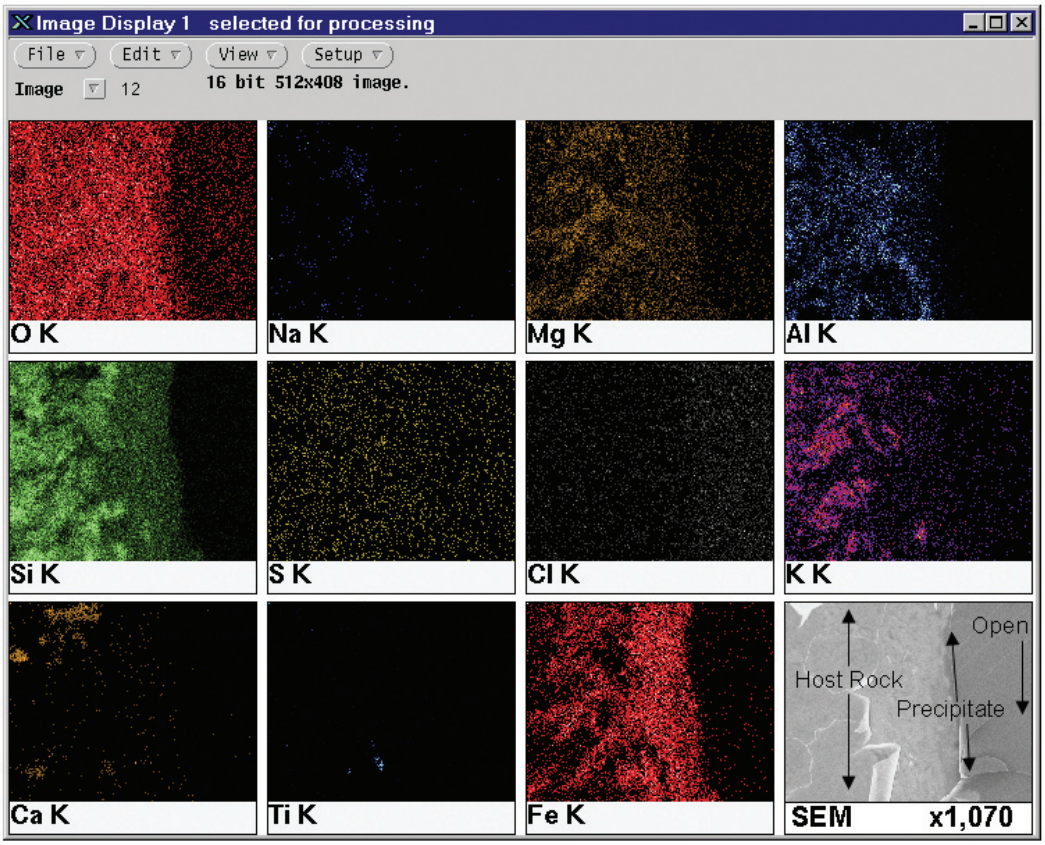

Figure 3.15 Element spatial map of microfracture MF07 thin section showing host rock and microfracture face in cross section. Each window is about 300 by 200 µm.

3.7 Mineralogy of Microfracture Surfaces and Host Rock Based on XRD

XRD was used to identify crystalline minerals in the BBC host rock and microfracture surface precipitate materials. Mineral identification was limited to those identified from matches with the ICDD database. Due to the complex nature of the diffractogram and the search/match process, it was not unusual to identify minerals that were not likely present in the sample. Despite this, XRD was still a useful method of analysis, especially when used in conjunction with other analytical methods.

Figures 3.16, 3.17, and 3.18 reflect the data processing method in several steps. Figure 3.16 is a typical raw XRD diffractogram for a microfracture sample. Figure 3.17 is the same diffractogram after background correction and smoothing to remove excessive noise. Figure 3.18 shows typical identification of minerals as determined by the search match program. Figure 3.19 shows a diffractogram of host rock material from microfracture MF07. Figure 3.20 shows a diffractogram of the microfracture surface precipitate of microfracture MF07. A high degree of crystallinity, as evidenced by the number of peaks observed, is apparent in both samples. Some common major peaks are present, but the diffractograms show significant differences in mineral composition.

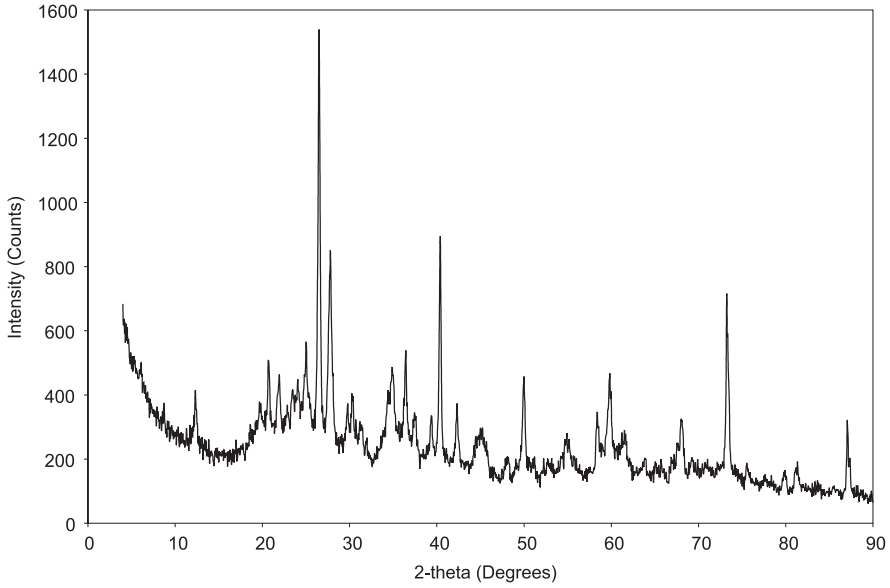

Figure 3.16 Typical raw diffractogram.

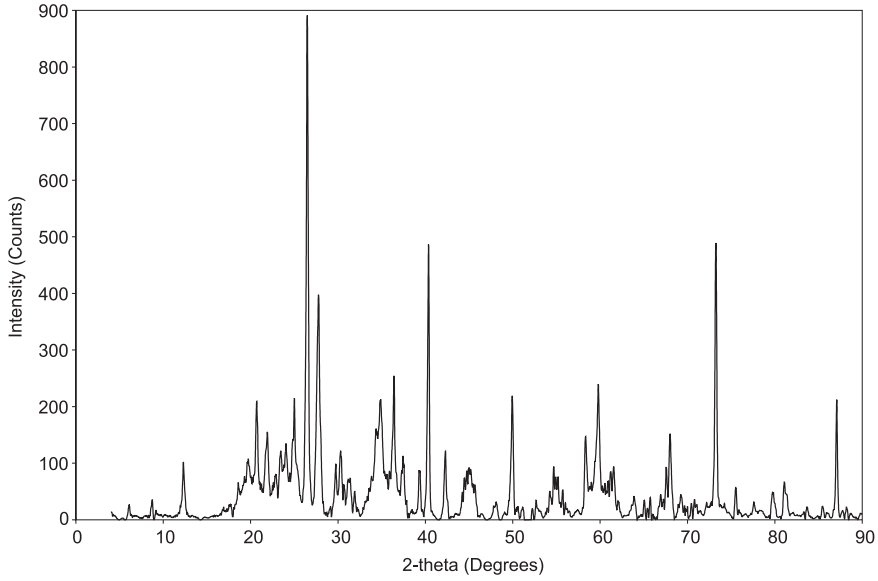

Figure 3.17 Typical diffractogram after background removal and smoothing.

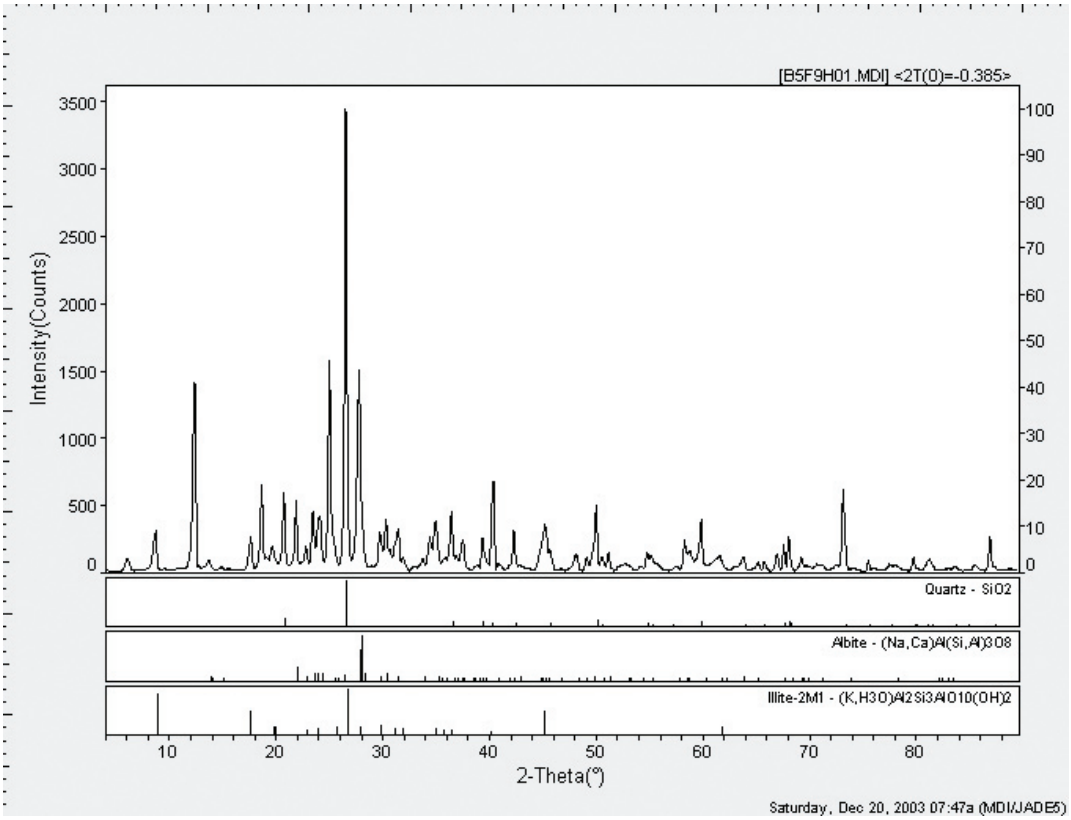

Figure 3.18 Typical peak ID as determined by search match routine. The right hand Y axis is relative intensity (%).

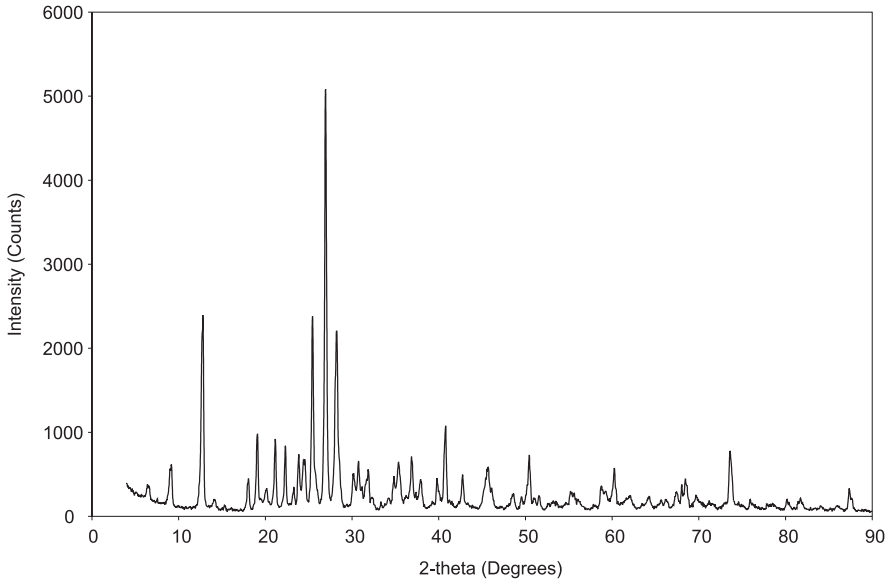

Figure 3.19 Diffractogram of host rock from microfracture MF07.

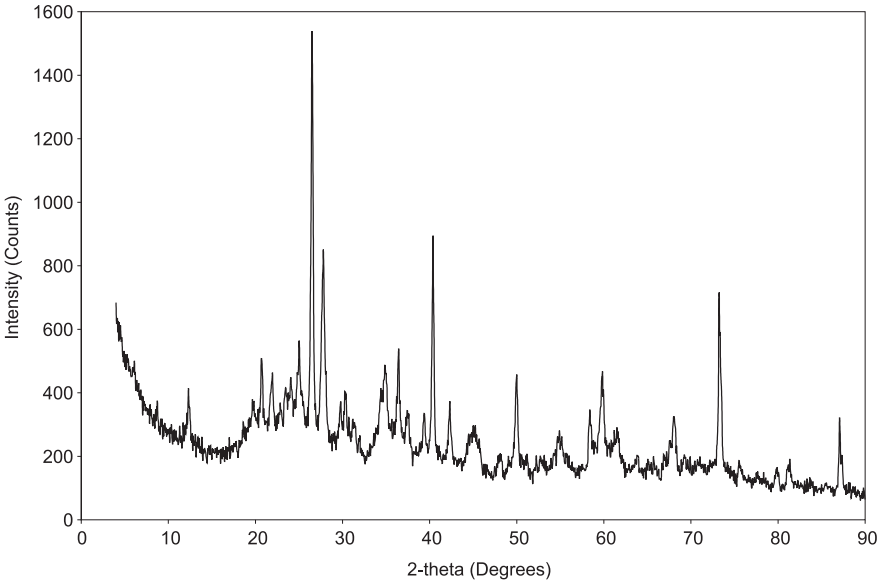

Figure 3.20 Diffractogram of microfracture surface precipitate from microfracture MF07.

Table 3.5 lists all reasonable candidate minerals identified in the host rock material. Dominant major candidate minerals included quartz (SiO_2), clinochlore (a chlorite), and albite ($(Na,Ca)Al(Si,Al)_3O_8$).

Table 3.5. Summary of Crystalline Minerals Identified in Host Rock Samples

Mineral Name (Formula)	Microfracture #, Mineral Phase Relative Abundance (Search-Match FOM)								
	MF01	MF02	MF04	MF06	MF07	MF08	MF09	MF10	MF11
Quartz (SiO_2)	3.0	2.2	0.6	0.6	3.0	2.6	0.7	1.3	3.0
Clinochlore ($(Mg,Fe^{2+},Fe^{3+},Mn,Al,)_{12}[(Si,Al)_8O_{20}](OH)_{16}$)	10.8	3.4			10.7		10.8	8.6	9.0
Albite ($(Na,Ca)Al(Si,Al)_3O_8$)	12.6	13.2		13.4	4.6		5.4		9.1
Potassium Mica ($KAl_3Si_3O_{11}$)					2.6			3.6	
Illite ($(K,H_3O)Al_2Si_3AlO_{10}(OH)_2$)					2.9			2.1	
Potassium Manganese Oxide Hydrate ($K_{0.5}Mn_2O_4$)					7.4				
$K(Mg,Al)_{2.04}(Si_{3.34}Al_{0.66})O_{10}(OH)_2$					12.4			12.5	
$(Mg, Fe^{2+}, Fe^{3+},Mn,Al)_{12}[(Si,Al)_8O_{20}](OH)_{16}$					14.7			10.9	
Zeolite (Na_2O-SiO_2-Al_2O_3)					15.0				
Lizardite Aluminian ($(Mg,Fe^{2+},Fe^{3+},Mn,Al)_{12}[(Si,Al)_8O_{20}](OH)_{16}$)					16.0				
Chamosite ($(Fe,Al,Mg)_6(Si,Al)_4O_{10}(OH)_8$)					19.2				
Anorthoclase ($(Na,K)(Si_3Al)O_8$)							19.1		
Anorthite ($Na[AlSi_3O_8]$-$Ca[Al_2Si_2O_8]$)							17.4		
Sanidine ($K_2(Mg,Fe^{2+})_6$-$4(Fe^{3+},Al,Ti)_0$-$2[Si_6$-$5Al_2$-$3O_{20}](OH,F)_4$)							16.3	5.6	
Baratovite ($Li_2KCa_8Ti_2Si_{12}O_{37}F$)							18.2		
Iron Silicate Hydroxide ($Fe_3Si_2O_5(OH)_4$)								14.0	
Muscovite ($(K,Na)(Al,Mg,Fe)_2(Si_{3.1}Al_{0.9})O_{10}(OH)_2$)								15.1	

Table 3.6 lists all reasonable minerals identified in the surface precipitates for each microfracture sample. Surface precipitates from microfractures MF03 and MF05 were not analyzed by XRD because an insufficient amount of surface precipitate material was recovered from the sample to allow for this analysis. The tables show that the surface precipitates were generally different from the host rock in mineral composition, generally containing carbonates ($CaCO_3$, $CaMg(CO_3)_2$, $FeMgCO_3$), chlorite ($((Mg,Al,Fe)_3(Si,Al)_4O_{10}(OH)_2 \bullet (Mg,Al,Fe)_3(OH)_6$), and quartz ($SiO_2$).

Table 3.6. Microfracture Surface Precipitate Candidate Minerals Based on XRD

Mineral Name (Formula)	Microfracture Number, Mineral Phase Relative Abundance (Search-Match FOM)								
	MF01	**MF02**	**MF04**	**MF06**	**MF07**	**MF08**	**MF09**	**MF10**	**MF11**
Calcite $CaCO_3$	Major (18.2)	Major (1.3)				Major (6.2)	Major (6.0)		Major (5.7)
Magnesian Calcite $(Ca,Mg)CO_3$		Major (14.3)							
Dolomite $CaMg(CO_3)_2$				Major (8.7)			Major (2.8)		
Kutnohorite $Ca(Mn,Mg)(CO_3)_2$				Major (8.8)					
Ankerite $Ca(Fe,Mg)(CO_3)_2$				Major (16.9)			Major (4.7)		
Quartz SiO_2			Major (1.4)	Major (1.0)	Major (3.6)		Major (6.3)	Major (3.1)	
Sanidine $K(AlSi_3)O_8$			Major (7.2)		Major (4.7)			Major (7.4)	
Clinochlore $Mg_3Mn_2AlSi_3AlO_{10}(OH)_8$			Minor (14.3)					Major (8.8)	
Microcline $KAlSi_3O_8$			Minor (16.4)						
Albite $NaAlSi_3O_8$					Major (9.1)				
Calcian Albite $(Na,Ca)Al(Si,Al)_3O_8$				Major (18.6)					
Anorthite $(Ca,Na)(Si,Al)_4O_8$					Major (17.0)				
Sodium Aluminum Silicate $NaAlSiO_4$	Major (20.4)								
Potassium Aluminum Silicate $K_{1+x}xAl_{1+x}Si_{1-x}O_4$					Major (17.9)				
Potassium Mica $KAl_3Si_3O_{11}$							Major (17.1)	Major (3.2)	
Illite $(K,H_3O)Al_2Si_3AlO_{10}(OH)_2$								Major (1.9)	
Badeleyite ZrO_2					Major (10.8)				
Aluminum Iron Zirconium $Al_{1.65}Fe_{0.35}Zr$					Minor (19.0)				
Wustite FeO							Minor (19.9)		

The colors of the microfracture faces varied between samples and were noted as white, blue, green, or black. Microfractures MF01, 02, 06, 07, 08, 09, 10, and MF11 were recorded as white, blue, or green. Microfracture MF04 was black in color. Calcite, dolomite, and other carbonate minerals were dominant in the white surface precipitates and present in the blue and green precipitate, but not identified in the black. The black surface precipitate may have been the host rock.

3.8 Element Speciation of Microfracture Surfaces Based on XPS

XPS was used to identify speciation of surface-associated elements. XPS offers one principal advantage as a surface spectroscopy--- it can provide speciation information for the surface in contact with the microfracture porewater. Mineral identification is limited by the NIST database which can result in the identification of irrelevant candidate minerals because initial searching is based on the binding energy of the fitted peak and the element and photoelectron in question. Because of the high surface sensitivity of the method (e.g., information from the top few nm), many of the minerals identified may reflect recent precipitation from porewater rather than the mineral phases in the bulk of the surface precipitate.

Figure 3.21 shows a typical low resolution survey scan and indicates which elements were identified in this scan of microfracture MF02. Figure 3.22 shows the curve fitting of the C1s photoelectron data from microfracture MF02. The example minerals identified by the NIST database are indicated for the fitted peaks.

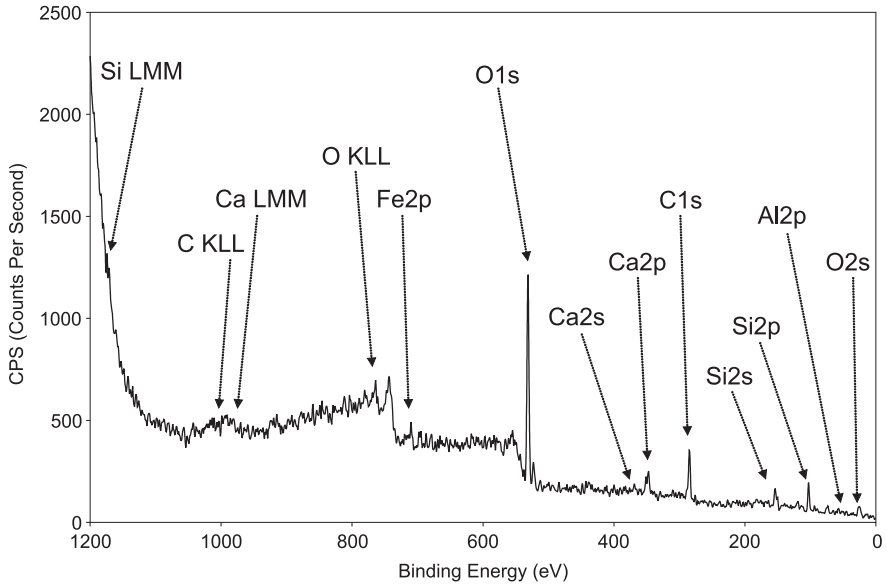

Figure 3.21 Typical XPS low resolution survey scan of microfracture MF02.

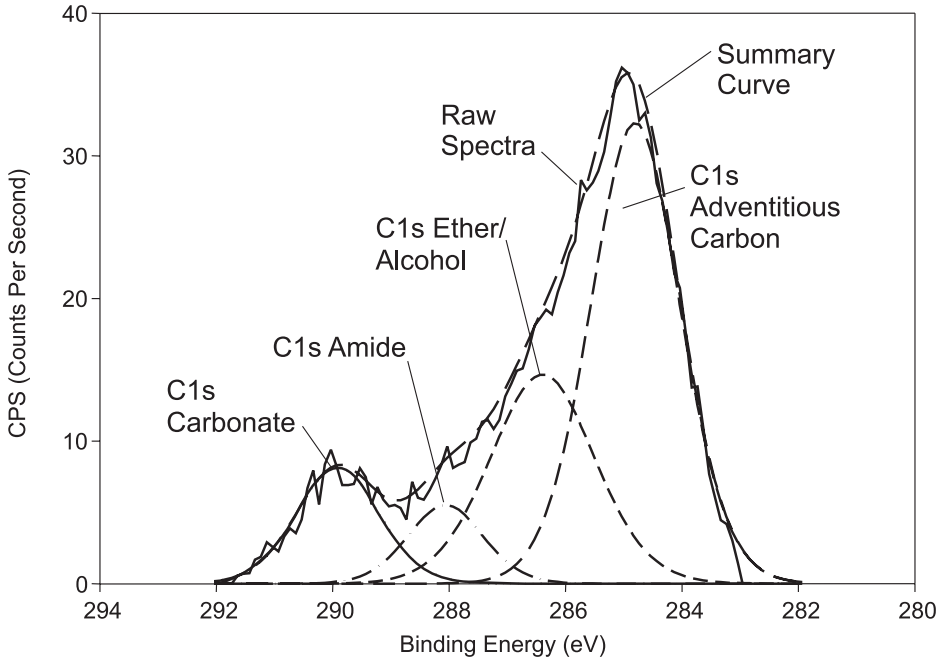

Figure 3.22 Typical component curve fit exercise for the C1s photoelectron from a high resolution scan for microfracture MF02.

Tables 3.7 – 3.15 show the final lists of candidate minerals for each of the microfractures as identified by XPS. Microfractures MF01 and MF11 were not analyzed due to spatial limitations of the sample holder in the vacuum chamber. A high degree of internal consistency was seen in the peak assignments. Most microfracture precipitate surfaces contained simple carbonates (calcite or dolomite), oxyhydroxides of Fe and Al, and silicates.

Table 3.7. Microfracture MF02 - Candidate Minerals by XPS

Element	Binding Energy (eV)	Peak Area %	Candidates (Range +/- 0.3 eV)
Al2p	74.15	100.0	Mol Sieve, Ca form (73.9-74.75)
			Al_2O_3 (71.47-77.3)
			$Al_{0.2}Si_{0.8}O_{2.2}$ (74.4)
C1s	284.80	71.7	Adventitious Carbon (284.8)
	286.53	4.8	NOM Ether or Alcohol (286.4-286.6)
	287.76	7.6	NOM Ketone or Aldehyde (287.5-287.7)
	289.38	15.9	$CaCO_3$ (288.2-290.4)
			$CaMg(CO_3)_2$ (289.8)
			NOM Carboxylic (289.1-289.3)
Ca2p	346.83	46.1	$CaCO_3$ (346.6-347.7)
			CaO (346.1-347.3)
			$CaSiO_3$ (346.7-347.3)
	347.54	15.3	$CaCO_3$ (346.6-347.7)
			$CaMg(CO_3)_2$ (347.3)
			CaO (346.1-347.3)
			$CaSiO_3$ (346.7-347.3)
	348.38	5.3	Mol Sieve, Ca form (347.9-348.6)
Fe2p	708.77	22.7	Fe_3O_4 (708.1-711.4)
			FeS_2 (706.6-708.6)
	709.84	22.5	Fe_3O_4 (708.1-711.4)
			FeO (709.2-710.7)
			Fe_2O_3 (709.9-711.6)
	711.22	35.9	Fe_3O_4 (708.1-711.4)
			Fe_2O_3 (709.9-711.6)
			FeS (710.3-713.6)
			Fe(OH)O (710.8-711.8)
			Fe_2O_3*nH_2O aged HFO (710.7-711.1)
			FeO(OH)*nH_2O (711.1-711.3)
			Fe_2O_3*nH_2O fresh HFO (711.3-711.9)
	714.14	18.8	Unidentified

Element	Binding Energy (eV)	Peak Area %	Candidates (Range +/- 0.3 eV)
O1s	530.14	13.8	FeO (529.8-530.1)
			Fe_2O_3 (529.5-530.3)
			Fe_3O_4 (529.1-530.1)
			CaO (529.4-531.3)
			Al_2O_3 (530.0-532.7)
	530.88	52.8	CaO (529.4-531.3)
			$CaCO_3$ (530.5-531.5)
			Al_2O_3 (530.0-532.7)
			Mol Sieve, Ca form (531.05-532)
	531.76	28.8	$CaCO_3$ (530.5-531.5)
			$CaMg(CO_3)_2$ (531.7)
			$CaSiO_3$ (531.5-531.6)
			Al_2O_3 (530.0-532.7)
			$Fe_2(SO_4)_3$ (531.6-532.2)
			SiO_2 (532-534.3)
	532.82	4.6	Al_2O_3 (530.0-532.7)
			SiO_2 (532-534.3)
Si2p	102.13	59.5	Mol Sieve, Ca form (101.8-102.8)
			$CaSiO_3$ (102.36)
	102.95	40.5	Mol Sieve, Ca form (101.8-102.8)
			SiO_2 (103.2-104.1)
			$Al_{0.2}Si_{0.8}O_{2.2}$ (103.2)

Table 3.8. Microfracture MF03 - Candidate Minerals by XPS

Element	Binding Energy (eV)	Peak Area %	Candidates (Range +/- 0.3 eV)
			Al_2O_3 (71.47-77.3)
			Mol Sieve, Ca form (73.9-74.75)
			Al_2OSiO_4 (74.58-74.8)
	74.54	60.6	$Al_{0.2}Si_{0.8}O_{2.2}$ (74.4)
	75.20	20.3	Al_2O_3 (71.47-77.3)
Al2p	75.92	19.1	Al_2O_3 (71.47-77.3)
	284.80	52.6	Adventitious Carbon (284.8)
	286.39	27.7	NOM Ether or Alcohol (286.4-286.6)
	288.06	7.5	NOM Amide (288.4-288.5)
			$CaCO_3$ (288.2-290.4)
			$CaMg(CO_3)_2$ (289.8)
C1s	289.82	12.2	NOM Carboxylic (289.1-289.3)
			Fe_3O_4 (708.1-711.4)
	709.32	20.3	FeO (709.2-710.7)
			Fe_3O_4 (708.1-711.4)
			FeO (709.2-710.7)
			Fe_2O_3 (709.9-711.6)
			FeS (710.3-713.6)
			Fe(OH)O (710.8-711.8)
			Fe_2O_3*nH_2O aged HFO (710.7-711.1)
	710.93	30.1	FeO(OH)*nH_2O (711.1-711.3)
	712.22	20.3	FeS (710.3-713.6)
	713.93	20.1	Unidentified
Fe2p	716.25	9.1	Unidentified

Element	Binding Energy (eV)	Peak Area %	Candidates (Range +/- 0.3 eV)
			$CaCO_3$ (530.5-531.5)
			CaO (529.4-531.3)
			$CaSiO_3$ (531.5-531.6)
			Al_2O_3 (530.0-532.7)
			Al_2OSiO_4 (531.3-531.88)
			Mol Sieve, Ca form (531.05-532)
	531.36	84.6	Fe(OH)O (530.1-531.8)
O1s	533.08	15.4	SiO_2 (532-534.3)
			$CaSiO_3$ (102.36)
			Mol Sieve, Ca form (101.8-102.8)
	102.34	12.3	Al_2OSiO_4 (102.6-103)
			Al_2OSiO_4 (102.6-103)
			$Al_{0.2}Si_{0.8}O_{2.2}$ (103.2)
	103.32	32.7	SiO_2 (103.2-104.1)
Si2p	104.32	55.0	SiO_2 (103.2-104.1)

Table 3.9. Microfracture MF04 - Candidate Minerals by XPS

Element	Binding Energy (eV)	Peak Area %	Candidates (Range +/- 0.3 eV)
			Al_2O_3 (71.47-77.3)
			Mol Sieve, Ca form (73.9-74.75)
			Al_2OSiO_4 (74.58-74.8)
	74.82	60.9	$Al_2(SO_4)_3$ (74.9)
Al2p	75.69	39.1	Al_2O_3 (71.47-77.3)
	284.80	50.3	Adventitious Carbon (284.8)
	285.46	31.1	NOM Carboxylic Neighbor (285.4-285.6)
	286.26	12.7	NOM Ether or Alcohol (286.4-286.6)
	287.78	4.3	NOM Ketone or Aldehyde (287.5-287.7)
			$CaCO_3$ (288.2-290.4)
C1s	289.49	1.6	NOM Carboxylic (289.1-289.3)
			$CaCO_3$ (346.6-347.7)
	346.62	10.3	CaO (346.1-347.3)
			$CaMg(CO_3)_2$ (347.3)
			$CaCO_3$ (346.6-347.7)
	347.56	52.4	$CaSO_4$ (347.6-348.4)
			Mol Sieve, Ca form (347.9-348.6)
Ca2p	348.64	37.4	$CaSO_4$ (347.6-348.4)
			Fe_2O_3 (709.9-711.6)
			Fe_3O_4 (708.1-711.4)
			FeO (709.2-710.7)
			FeS_2 (706.6-708.6)
	710.50	49.0	FeS (710.3-713.6)
	713.26	30.1	FeS (710.3-713.6)
Fe2p	716.42	20.9	Unidentified

Element	Binding Energy (eV)	Peak Area %	Candidates (Range +/- 0.3 eV)
			FeO (529.8-530.1)
			Fe_3O_4 (529.1-530.1)
			Fe_2O_3 (529.5-530.3)
			CaO (529.4-531.3)
			$CaCO_3$ (530.5-531.5)
	530.43	6.2	Al_2O_3 (530.0-532.7)
			CaO (529.4-531.3)
			$CaCO_3$ (530.5-531.5)
			$CaMg(CO_3)_2$ (531.7)
			Al_2O_3 (530.0-532.7)
			Al_2OSiO_4 (531.3-531.88)
			Mol Sieve, Ca form (531.05-532)
			Al_2O_3 (530.0-532.7)
			SiO_2 (532-534.3)
			SiO (532.5)
			$CaSO_4$ (532-532.9)
	532.49	50.8	$Al_2(SO_4)_3$ (532.4)
O1s	533.49	18.1	SiO_2 (532-534.3)
			SiO (101.7-102.7)
	101.98	12.4	Mol Sieve, Ca form (101.8-102.8)
			SiO (101.7-102.7)
			Mol Sieve, Ca form (101.8-102.8)
	102.84	37.4	Al_2OSiO_4 (102.6-103)
Si2p	103.70	50.2	SiO_2 (103.2-104.1)

Table 3.10. Microfracture MF05 - Candidate Minerals by XPS

Element	Binding Energy (eV)	Peak Area %	Candidates (Range +/- 0.3 eV)
			Al_2O_3 (71.47-77.3)
			Mol Sieve, Ca form (73.9-74.75)
			Al_2OSiO_4 (74.58-74.8)
Al2p	74.45	100.0	$Al_{0.2}Si_{0.8}O_{2.2}$ (74.4)
	284.80	82.1	Adventitious Carbon (284.8)
	286.39	12.9	NOM Ether or Alcohol (286.4-286.6)
			$CaCO_3$ (288.2-290.4)
			$FeCO_3$ siderite (289.6)
C1s	289.45	5.1	NOM Carboxylic (289.1-289.3)
			$CaCO_3$ (346.6-347.7)
			$CaMg(CO_3)_2$ (347.3)
			CaO (346.1-347.3)
	347.57	69.8	$CaSiO_3$ (346.7-347.3)
Ca2p	348.47	30.2	Mol Sieve, Ca form (347.9-348.6)
			Fe_3O_4 (708.1-711.4)
	709.32	7.8	FeO (709.2-710.7)
			$FeCO_3$ siderite (710.4-710.7)
			Fe_2O_3 (709.9-711.6)
			Fe_3O_4 (708.1-711.4)
			FeO (709.2-710.7)
	710.88	87.4	Fe(OH)O (710.8-711.8)
Fe2p	712.41	4.8	$FeSO_4$ (711.2-713.6)

Element	Binding Energy (eV)	Peak Area %	Candidates (Range +/- 0.3 eV)
			FeO (529.8-530.1)
			Fe_3O_4 (529.1-530.1)
			Fe_2O_3 (529.5-530.3)
			FeOOH (529.7-531.7)
	529.66	4.6	CaO (529.4-531.3)
			FeOOH (529.7-531.8)
			CaO (529.4-531.3)
			$CaCO_3$ (530.5-531.5)
			$CaMg(CO_3)_2$ (531.7)
			$CaSiO_3$ (531.5-531.6)
			Al_2O_3 (530.0-532.7)
			Al_2OSiO_4 (531.3-531.88)
	531.44	69.5	Mol Sieve, Ca form (531.05-532)
			$FeCO_3$ siderite (532.1)
			$FeSO_4$ (532.3)
			Al_2O_3 (530.0-532.7)
			Mol Sieve, Ca form (531.05-532)
			SiO_2 (532-534.3)
			SiO (532.5)
			$CaSO_4$ (532-532.9)
	532.31	22.1	$Al_2(SO_4)_3$ (532.4)
O1s	533.80	3.7	SiO_2 (532-534.3)
			$FeSO_4$ (168.7-168.8)
			$Fe_2(SO_4)_3$ (168.6-169.1)
			FeS_2 (161.7-162.9)
	168.72	33.2	$CaSO_4$ (169-170.1)
			$Fe_2(SO_4)_3$ (168.6-169.1)
			$Al_2(SO_4)_3$ (169.5)
S2p	169.41	66.8	$CaSO_4$ (169-170.1)
			SiO (101.7-102.7)
			Mol Sieve, Ca form (101.8-102.8)
			$CaSiO_3$ (102.36)
	102.06	7.8	Al_2OSiO_4 (102.6-103)
			Al_2OSiO_4 (102.6-103)
			$Al_{0.2}Si_{0.8}O_{2.2}$ (103.2)
	103.11	54.1	SiO_2 (103.2-104.1)
	103.52	16.3	SiO_2 (103.2-104.1)
Si2p	103.94	21.8	SiO_2 (103.2-104.1)

Table 3.11. Microfracture MF06 - Candidate Minerals by XPS

Element	Binding Energy (eV)	Peak Area %	Candidates (Range +/- 0.3 eV)
			Al_2O_3 (71.47-77.3)
			Mol Sieve, Ca form (73.9-74.75)
			Al_2OSiO_4 (74.58-74.8)
			$Al_{0.2}Si_{0.8}O_{2.2}$ (74.4)
	74.75	64.6	$Al_2(SO_4)_3$ (74.9)
Al2p	75.65	35.4	Al_2O_3 (71.47-77.3)
	284.80	57.6	Adventitious Carbon (284.8)
	285.66	22.4	NOM Carboxylic Neighbor (285.4-285.6)
	286.92	10.4	NOM Ether or Alcohol (286.4-286.6)
	288.24	4.2	NOM Amide (288.4-288.5)
			$CaCO_3$ (288.2-290.4)
C1s	289.45	5.3	$CaMg(CO_3)_2$ (289.8)
			$CaCO_3$ (346.6-347.7)
			$CaMg(CO_3)_2$ (347.3)
			CaO (346.1-347.3)
	347.32	26.7	$CaSO_4$ (347.6-348.4)
			Mol Sieve, Ca form (347.9-348.6)
	348.13	52.9	$CaSO_4$ (347.6-348.4)
Ca2p	349.09	20.4	Unidentified
			Fe(OH)O (711-711.8)
	710.88	69.8	FeS (710.3-713.6)
Fe2p	714.67	30.2	Unidentified
Mg2p	50.51	100.0	$CaMg(CO_3)_2$ (50.5)

Element	Binding Energy (eV)	Peak Area %	Candidates (Range +/- 0.3 eV)
			Fe(OH)O (530.1-531.8)
			$CaCO_3$ (530.5-531.5)
			CaO (529.4-531.3)
			Mol Sieve, Ca form (531.05-532)
			Al_2O_3 (530.0-532.7)
	531.14	21.1	Al_2OSiO_4 (531.3-531.88)
			$Al_2(SO_4)_3$ (532.4)
			Al_2O_3 (530.0-532.7)
			Al_2OSiO_4 (531.3-531.88)
			$CaSO_4$ (532-532.9)
			Fe(OH)O (530.1-531.8)
			Mol Sieve, Ca form (531.05-532)
	532.10	54.6	SiO_2 (532-534.3)
			$Al_{0.2}Si_{0.8}O_{2.2}$ (532.9)
			$CaSO_4$ (532-532.9)
	533.05	20.6	SiO_2 (532-534.3)
O1s	534.38	3.7	SiO_2 (532-534.3)
	101.80	6.8	Mol Sieve, Ca form (101.8-102.8)
			Mol Sieve, Ca form (101.8-102.8)
	102.87	44.0	Al_2OSiO_4 (102.6-103)
	103.63	41.7	SiO_2 (103.2-104.1)
Si2p	104.69	7.5	Unidentified

Table 3.12. Microfracture MF07 - Candidate Minerals by XPS

Element	Binding Energy (eV)	Peak Area %	Candidates (Range +/- 0.3 eV)
			Al_2O_3 (71.47-77.3)
			Mol Sieve, Ca form (73.9-74.75)
			Al_2O_3 (71.47-77.3)
			$Al_2(SO_4)_3$ (74.9)
	74.07	50.0	Mol Sieve, Ca form (73.9-74.75)
Al2p	74.93	50.0	Al_2OSiO_4 (74.58-74.8)
	284.80	83.0	Adventitious Carbon (284.8)
	285.92	5.8	NOM Carboxylic Neighbor (285.4-285.6)
	286.88	6.2	NOM Ether or Alcohol (286.4-286.6)
			$CaCO_3$ (288.2-290.4)
	288.67	2.3	NOM Amide (288.4-288.5)
C1s	290.28	2.8	$CaCO_3$ (288.2-290.4)
			$CaCO_3$ (346.6-347.7)
			$CaMg(CO_3)_2$ (347.3)
	347.29	24.1	CaO (346.1-347.3)
			$CaCO_3$ (346.6-347.7)
	347.88	57.3	Mol Sieve, Ca form (347.9-348.6)
Ca2p	348.55	18.5	Mol Sieve, Ca form (347.9-348.6)
			Fe_3O_4 (708.1-711.4)
			FeO (709.2-710.7)
	709.6	27.2	Fe_2O_3 (709.9-711.6)
			Fe_3O_4 (708.1-711.4)
			Fe_2O_3 (709.9-711.6)
			FeS (710.3-713.6)
			FeO (709.2-710.7)
			Fe(OH)O (710.8-711.8)
			Fe_2O_3*nH_2O aged HFO (710.7-711.1)
			FeO(OH)*nH_2O (711.1-711.3)
	711.37	38.2	Fe_2O_3*nH_2O fresh HFO (711.3-711.9)
			FeS (710.3-713.6)
	713.15	25.5	$Fe_2(SO_4)_3$ (713.3)
Fe2p	715.41	9.1	Unidentified
Mg2p	50.79	100.0	$CaMg(CO_3)_2$ (50.5)

Element	Binding Energy (eV)	Peak Area %	Candidates (Range +/- 0.3 eV)
			Fe_2O_3 (529.5-530.3)
			Fe_3O_4 (529.1-530.1)
			Fe(OH)O (530.1-531.8)
			CaO (529.4-531.3)
			$CaCO_3$ (530.5-531.5)
			Mol Sieve, Ca form (531.05-532)
	530.39	6.0	Al_2O_3 (530.0-532.7)
			$CaCO_3$ (530.5-531.5)
			$CaMg(CO_3)_2$ (531.7)
			Fe(OH)O (530.1-531.8)
			Al_2O_3 (530.0-532.7)
	531.64	54.8	Al_2OSiO_4 (531.3-531.88)
			SiO_2 (532-534.3)
	532.58	35.0	Al_2OSiO_4 (531.3-531.88)
O1s	534.07	4.3	SiO_2 (532-534.3)
			$FeSO_4$ (168.7-168.8)
			$Fe_2(SO_4)_3$ (168.6-169.1)
	169.01	49.6	$CaSO_4$ (169-170.1)
S2p	170.03	50.4	$CaSO_4$ (169-170.1)
			SiO_2 (103.2-104.1)
			$Al_{0.2}Si_{0.8}O_{2.2}$ (103.2)
			Al_2OSiO_4 (102.6-103)
Si2p	103.08	100.0	Mol Sieve, Ca form (101.8-102.8)

Table 3.13. Microfracture MF08 - Candidate Minerals by XPS

Element	Binding Energy (eV)	Peak Area %	Candidates (Range +/- 0.3 eV)
			Al_2O_3 (71.47-77.3)
			Mol Sieve, Ca form (73.9-74.75)
	74.23	9.9	$Al_{0.2}Si_{0.8}O_{2.2}$ (74.4)
			Al_2O_3 (71.47-77.3)
			$Al_2(SO_4)_3$ (74.9)
	74.93	25.6	Al_2OSiO_4 (74.58-74.8)
Al2p	75.22	64.4	$Al_2(SO_4)_3$ (74.9)
	284.8	62.8	Adventitious Carbon (284.8)
	285.83	27.3	NOM Carboxylic Neighbor (285.4-285.6)
	287.8	2.5	NOM Ketone or Aldehyde (287.5-287.7)
			$CaCO_3$ (288.2-290.4)
	288.93	2.5	NOM Carboxylic (289.1-289.3)
C1s	290.38	4.9	$CaCO_3$ (288.2-290.4)
			$CaMg(CO_3)_2$ (347.3)
			$CaCO_3$ (346.6-347.7)
	347.30	16.6	CaO (346.1-347.3)
			$Ca(OH)_2$ (347.7)
			$CaCO_3$ (346.6-347.7)
	347.67	25.5	Mol Sieve, Ca form (347.9-348.6)
			Mol Sieve, Ca form (347.9-348.6)
Ca2p	348.24	57.9	$CaSO_4$ (348)
			Fe_3O_4 (708.1-711.4)
			FeO (709.2-710.7)
			Fe_2O_3 (709.9-711.6)
	710.24	25.52	FeS (710.3-713.6)
			FeS (710.3-713.6)
	712.15	36.98	Fe_2O_3*nH_2O fresh HFO (711.3-711.9)
	713.92	24.06	Unidentified
Fe2p	715.79	13.44	Unidentified
Mg2p	50.73	100.0	$CaMg(CO_3)_2$ (50.5)

Element	Binding Energy (eV)	Peak Area %	Candidates (Range +/- 0.3 eV)
			Fe(OH)O (530.1-531.8)
			CaO (529.4-531.3)
			$CaCO_3$ (530.5-531.5)
			$CaMg(CO_3)_2$ (531.7)
	530.59	1.4	Al_2O_3 (530.0-532.7)
			Fe(OH)O (530.1-531.8)
			$CaMg(CO_3)_2$ (531.7)
			Al_2O_3 (530.0-532.7)
			Al_2OSiO_4 (531.3-531.88)
			Mol Sieve, Ca form (531.05-532)
			SiO_2 (532-534.3)
	531.98	12.0	$CaSO_4$ (532-532.9)
			SiO_2 (532-534.3)
			$CaSO_4$ (532-532.9)
			$Al_2(SO_4)_3$ (532.4)
			$Al_{0.2}Si_{0.8}O_{2.2}$ (532.9)
	532.38	55.6	Al_2O_3 (530.0-532.7)
			$Al_{0.2}Si_{0.8}O_{2.2}$ (532.9)
			$CaSO_4$ (532-532.9)
O1s	532.98	31.0	Al_2O_3 (530.0-532.7)
			Al_2OSiO_4 (102.6-103)
			$Al_{0.2}Si_{0.8}O_{2.2}$ (103.2)
	103.12	61.0	SiO_2 (103.2-104.1)
			$Al_{0.2}Si_{0.8}O_{2.2}$ (103.2)
	103.45	14.4	SiO_2 (103.2-104.1)
Si2p	104.06	25.5	SiO_2 (103.2-104.1)

Table 3.14. Microfracture MF09 - Candidate Minerals by XPS

Element	Binding Energy (eV)	Peak Area %	Candidates (Range +/- 0.3 eV)
			Al_2O_3 (71.47-77.3)
			Mol Sieve, Ca form (73.9-74.75)
			Al_2OSiO_4 (74.58-74.8)
			$Al_2(SO_4)_3$ (74.9)
Al2p	74.72	100.0	$Al_{0.2}Si_{0.8}O_{2.2}$ (74.4)
	284.8	59.6	Adventitious Carbon (284.8)
	286.14	3.1	NOM Ether or Alcohol (286.4-286.6)
	287.04	1.6	Unidentified
	288.53	1.5	NOM Amide (288.4-288.5)
C1s	290.33	34.2	$CaCO_3$ (288.2-290.4)
			$CaMg(CO_3)_2$ (347.3)
			$CaCO_3$ (346.6-347.7)
			CaO (346.1-347.3)
	347.35	58.2	$CaSO_4$ (347.6-348.4)
			$CaCO_3$ (346.6-347.7)
			$Ca(OH)_2$ (347.7)
			Mol Sieve, Ca form (347.9-348.6)
	347.63	34.3	$CaSO_4$ (347.6-348.4)
Ca2p	348.72	7.5	Mol Sieve, Ca form (347.9-348.6)
			Fe_3O_4 (708.1-711.4)
	709.44	40.4	FeO (709.2-710.7)
			Fe_3O_4 (708.1-711.4)
			Fe_2O_3 (709.9-711.6)
			FeS (710.3-713.6)
			Fe(OH)O (710.8-711.8)
			$FeO(OH)*nH_2O$ (711.1-711.3)
	711.51	33.0	$Fe_2O_3*nH_2O$ fresh HFO (711.3-711.9)
Fe2p	714.14	26.6	Unidentified

Element	Binding Energy (eV)	Peak Area %	Candidates (Range +/- 0.3 eV)
			$Ca(OH)_2$ (531.2)
			$CaCO_3$ (530.5-531.5)
			Fe(OH)O (530.1-531.8)
			Mol Sieve, Ca form (531.05-532)
			$(Mg/Fe)SiO_4$ (531.2)
	530.97	13.4	Al_2O_3 (530.0-532.7)
			$(Mg/Fe)SiO_3$ (531.7)
			Al_2O_3 (530.0-532.7)
			Al_2OSiO_4 (531.3-531.88)
			$CaCO_3$ (530.5-531.5)
			$CaMg(CO_3)_2$ (531.7)
			$CaSO_4$ (532-532.9)
			Fe(OH)O (530.1-531.8)
			Mol Sieve, Ca form (531.05-532)
	531.80	81.2	SiO_2 (532-534.3)
O1s	533.36	5.4	SiO_2 (532-534.3)
			Al_2OSiO_4 (102.6-103)
			$Al_{0.2}Si_{0.8}O_{2.2}$ (103.2)
	103.22	68.8	SiO_2 (103.2-104.1)
	103.81	17.0	SiO_2 (103.2-104.1)
Si2p	104.12	14.2	SiO_2 (103.2-104.1)

Table 3.15. Microfracture MF10 - Candidate Minerals by XPS

Element	Binding Energy (eV)	Peak Area %	Candidates (Range +/- 0.3 eV)
Al2p	74.18	11.7	Al_2O_3 (71.47-77.3)
			Mol Sieve, Ca form (73.9-74.75)
			$Al_{0.2}Si_{0.8}O_{2.2}$ (74.4)
	75.12	70.4	Al_2O_3 (71.47-77.3)
			$Al_2(SO_4)_3$ (74.9)
	75.63	17.8	Al_2O_3 (71.47-77.3)
C1s	284.8	69.9	Adventitious Carbon (284.8)
	286.73	10.4	NOM Ether or Alcohol (286.4-286.6)
	288.62	2.3	NOM Amide (288.4-288.5)
	290.21	17.4	$CaCO_3$ (288.2-290.4)
Ca2p	347.31	20.3	$CaCO_3$ (346.6-347.7)
			$CaMg(CO_3)_2$ (347.3)
			CaO (346.1-347.3)
			$CaSiO_3$ (346.7-347.3)
			$CaSO_4$ (347.6-348.4)
	347.69	48.0	$Ca(OH)_2$ (347.7)
			$CaCO_3$ (346.6-347.7)
			Mol Sieve, Ca form (347.9-348.6)
			$CaSO_4$ (347.6-348.4)
	348.23	31.7	Mol Sieve, Ca form (347.9-348.6)
			$CaSO_4$ (347.6-348.4)
Fe2p	709.97	25.8	Fe_3O_4 (708.1-711.4)
			FeO (709.2-710.7)
			Fe_2O_3 (709.9-711.6)
			FeS (710.3-713.6)
	711.62	33.1	Fe_3O_4 (708.1-711.4)
			Fe_2O_3 (709.9-711.6)
			FeS (710.3-713.6)
			Fe(OH)O (710.8-711.8)
			Fe_2O_3*nH_2O fresh HFO (711.3-711.9)
	712.85	21.4	FeS (710.3-713.6)
	714.55	19.7	Unidentified
Mg2p	50.81	100.0	$CaMg(CO_3)_2$ (50.5)

Element	Binding Energy (eV)	Peak Area %	Candidates (Range +/- 0.3 eV)
O2p	530.04	6.5	Al_2O_3 (530.0-532.7)
			CaO (529.4-531.3)
			Fe(OH)O (530.1-531.8)
			Fe_2O_3 (529.5-530.3)
			Fe_3O_4 (529.1-530.1)
			FeO (529.8-530.1)
	531.67	82.7	$CaCO_3$ (530.5-531.5)
			$CaMg(CO_3)_2$ (531.7)
			$CaSiO_3$ (531.5-531.6)
			Fe(OH)O (530.1-531.8)
			Al_2O_3 (530.0-532.7)
			Al_2OSiO_4 (531.3-531.88)
			Mol Sieve, Ca form (531.05-532)
	532.71	10.8	SiO_2 (532-534.3)
			$CaSO_4$ (532-532.9)
			Al_2O_3 (530.0-532.7)
			$Al_2(SO_4)_3$ (532.4)
			$Al_{0.2}Si_{0.8}O_{2.2}$ (532.9)
Si2p	103.16	67.4	Al_2OSiO_4 (102.6-103)
			$Al_{0.2}Si_{0.8}O_{2.2}$ (103.2)
			SiO_2 (103.2-104.1)
	103.87	32.6	SiO_2 (103.2-104.1)

Carbonates were the dominant minerals observed on the microfracture surfaces. Candidate minerals included siderite ($FeCO_3$), calcite ($CaCO_3$), and dolomite (($CaMgCO_3)_2$). Generally, calcite was more prevalent than dolomite and in almost all cases, was identified with the $Ca2p_{3/2}$, C1s and O1s photoelectrons.

Iron was also detected in high resolution scans of all the microfracture surfaces. A number of candidate minerals were identified, including both ferrous (e.g., siderite, pyrrhotite (FeS), wüstite ((FeO)), ferric minerals (e.g., goethite (α-FeOOH)), hematite (Fe_2O_3), aged hydrous ferric oxide ($Fe_2O_3 \bullet 1.57\ H_2O$, limonite (($Fe_2O_3 \bullet nH_2O$)), and mixed ferrous and ferric minerals (e.g., magnetite ((Fe_3O_4)). The presence of ferric minerals such as goethite indicated that iron reduction was possible on the microfracture surface. The presence of Fe(II) minerals such as siderite is perhaps evidence of Fe(III) reduction.

Sulfur was directly detected in some of the high resolution spectra for microfractures MF05 and MF07. Species assignments were for sulfates ($Fe_2(SO_4)_3$). It was also indirectly detected in Fe spectra. The assignment of FeS or FeS_2 was tentative, largely based on the fact that pyrites were seen with petrography and SEM/EDAX.

In all cases, organic carbon was also observed on the microfracture surfaces. Some of this carbon was adventitious (e.g., at 284.80 eV) and an artifact of analysis under high vacuum. Though the presence of TCE or its daughter products on the surface was suspected using SIMS at extremely low detection limits (see Section 3.10), the detection limit of XPS for the C1s photoelectron for sorbed TCE was likely not sufficiently low enough to detect the TCE. The bulk of the carbon is at much higher binding energy values typical of NOM functional groups. NOM can form conditioning films on inorganic surfaces in aquatic settings (Leis *et al.*, 2000). The sorption of NOM model compounds to mineral surfaces has also been demonstrated (Evanko and Dzombak, 1998). On the microfracture surfaces, ethers, alcohols, ketones, aldehydes, amides, and carboxylic acids were observed that are characteristic of a variety of humic substances (Monteil-Rivera *et al.*, 2000) and aquatic NOM (Boughriet *et al.*, 1992) on particulates from the Seine River.

3.9 Packer Water Characterization and Geochemical Modeling

Straddle packers were used to isolate the bore holes over 1.52 m (5.0 ft) intervals where some of the microfractures were situated. The packer intervals (28 L) were purged for at least two interval volumes prior to sample collection. During purging, conductivity and pH were monitored and would stabilize over the purge cycle. The packer intervals were purged for at least two interval volumes prior to sample collection (termed packer water). In some cases (Clusters 2 and 4), this purging required 2 or 3 days of continuous pumping. Four sampling events were conducted (Table 3.16). Microfracture MF04 (Cluster 2) was sampled on July 20, 2002. Microfractures MF05-MF06-MF07 (Cluster 3) were sampled on April 15, 2002, and May 29, 2002, and microfractures MF10-MF11 (Cluster 4) were sampled on June 3, 2003. Cluster 1 in borehole BBC5 (microfractures MF01-MF02-MF03) was not sampled as the location was too close to the bottom of the telescoping casing.

The sample collection times and volumes collected after purging for the samples were 3 h and 5.4 L for microfracture MF04 (Cluster 2) on July 20, 2002, 1.45 h and 224 L for microfractures MF05-MF06-MF07 (Cluster 3) on April 15, 2002, and 0.83 h minutes and 224 L for microfractures MF05-MF06-MF07 (Cluster 3) on May 29, 2002, and 1.167 h and 14.35 L for microfractures MF10-MF11 (Cluster 4) on June 3, 2003. These differential volumes reflect the different hydraulic conductivities across the intervals. The longer sample collection times for Clusters 2 and 4 suggest that these intervals had relatively low hydraulic conductivities.

Generally, the packer waters were typical of groundwater temperatures (10°C). Observed pH values (8.79-9.56) were in agreement with the alkaline nature of the water (131-190 mg/L alkalinity as $CaCO_3$). Dissolved oxygen values were low (0.4 to 2.5 mg/L), but conditions were not always anaerobic. Non-purgeable organic carbon concentrations were generally low (0.82-1.66 mg/L). As noted previously, it is not clear what signatures were derived from the microfracture network relative to the more open fracture system comprising the bulk of the sample collected in the straddle packers.

Eh values as determined by polished platinum electrode were mildly reducing (+160 to -208 eV). Interestingly, both Fe^{2+} and Fe^{3+} were observed, usually both at low concentrations. This suggested that the biogeochemistry of the system was poised around the Fe^{2+}/Fe^{3+} couple. Geochemical modeling with Visual MINTEQ with a Fe^{2+}/Fe^{3+} couple at the observed concentrations showed the system to have mildly reducing Eh values based on Nernst equation calculations, suggesting that the observed Eh values in the field were reasonable estimates.

Table 3.16. Packer Water Characterizations

Well			BBC5	BBC5	BBC5	BBC6
Interval			95.4 - 100.4 ft	121.4 - 126.4 ft	121.4 - 126.4 ft	112.0 - 117.0 ft
Cluster			2	3	3	4
Applicable Microfractures			MF04	MF05-MF07	MF05-MF07	MF10-MF11
Sampling Date	Units	DL	7/20/02	4/15/02	5/29/02	6/3/03
Packer Volume Collected	L	-	5.4	224	224	14.35
Collection Time	h	-	3	1.45	0.83	1.167
Temperature	°C	-	10.29	ND	10.33	NA
pH	pH	-	9.56	8.79	9.00	8.94
Conductivity	mS	-	0.56	0.60	0.60	0.56
DO	mg/L	0.1	2.5	0.40	0.40	0.7
Eh	mV	-	-84.8	NA	160.9	-208.8
TCE	µg/L	2	43	110	NA	33
trans-1,2-DCE	µg/L	2	45	76	NA	37
cis-1,2,DCE	µg/L	2	320	480	NA	340
1,1-DCE	µg/L	1	ND	2	NA	1
VC	µg/L	2	14	25	NA	15
Acetone	µg/L	10	120	ND	NA	ND
Methane	µg/L	4	260	360	NA	170
Ethane	µg/L	4	ND	ND	NA	ND
Ethene	µg/L	1	11	15	NA	6
NPDOC	mg C/L	0.10	NA	0.80	0.82	1.66
NH_4^+	µg N/L	5	ND	ND	ND	72
Alkalinity (as $CaCO_3$)	mg/L	1	131	158	190	165
Cl^-	mg/L	4	14	11	12	12
SO_4^{2-}	mg/L	10	110	110	120	120
NO_3^-	mg/L	0.1	ND	ND	ND	ND
S^{2-}	mg/L	0.004	ND	ND	ND	ND
Fe^{2+}	mg/L	0.10	0.10	0.10	0.10	0.1
Al	mg/L	0.1	0.76	ND	0.09	ND
As	mg/L	0.04	ND	ND	0.01	ND
Ba	mg/L	0.002	0.007	ND	0.02	ND
B	mg/L	0.3	ND	ND	0.03	ND
Ca	mg/L	1	3.6	7.40	8.60	3.8
Cr	mg/L	0.001	0.02	ND	0.002	ND
Cu	mg/L	0.001	NA	ND	0.002	ND
Fe	mg/L	0.05	0.18	0.30	0.11	0.11
Pb	mg/L	0.02	ND	ND	ND	ND
Mg	mg/L	1	1.6	2.90	3.20	1.3
Mn	mg/L	0.05	ND	ND	0.03	ND
K	mg/L	1	6.8	8.00	6.00	4.4
Si	mg/L	0.3	4.4	4.10	5.20	7
Na	mg/L	10	77	110.00	120.00	140
Zn	mg/L	0.1	0.07	ND	0.02	ND

DL = Detection Limit; ND = Not Determined; NA = Not Analyzed; - = Not relevant.

The presence of dissolved oxygen at relatively low concentrations around 0.5 mg/L and detectable Fe(II) concentrations in the packer samples warrant some discussion. Similar occurrences of detectable Fe(II) and low dissolved oxygen concentrations have been observed at TCE-contaminated field sites before (Yager *et al.*, 1997). The system was poised at the redox boundary between Fe(II) oxidation and Fe(III) reduction. However, it is not clear if the system is at pseudo-equilibrium. The data suggest that perhaps either Fe(II) oxidation was kinetically constrained or that mixing of two sample types (more oxic open fracture groundwater with small volumes of more reducing microfracture network porewater) may have occurred. The high O_2 value of the one sample (2.5 mg/L) could also reflect improper packer operation in that case. Fe(II) oxidation in controlled aqueous solutions (with respect to pH, CO_2 partial pressures, ionic strength) is typically first order with respect to Fe(II) and O_2 concentrations and second order with respect to OH^- concentrations. Oxidation rates are dramatically slower at lower pH values (<5). The presence of reactive surfaces, solution-phase complexants, and microbial catalysts can also influence aqueous oxidation rates. Abiotic reductive dissolution of Fe(III) oxides is also kinetically constrained by slow detachment of the Fe(II) ion.

No nitrates or sulfides were detected in the packer water samples. The dominant form of sulfur in the packer water samples was sulfate (110 to 120 mg/L), suggesting that sulfate reduction was probably not occurring in the open fracture system or that sulfate was not limiting in the open fracture system. Pyrite (FeS_2) was found in all 11 of the host rock samples with petrography. Pyrite was also seen in some of the microfracture samples (microfractures MF02, MF04, MF05, and MF09) with SEM/EDAX. This method has the ability to detect mineral associations at depths of up to 1 µm. In a few cases, pyrite was inferred with XPS based on Fe spectra in microfractures MF04, MF05, MF06, MF08, and MF09 though S was seen on only two microfracture surfaces (microfractures MF05, MF07) and both spectra indicated oxidized sulfur was present. This spectroscopy is a surface sensitive technique (penetration depths of ca. 10 Å). No significant levels of S were detected by SIMS, another surface spectroscopy (ejection depths of ca. 100 Å). These data collectively suggest that much of the source of sulfate in the system may have been derived from pyrite oxidation, but less pyrite was available at the microfracture surface, either by depletion or by occlusion from calcite-dominated surface precipitates, for oxidation.

In all cases where it was analyzed, dissolved methane was detected (170 to 360 µg/L) in the packer waters during three sampling events. These data suggest that some level of methanogenesis is occurring in the open fracture system or in the microfracture networks. The import of more surficial overburden waters containing methane cannot be discounted. The surficial and groundwater hydrology is discussed in greater detail in Volume 3: Fractured Rock Hydraulics.

In terms of contaminants, *cis*-1,2 DCE was by far the dominant chlorinated compound (320 to 480 µg/L). Some *trans*-1,2 DCE was observed as well, but at low concentrations (37-76 µg/L). Very little 1,1-DCE was observed (ND to 2 µg/L). TCE concentrations were moderate (33 to 110 µg/L). VC concentrations were also low (14-25 µg/L). Interestingly, ethene was detected (ND to 11 µg/L). These data suggest that some mechanism of biodegradation of TCE had occurred, resulting in some of the TCE becoming completely dechlorinated. However, much of the contaminant had undergone only partial dechlorination to DCE.

The packer water composition was dominated by Na, Cl, K, Ca, Mg, Si, and carbonate. Other constituents (e.g., Al, Fe, Mn, As) were present at lower concentrations. As shown in Table 3.17, the likely controlling solids for these packer waters were carbonates, quartz, and simple oxyhydroxides (e.g. $Fe(OH)_3$, FeOOH, $Al(OH)_3$, AlOOH). These phases were all identified by XPS, XRD, and petrography. If detection limit values for S^{2-} were introduced into the model, saturation index values for amorphous FeS and mackinawite (FeS) were slightly under saturated (e.g., saturation indices of -0.749 to -1.399).

As noted earlier, the use of thermodynamic models to interpret solid phase control of dominant dissolved constituents, buffer systems, redox reactions, and related geochemical processes must be done with some caution. Analyses suggest that with respect to simple acid-base reactions (e.g., carbonate dissolution, hydrolysis reactions), the microfracture network may be closer to pseudo-equilibrium. The principal buffer in network, dominated by carbonates from calcite and Ca-Mg carbonates, is found as a dominant mineral in the closed microfractures, open microfractures, and on the borehole walls of the wells.

The bulk of the data suggests that the presence of methane, Fe(II), hydrogen, and low DO values points to some type of reduced environments somewhere in the fracture system, likely within the microfracture networks. This is discussed later in Section 3.13.

Table 3.17. Candidate Controlling Solid Minerals in Packer Waters Identified by Geochemical Modeling

Mineral	Formula	MF04 (7/20/02)		MF05-MF07 (4/15/02)		MF05-MF07 (5/29/02)		MF1—MF11 (6/3/03)	
		Log IAP	SI	Log IAP	SI	Log IAP	SI	Log IAP	SI
$Al(OH)_3$ (Soil)	$Al(OH)_3$	-	-	8.36	0.07	8.73	0.44	-	-
$BaHAsO_4 \bullet H_2O$	$BaHAsO_4 \bullet H_2O$	-	-	-25.39	-0.75	-	-	-	-
Barite	$BaCO_3$	-	-	-10.14	-0.16	-10.61	-0.63	-	-
Boehmite	AlOOH	-	-	8.36	-0.22	8.73	0.16	-	-
$CaCO_3 \bullet H_2O$	-	-	-	-7.81	-0.67	-7.93	-0.79	-8.26	-1.12
Calcite	$CaCO_3$	-8.10	0.38	-7.81	0.68	-7.93	0.55	-8.26	0.22
Dolomite (dis.)	$CaMg(CO_3)_2$	-16.36	0.19	-15.76	0.76	-15.93	0.61	-16.73	-0.19
Dolomite (ord.)	$CaMg(CO_3)_2$	-16.36	0.73	-15.76	1.31	-15.93	1.16	-16.73	0.36
$Fe(OH)_2$ (am.)	-	11.55	-1.94	11.92	-1.57	12.86	-0.63	11.82	-1.67
$Fe(OH)_2$ (c)	-	11.55	-1.34	11.92	-0.97	12.86	-0.03	11.82	-1.07
Gibbsite (c)	$Al(OH)_3$	-	-	8.36	0.62	8.73	0.99	-	-
Goethite	FeOOH	-	-	-	-	7.25	6.76	-	-
Halloysite	$Al_2SiO_2(OH)_6 \bullet H_2O$	-	-	9.20	-0.37	9.54	-0.04	-	-
Huntite	$CaMg_3(CO_3)_4$	-	-	-31.75	-1.78	-31.94	-1.97	-	-
Hydrozincite	$Zn_5(CO_3)_2(OH)_6$	-	-	6.79	-1.90	8.94	0.24	-	-
Imogolite	$Al_2SiO_4(OH)_2 \bullet H_2O$	-	-	12.96	-0.04	13.50	0.50	-	-
K-Jarosite	$Fe_3(SO_4)(OH)_5 \bullet 2H_2O$	-12.30	-1.30	-	-	-	-	-	-
Magnesite	$MnCO_3$	-	-	-7.98	-0.52	-8.00	-0.54	-8.47	-1.01
$MnCO_3$ (am.)	-	-	-	-11.06	-0.56	-	-	-	-
Quartz	SiO_2	-3.84	0.16	-3.76	0.24	-3.97	0.03	-3.62	0.38
Rhodochrosite	$MnCO_3$	-	-	-11.06	-0.05	-	-	-	-
Sepiolite	$Mg_2Si_3O_8 \bullet 2H_2O$	15.35	-0.41	16.47	0.71	17.47	1.71	15.87	0.11
Sepiolite (am.)	$Mg_2Si_3O_8 \bullet 2H_2O$	-	-	-	-	17.47	-1.31	-	-
Siderite	$FeCO_3$	-10.15	0.441	-9.93	0.66	-9.83	0.76	-10.03	0.56
SiO_2 (am, gel)	-	-3.84	-1.13	-3.76	-1.05	-3.97	-1.25	-3.62	-0.91
SiO_2 (am, ppt)	-	-3.84	-1.10	-3.76	-1.02	-3.97	-1.23	-3.62	-0.88
Smithsonite	$ZnCO_3$	-	-	-11.75	-0.85	-11.83	-0.92	-	-
Zincite	ZnO	-	-	10.10	-1.13	10.86	-0.37	-	-
$Zn(OH)_2$	$Zn(OH)_2$ (beta)	-	-	10.10	-1.65	10.86	-0.89	-	-
$ZnCO_3$	-	-	-	-11.75	-0.95	-11.82	-1.02	-	-
$ZnCO_3 \bullet H_2O$	-	-	-	-	-	-11.75	-1.49	-	-

IAP = Ion Activity Product
SI = Saturation Index

3.10 Mass Fragment Fingerprints of Microfracture Surfaces

The static SIMS work conducted on microfracture MF03 was preliminary, but illustrative of the organics and contaminants present. Significant problems were experienced with sample charging.

Negative (0-50 atomic mass units) and positive mass fragments (0-50, 50-100 atomic mass units) observed with SIMS are shown in Figures 3.23, 3.24, and 3.25, respectively. A number of mass fragments associated with dominant isotopes of major elements were observed. These included Fe, Na, Si, Mg, K, Ca, and Ti, all of which were seen with other spectroscopic methods. Additionally, Ga was seen as it was implanted during ion bombardment. Isotope mass distributions observed generally reflected their natural abundances: $^{28}Si^+/^{29}Si^+/^{30}Si^+$ of 92/5/3 %, $^{39}K^+/^{41}K^+$ of 93/7 %, $^{40}Ca^+/^{44}Ca^+$ of 97/2 %, and $^{35}Cl^-/^{37}Cl^-$ of 76/24 %.

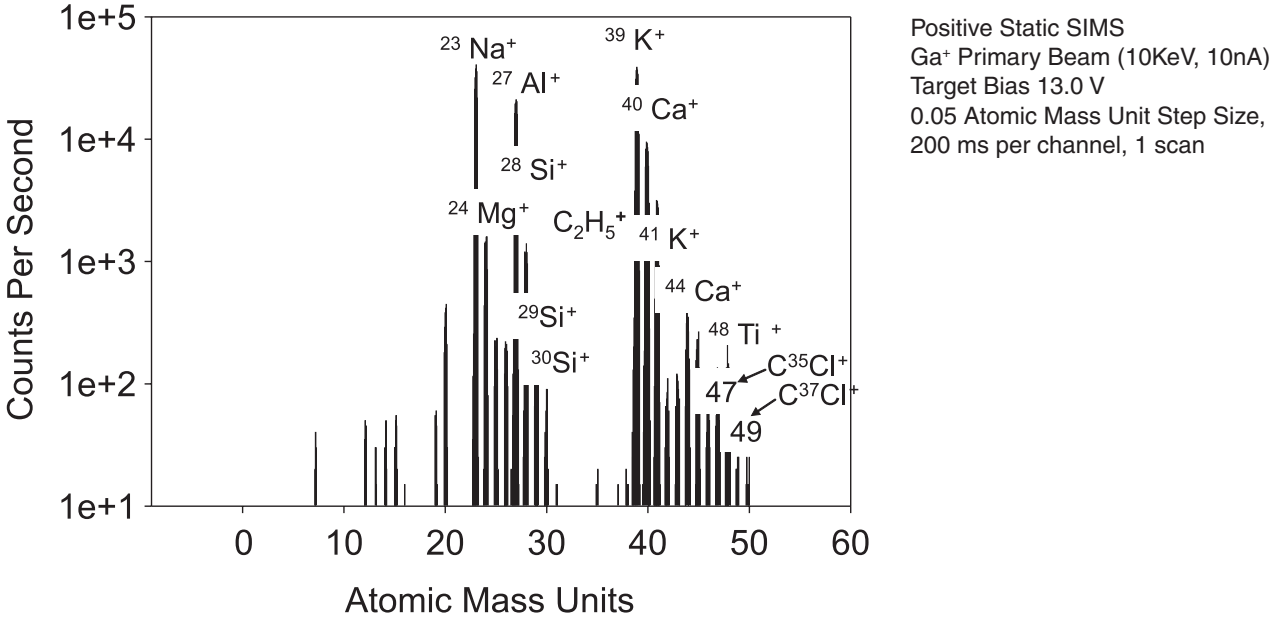

Figure 3.23 SIMS negative mass fragment (0-50 atomic mass units) fingerprint. The sample was microfracture MF03.

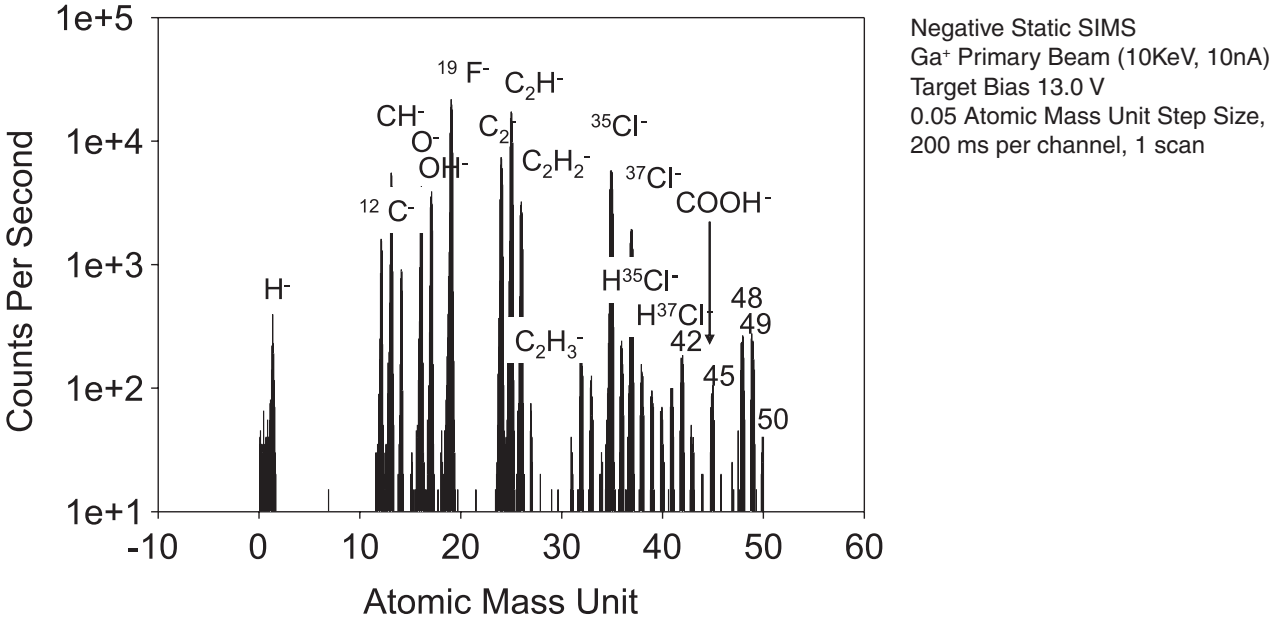

Figure 3.24 SIMS positive mass fragment (0-50 atomic mass units) fingerprint. The sample was microfracture MF03.

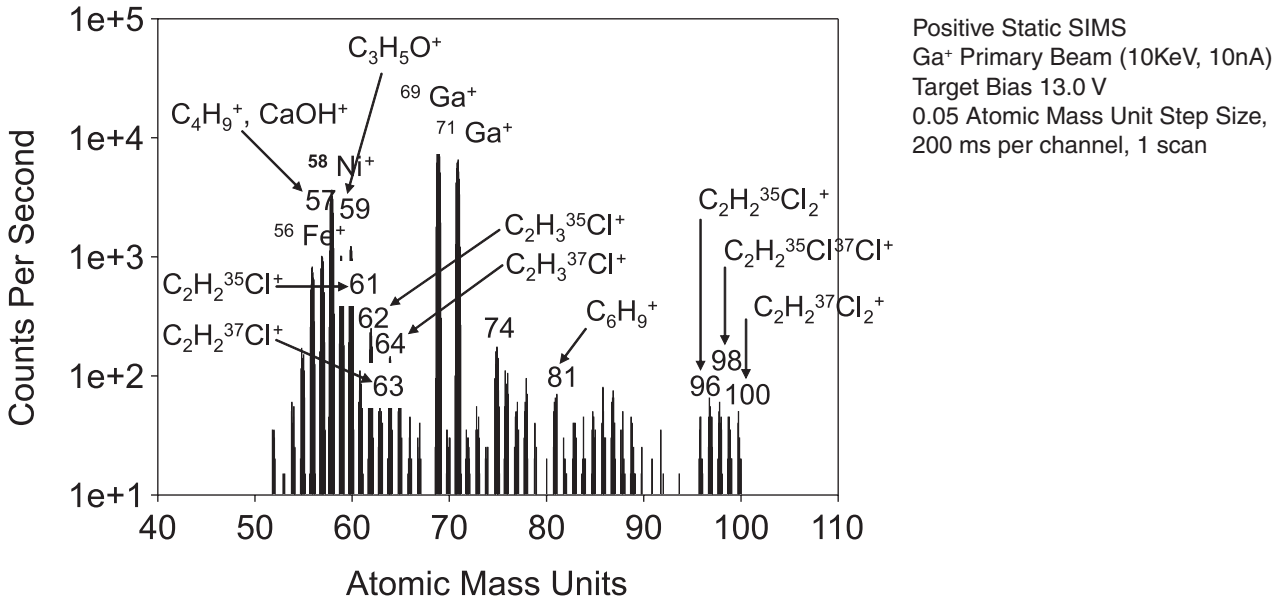

Figure 3.25 SIMS positive mass fragment (50-100 atomic mass units) fingerprint. The sample was microfracture MF03.

Organic carbon was also observed in the spectra. This was not surprising given the propensity of NOM to form conditioning films on wetted mineral surfaces (Leis *et al*., 2000; Evanko and Dzombak, 1998). NOM is comprised of humic substances; typically, humic acids, fulvic acids, and humin (Hayes, 1997). Fulvic acids have lower molecular weights, higher oxygen to carbon ratios, and higher ratios of acidic functional groups than humic acids. Humin is more strongly mineral bound than either humic or fulvic acids. All three components represent a continuum of molecular weights and functional group distributions. Typically, humic substances originate from proteins, carbohydrates, lipids, waxes, aliphatics, and aromatics. These compounds have defined functional groups or moieties: carboxylic acids, phenols, alcohols, amines, imides, Schiff bases, esters, ethers, and S- and P-moieties (Stevenson, 1994). A number of mass fragments typical of NOM were seen on the microfracture sample (Leis *et al*., 2000). These included CH^-, CH_2^-, C_2H^-, $C_2H_2^-$, $C_2H_3^-$, $COOH^-$, $C_4H_9^+$, $C_3H_5O^+$, and $C_6H_9^+$.

If either TCE, DCE, or VC were present on the surface, then a number of mass fragments would be evicted under ion bombardment with SIMS. C-Cl fragments observed from microfracture MF03 included $H^{35}Cl^-$, $H^{37}Cl^-$, $C^{35}Cl^+$, $C^{37}Cl^+$, $C_2H_2{}^{35}Cl^+$, $C_2H_2{}^{37}Cl^+$, $C_2H_3{}^{35}Cl^+$, $C_2H_3{}^{37}Cl^+$, $C_2H_2{}^{35}Cl_2{}^+$, $C_2H_2{}^{35}Cl^{37}Cl^+$, and $C_2H_2{}^{37}Cl_2{}^+$. All of these fragments were observed by Briggs *et al*. (2002) using TOF SIMS on poly (vinyl chloride) polymers. Only one expected fragment was not observed: $CH^{35}Cl^+/CH^{37}Cl^+$. This is reasonably strong evidence that TCE, DCE, or VC was present on the microfracture surface.

The mechanism of partitioning of TCE, DCE, or VC to the microfracture surface is not known. However, nonionic organic contaminants such as TCE, DCE, and VC are non-polar and hydrophobic and can sorb to hydrophobic NOM. NOM was present on the surface, but the mass of sorbed NOM as well as its degree of surface coverage is not clearly known (e.g., some of the SEM work suggests that sorbed NOM is patchy and visible as blankets). Partitioning could have occurred if the non-polar TCE will dissolve into the non-polar fraction of the NOM. TCE has an aqueous solubility of $10^{-2.04}$ mol/L and a K_{ow} of $10^{2.42}$. VC has an aqueous solubility of $10^{-1.35}$ mol/L and a K_{ow} of $10^{0.60}$. Organic matter-water partition coefficients (K_{om}) or organic carbon-water partition coefficients (K_{oc}) can be used to describe the partitioning of halogenated organics to NOM. Generally, a strong, positive linear-free energy relationship exists between K_{om} or K_{oc} and K_{ow} (Schwarzenbach *et al*., 1993). The more hydrophobic TCE would expect to partition more to NOM than VC. K_{om} values for TCE are theoretically expected to be $10^{1.5}$ to $10^{2.5}$ based on the inverse linear relationship between aqueous solubility and K_{om}. Therefore, the C-Cl fragments observed are more likely to have come from hydrophobically-partitioned TCE.

Garbarini and Lion (1986) studied the partitioning of TCE to many types of NOM and found a strong positive relationship between the NOM oxygen content and carbon content to TCE partitioning. They found K_{oc} values ranging from 2.0 (cellulose) to 120 (lignin), depending on the NOM. K_{oc} values for TCE partitioning to humic acids were around 57-65. Xing *et al*. (1996) also have documented TCE sorption to soil, peat, humic acid, and silica. More recently, Chiou and Kile (1998) found non-linear adsorption of TCE to peat-based soils at very low TCE aqueous concentrations (< 15% of saturation). They reported a TCE K_{om} of 49.

In related work, Zhu *et al*. (2003) studied the partitioning of halogenated organics to soils and clays precoated with a cationic surfactant. The degree of partitioning to the solid phase depended on the degree of coverage of the surfactant. Partitioning to the sorbed surfactant was stronger than the partitioning into the organic matter in the soil particles.

3.11 Porosity and Pore Size Distribution of Host Rock

The core material was generally insufficiently porous to be characterized by MIP. Samples, despite apparent sealed microfractures on the surface, did not allow the minimum mercury intrusion volumes needed to gather reliable data. Samples with larger, less sealed fractures broke apart during the cube cutting process and so could not be characterized.

Of the 10 sample cubes from borehole BBC5 analyzed by MIP, one sample was sufficiently porous to provide reliable mercury intrusion data. Figure 3.26 shows the cumulative porosity and the differential pore size distribution, respectively, collected from this sample cube. Peaks on the differential pore size distribution plot corresponded to threshold pore widths and represented pore diameters where an increased amount of Hg was intruded into the sample. This plot indicated the relative population of pores of a given width based on the increased Hg intrusion at that pore width.

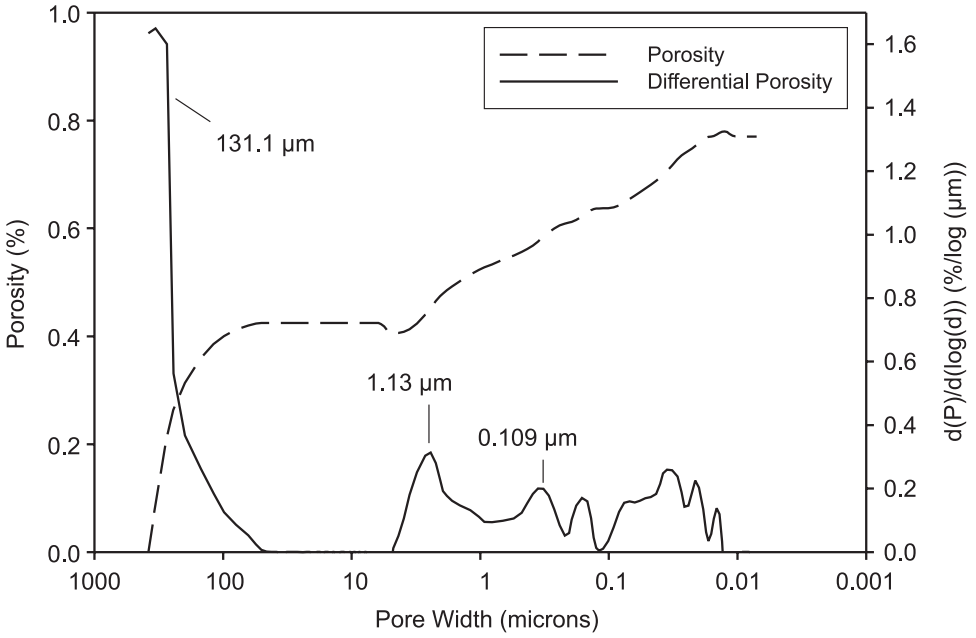

Figure 3.26 MIP cumulative porosity and pore size distribution for borehole BBC5 host rock specimen.

The MIP data for this sample showed three significant pore throat sizes, reflected as peaks in the plot in Figure 3.26. These pore throat sizes were 131.1 µm, 1.136 µm, and 0.109 µm. The sample was found to have a porosity of 0.8% and density of 2.65 g/cm^3. These data are typical for the type of rock that was studied (e.g., Guillot *et al.*, 2000; Colwell *et al.*, 1997; Fredrickson *et al.*, 1997; Onstott *et al.*, 2003). Estimated permeabilities for this sample, based on the method of Swanson (1981), were < 1 µDarcy.

In the case of the rock sample from borehole BBC5, the observed pore throat sizes were more similar to those observed by Colwell *et al.* (1997) than those reported by Onstott *et al.* (2003). The borehole BBC5 sample was found to have a porosity of 0.8%, a value closer to those reported by Onstott *et al.* (2003). The borehole BBC5 host rock sample had an estimated permeability of < 1 µDarcy, a value closer to values reported by Onstott *et al.* (2003) than those reported by Colwell *et al.* (1997).

3.12 Microbes Identified on Microfractures

Amplification with specific primer sets (Table 3.18) showed the presence of both bacteria and *Archaea* in all of the borehole BBC5 microfracture samples. Positive results were also observed for *Dehalococcoides* sp., except for microfracture MF06, and sulfate-reducing bacteria, except microfractures MF05 and MF07. *Geobacteraceae* were observed only on microfracture MF04. No *Desulfuromonas* species were detected with the primer set used. These genes, amplified by polymerase chain reaction, are for partial 16S rDNA sequence for these prokaryotic groups and do not imply active metabolism. In the case of the *Archaea* domain, the presence of 16S rDNA could indicate the presence of methanogens. Further, in the case of iron-reducing bacteria, the *Geobacteraceae* 16S rDNA does not include all genera of iron-reducing bacteria.

Table 3.18. Presence or Absence of Prokaryotic Groups on Borehole BBC5 Microfracture Surfaces as Determined by Amplification with Specific Primer Sets

Microfracture	Specific Primer Set					
	Bacteria	*Geobacteracea*	SRB	*Dehalococcoides* sp.	*Desulfuromonas* sp.	Archaea
01	+	-	+	+	-	+
02	+	-	+	+	-	+
03	+	-	+	+	-	+
04	+	+	+	+	-	+
05	+	-	-	+	-	+
06	+	-	+	-	-	+
07	+	-	-	+	-	+
SRB = Sulfate Reducing Bacteria						

A culture-independent approach, denaturing gradient gel electrophoresis molecular fingerprinting using bacterial primers, was used to determine the diversity of prokaryotic microbial communities found associated with the fracture surfaces of borehole BBC5 microfractures and their mineral deposits. The community profiles of the polymerase chain reaction-amplified 16S rDNA (Figure 3.27) showed the number of denaturing gradient gel electrophoresis bands observed varied between microfractures. The number of discrete bands was distributed as follows for the indicated microfractures: MF01: 23, MF02: 23, MF03: 25, MF04: 27, MF05: 12, MF06: 10, and MF07: 7.

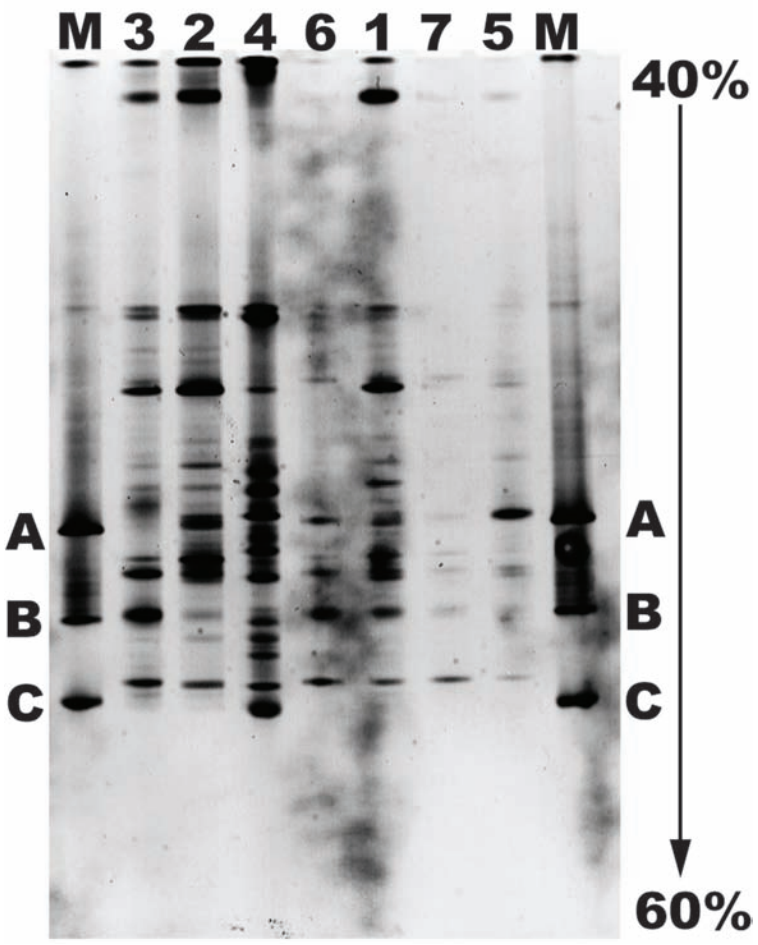

Figure 3.27 Polymerase chain reaction-denaturing gradient gel electrophoresis bacterial community profiles of borehole BBC5 microfractures MF01-MF07. Lanes labeled (M) include markers (A) *Shewenalla algae* BrY, (B) *Bacillus subtilus*, (C) *Streptomyces griseus*.

The moderate number of bands observed indicates a significant level of microbial diversity within and between the microfracture surfaces. The banding patterns from each microfracture surface were analyzed by unweighted paired group method with arithmetic averages to determine the similarity of the samples (Figure 3.28). The dendrogram shows the similarity coefficient of the samples. Only the banding patterns of microfractures MF01 and MF03 were shown to be similar, with a similarity coefficient of 0.82. All other samples showed significantly different banding patterns, indicating the bacterial communities on the fracture surfaces were, in most cases, compositionally unique. It is important to note the lack of similarity in community composition, despite their relative spatial proximity of microfractures (even within a cluster) and the general similarity of surface precipitates among microfractures. The degree of hydraulic connection between microfractures MF01 and MF03 is unknown.

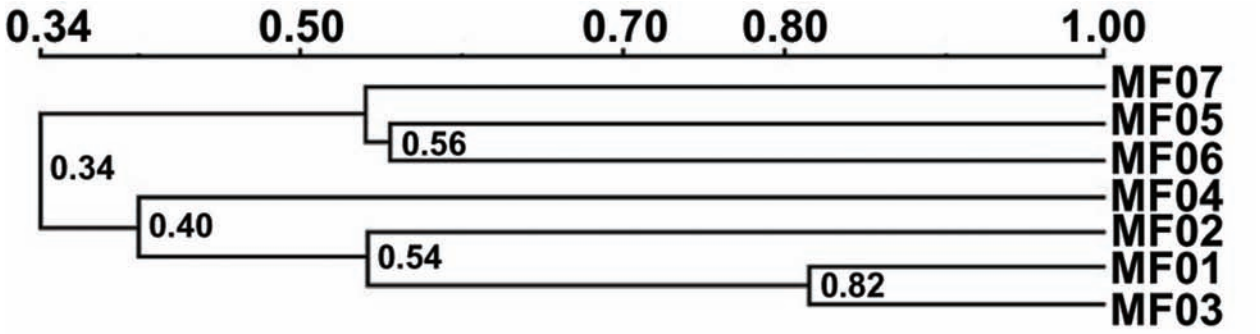

Figure 3.28 Cluster analysis of the denaturing gradient gel electrophoresis banding patterns of borehole BBC5 microfracture surfaces based on the position of bands using unweighted paired group method with arithmetic averages. The numbers denote the similarity coefficients. Values > 0.75 are deemed similar in community composition.

The observed banding patterns in the denaturing gradient gel electrophoresis gel differ from banding patterns from boreholes BBC5 and BBC6 packer water samples (See Volume 4: Fractured Rock Microbiology.). The banding patterns for unattached prokaryotes in the packer waters show remarkable consistency and little variation (See Volume 4.) and likely represent the blending of significant volumes of open fracture water with small volumes of microfracture network water. These data suggested that the communities on the microfracture surfaces were specialized and perhaps adapted to a surface-associated (thigmotrophic) existence.

Bands from microfracture MF04 were excised, purified, and sequenced to identify the closest phylogenetic group. Partial sequences of the V3 region of the 16S rDNA (~500bp) of the denaturing gradient gel electrophoresis bands showed the closest phylogenetic affiliation with an uncultured bacterial clone P39B-52 (98% sequence identity; #AF414577), a uranium mine sediment isolate; *Ultrabacterium* strain D-7, (99% sequence identity; #AB008505), a soil isolate; and an uncultured bacterial clone RA13C10 (99% sequence identity; #AF407400), a chlorobenzene-contaminated groundwater isolate. These data suggested that the microbes associated with the microfracture surfaces were similar to those found in other subsurface environments (Pedersen, 1997).

Given the large number of bands and the suggestion of diverse metabolic potential on the microfracture surfaces, the identity of the remaining bands is important. It might help to elucidate syntrophic relationships, dependency upon mineral abundance for redox reactions and mineral cycling, and the nature of the advantages offered by surface growth.

3.13 Relationship Between Packer Water Samples and Microfracture Geochemical Environment

The packer water sampling and characterization of microfractures from boreholes BBC5 and BBC6 represent a spatially discrete and very small sub-sample from the entire contaminated bedrock plume at Site 32. Further, the pump and treat remediation strategy instituted in 1997 likely altered initial discrete redox zonation within the plume by changing the hydraulic conditions (e.g., drawing groundwater back towards the sheetpile). Comparison of packer water and microfracture snapshots may not necessarily reflect temporal and spatial trends within the plume because they were, by necessity, collected at different times. Further, the installation of boreholes introduced hydraulic connections that may not have existed prior to drilling and will most likely have impacted the chemical signature of the packer water samples. Nevertheless, it is useful to compare the results from packer water samples and the likely microenvironments that existed in the porewater and microfracture surfaces within the microfracture network.

Even with the assumption of a relatively high microfracture-specific surface area, the total volume of porewater available in the microfractures was likely many orders of magnitude less than those volumes collected during packer water sample collection, particularly for highly transmissive intervals (e.g., Cluster 2, 3). This suggested that open fractures likely contributed the most significant proportion (e.g., > 99%) to the packer water samples. The estimated permeability of the microfracture network in the host rock (< 1 µd) also implied that diffusive, rather than advective, transport was probably occurring between the microfracture network and the more open fracture system. As a result, discerning the exact composition of the microfracture porewaters using packer sampling is difficult and subject to some uncertainty for quantitative estimation.

Some evidence suggested that the porewaters in contact with the microfracture surfaces were somewhat similar to the packer water and thus connected (though not necessarily similar from a geochemical perspective). For example, TCE or its transformation products were possibly identified on the one microfracture surface that was analyzed (microfracture MF03) using SIMS and in the packer water for that packer water interval, suggesting similar groundwater moving through them. Additionally, *Dehalococcoides* sp. primers were identified on a number of microfracture surfaces. This suggested that TCE or its transformation products had migrated from the open fracture system to the tighter microfracture network and that *Dehalococcoides* sp. present there may have been able to metabolize it. Finally, the dominant minerals such as carbonates identified on the microfracture surfaces were generally in local pseudo-equilibrium, as determined by the geochemical model Visual MINTEQ, with aqueous constituents measured in the packer waters, suggesting either some degree of communication between the packer water and the microfracture network or, more likely, the presence of similar minerals in the microfracture network and open fracture system.

A stronger body of evidence suggests that the packer water was not very representative of the local biogeochemical environment in the microfracture network. The microfracture network may have been more reducing than the open fracture system based on the preponderance of primer data. Primers for *Archaea* (including anaerobic methanogens) were found on all seven of the microfracture surfaces tested, yet the concentrations of methane in the packer samples were relatively low (170-360 µg/L). Primers for anaerobic *Dehalococcoides* sp. were found on six of the seven microfractures. Primers for anaerobic sulfate-reducing bacteria were found on five of the seven microfractures, yet no sulfide was quantified in the packer waters, and the packer waters were dominated by very high levels of sulfate (110-120 mg/L). If the packer waters were reflective of clearly delineated zones associated with methanogenesis or sulfate reduction, higher levels of methane or sulfide might be expected.

One reason for the low cell densities on the microfracture surfaces and the reducing conditions in the microfractures was the low levels of NPDOC in the groundwater at Site 32. This, in turn, limits H_2 production which is required as an electron donor for *Dehalococcoides* sp. In contrast, Wiedemeier *et al*. (1997) observed 1,420 to 1,600 µg/L of methane in the methanogenic zone of a sandy aquifer TCE contaminant plume at Plattsburgh Air Force Base. NPDOC levels were up to 80 mg/L. Chapelle (1997) observed up to 8,000 µg/L of methane in the methanogenic zone and up to 60 mg/L sulfide in the sulfate reducing zone of a TCE contaminant plume in a shallow, sandy aquifer at the Cecil Field Naval Air Station in Florida. While NPDOC levels were not reported, hydrocarbon contaminants were also present in the contaminant plume.

Perhaps the most likely scenario is that the microfracture network, by virtue of its smaller volume, reduced communication with the open fracture system, and likely mass transfer limitations into and out of the microfractures from the open fracture system, does not significantly contribute to the contaminant or biogeochemical signatures seen in the packer waters collected under fairly transmissive conditions for fractured bedrock at the site. The region around Cluster 3 (borehole BBC5) had a borehole transmissivity of 0.139 m^2/d (1.5 ft^2/d). The general region around Cluster 4 (borehole BBC6) had a borehole transmissivity of 0.185 m^2/d (2 ft^2/d). Based on the observed permeability of the borehole BBC5 host rock, water movement through the microfractures was unlikely to have been this high.

3.14 Likely Terminal Electron Accepting Processes in the Open Fracture System

The succession of terminal electron accepting processes in order of decreasing redox potential and free energy yield is generally: oxygen reduction, nitrate reduction, manganese reduction, Fe(III) reduction, sulfate reduction, and methanogenesis (McGuire *et al*., 2000). Using the general guide provided by Chapelle *et al*. (2003), the following observations were noted about the packer water samples.

While H_2 was not measured in the packer samples, it was measured in borehole BBC6 in regions within 3 m (10 ft) to sampled packer intervals. Sampling occurred on June 24-26, 2003. Concentrations ranged from 2.2 to 7.3 nM. H_2 was detected at 32.6 m (107 ft) at concentrations of 2.7 nM (depths relative to top of telescoping casing). It was also detected at 40.53 m (133 ft) at concentrations of 7.3 nM. It was also detected at 54.5 m (179 ft) at concentrations of 2.2 nM.

The presence of H_2 is indicative of hydrogenotrophic fermentive reactions that can result in a pool of H_2 that can have signature steady state concentrations with high turnover. The H_2 values observed for borehole BBC6 suggested sulfate reduction and possible methanogenesis (Chapelle *et al.*, 2003) at 40.53 m (133 ft). However, the high levels of sulfate (up to 120 mg/L), the absence of sulfide (<0.04 mg/L), and the low NPDOC in the packer water samples suggested that sulfate reduction was not the dominant terminal electron accepting process in the open fracture system. Interestingly, hydraulic testing showed a clear connection between 32.6 m (107 ft) and 54.5 m (179 ft) where lower methane concentrations were present and little to no connection at 40.53 m (133 ft) where methane was higher.

The dissolved oxygen concentrations in the packer samples ranged from 0.4 to 2.5 mg/L. Three of the four determinations were low (0.4, 0.4, 0.7 mg/L). The high value may be erroneous. These data suggested that DO was depleted in the open fracture system. The low values indicated a system dominated by nitrate, ferric iron, sulfate, or carbon dioxide reduction (Chapelle *et al.*, 2002). When compared and contrasted with the NPDOC data (concentrations ranging from 0.80 to 1.66 mg/L), the open fracture system seemed poised for sulfate reduction, but was likely limited by organic carbon bioavailability. At this time, the exact nature of the NPDOC (e.g., molecular weight distribution, hydrophobicity/hydrophilicity, aromaticity, functional group distribution, biodegradability) nor its source has been determined.

The supply of fixed nitrogen was limited in the packer samples. Both ammonium and nitrate concentrations were very low to non-detect. These data suggest that nitrate reduction was not a dominant terminal electron accepting process in the open fracture system. This was expected, given the low levels of N in the system.

Fe(II) and Fe(III) were present as dissolved constituents in the packer samples at modest concentrations. A comparison between measured Eh values using a polished platinum inert electrode and Ag/AgCl reference electrode in the packer water samples and predicted Eh values based on Nernst Equation calculations using the Fe(II)/Fe(III) couple with Visual MINTEQ modeling, showed the following: for microfracture MF04 (Cluster 2) on July 20, 2002, -84.8 mV versus -126.5 mV; microfractures MF05-MF06-MF07 (Cluster 3) on May 29, 2002, 160.9 mV versus -61.1 mV; and microfractures MF10-MF11 (Cluster 4) on June 3, 2003, -208.8 mV versus -48.47 mV. There are limitations to using platinum electrodes, mostly related to reactivity on the electrode's surface. This can be minimized by polishing. The electrode is responsive to the predominant aqueous electron-donating and electron-receiving species in solution and may not be responsive to kinetically-restrained reactions. Given these limitations, these data suggested that the observed redox conditions and dissolved iron species were in general agreement and that ferric iron reduction might have been the dominant terminal electron accepting process in the open fracture system.

Yager *et al.* (1997) developed similar conclusions about a TCE plume in highly fractured and weathered dolomite at a contaminated bedrock site near Niagara, NY. They observed pH values of 6.6 to 6.9, alkalinity values of 250 to 340 mg/L as $CaCO_3$, low DO values (<0.01 mg/L), fairly low values of NPDOC (1.4 to 3.2 mg/L), high levels of chloride (21-790 mg/L) and sulfate (500 to 1800 mg/L, largely influenced by gypsum dissolution in the formation), and detectable levels of sulfide (0.13 to 75 mg/L), Fe(II) (<0.2 to 1 mg/L), H_2 (0.26 to 1.4 nM), methane (1.5 to 37 mg/L), as well as TCE, DCE, VC, and ethene. The observed levels of H_2 and Fe(II) were used to determine that Fe(III) reduction was the dominant terminal electron accepting process at the site.

The presence of methane in the packer water samples indicated that methanogenesis was occurring somewhere in the open fracture system, most likely in the microfracture network. However, as noted previously in Section 3.14, it was not a likely dominant terminal electron accepting process in the open fracture system. Methane is soluble in water and can be readily transported. Its presence in the packer samples may not be indicative of local generation.

3.15 Likely Terminal Electron Accepting Processes in the Microfracture Network

Surface spectroscopies, particularly XPS, were used to look at element speciation on microfracture surfaces where adherent microbes were present and where porewaters were in contact with those surfaces. These spectroscopic methods were useful in deducing which terminal electron accepting process might dominate in the microfracture network, particularly as related to C, S, and Fe metabolism. For instance, Haveman *et al.* (1999) characterized the microbiology and geochemistry of groundwater samples from deep igneous rock sites in Finland dominated by gneiss, granodiorite, and Fe-rich granite. They found that free-swimming, sulfate-reducing bacteria in the fracture porewater predominated where iron sulfide fracture-filling minerals were present. Further, they found that free-swimming, iron-reducing bacteria in the fracture porewater were dominant where iron hydroxide fracture minerals were prevalent. Such relations may exist between adherent microbes and the dominant mineral forms on the BBC microfracture surfaces.

Both organic and inorganic C were ubiquitously observed on all microfracture surfaces. The bioavailability of the sorbed NOM is not known; however, its localized concentration on the microfracture surface was quite high relative to the

concentrations found in solution in the packer water samples. Using XPS, C concentrations in the top few atomic layers of the microfracture surfaces ranged from 18,555 to 330,000 mg/kg (data not shown). The majority (>80%) of this C was organic. This carbon may have been available for aerobic or anaerobic respiration. The inorganic carbon, also present at locally high concentrations on the microfracture surfaces, was a ready source of inorganic C for methanogenesis.

Sulfur was also observed on some of the microfracture surfaces (microfractures MF05, MF07). Concentrations were much less significant than those seen for C or Fe. Using XPS, S concentrations ranged from 5,000 to 16,000 mg/kg on two microfracture surfaces (data not shown). Most of the observed species were S (VI) and not (-II). Sulfides were below detection limits in the packer water samples (< 0.04 mg/L). No likely candidate controlling solids were observed for sulfate minerals with Visual MINTEQ. If detection limit values for S^{2-} were introduced into the model, then saturation index values for amorphous FeS and mackinawite (FeS) were slightly under saturated (-0.749 to -1.399). This indicated that the packer waters might be close to pseudo-equilibrium for FeS as a controlling solid if actual sulfide concentrations were just below detection limits. If sulfate reduction was occurring on the microfracture surfaces, then no spectroscopic evidence of a solid precipitate was detected using the various spectroscopies.

Iron was a dominant microfracture surface element on all microfracture surfaces. Using XPS, Fe concentrations ranged from 25,300 to 201,600 mg/kg (data not shown). Both Fe(II) and Fe(III) candidate minerals were identified on the microfracture surfaces, including pyrrhotite (FeS), wüstite (FeO), goethite (α-FeOOH), hematite (Fe_2O_3), aged hydrous ferric oxide ($Fe_2O_3 \bullet 1.57\ H_2O$), limonite ($Fe_2O_3 \bullet nH_2O$)), and mixed ferrous and ferric minerals (e.g., magnetite (Fe_3O_4)). Some oxidized Fe species (e.g., goethite (α-FeOOH)) are known substrates for iron-reducing bacteria (Lower *et al*., 2001; Dong *et al*., 2003). Iron-reducing bacteria are capable of reducing poorly crystalline Fe(III) oxide minerals during the redox reaction (Shelobolina *et al*., 2003). The spatial prevalence of Fe, as well as its situation in the top few nm of the microfracture surfaces, suggested that Fe(III) was available for iron-reducing bacteria. The occurrence of Fe(II) on the microfracture surface may reflect bacteria-mediated Fe(III) reduction reactions. The spectroscopic characterization of the microfracture surfaces points to Fe(III) reduction as perhaps a dominant terminal electron accepting process in the microfracture network.

Based on these spectroscopic observations, all three likely terminal electron accepting processes (ferric iron, sulfate, or carbonate reduction) may have been occurring. Further, some degree of redox zonation may occur spatially within the microfracture network depending on the network's proximity to the open fracture system, diffusivities, and diffusion gradients.

3.16 Microfracture Surface Speciation and Adherent Microbial Population Metabolism and Diversity

Table 3.19 summarizes the known speciation information for C, Fe, and S species within or on the microfracture surface precipitates. These three elements were likely candidates for terminal electron accepting processes. The speciation information was related to adherent microbial population community structure and to identified primers for microfractures MF01 through MF07.

There is generally good agreement between SEM-EDAX, XRD, and XPS about identification of C, S, and Fe with the microfracture surface precipitates on their surfaces. However, the observed population diversity as determined by denaturing gradient gel electrophoresis community similarity indices or denaturing gradient gel electrophoresis banding numbers cannot be precisely related to the speciation of any of the three elements on the microfracture surfaces. The situation is analogous for the primers that were identified on the microfracture surfaces. In all cases, carbonates were seen on microfracture surfaces where *Archaea* primers were seen. In two of four cases where sulfate-reducing bacteria primers were seen, oxidized or reduced S was seen. In the one case where iron-reducing bacteria primer was seen, oxidized and reduced Fe was detected. The problem stems from a lack of spatial resolution in identifying direct association between adherent microbial populations and the heterogeneous distribution of minerals on the microfracture surfaces.

The fact that the attached microbial populations differed in composition from the unattached populations (See Volume 4: Fractured Rock Microbiology.) suggested some role of the microfracture surface in influencing community diversity. Haveman *et al*. (1999) found a similar relationship. For example, they observed that free-swimming, sulfate-reducing bacteria predominated in groundwater samples from 200- to 950-m depths in four igneous rock sites in Finland where iron sulfide fracture filling minerals are common. The iron-reducing bacteria were the main population in one site where iron sulfide fracture minerals were not present, but iron hydroxide fracture minerals predominated. They observed that fracture filling minerals were a better indicator of microbial populations than was groundwater chemistry.

Table 3.19. Prokaryotic Groups on Borehole BBC5 Microfracture Surfaces Relative to Fe, S and C

Microfracture #	Petrography	SEM/EDAX	XRD	XPS	$[C]_s$ (mg/kg)	$[Fe]_s$ (mg/kg)	$[S]_s$ (mg/kg)	Primers
01	Insufficient Thickness for Modal Analysis	None	$CaCO_3$	Sample Size Constraints	–	–	–	Bacteria Archaea *Dehalococcoides* SRB
02	$CaCO_3$ $CaMg(CO_3)_2$ $(Fe,Mg)CO_3$ FeS_2	Fe-S	$CaCO_3$ $(Ca, Mg)CO_3$	$CaCO_3$ $CaMg(CO_3)_2$ α-Fe_2O_3 α-FeOOH Fe_3O_4	185,000	97,000	None Observed	Bacteria Archaea *Dehalococcoides* SRB
03	Insufficient Thickness for Modal Analysis	Si-Al-K-Mg-Fe-O Al-Mg-Fe-O Fe-S	Insufficient Surface Precipitate	$CaCO_3$ $CaMg(CO_3)_2$ α-Fe_2O_3 α-FeOOH $FeOOH \bullet nH_2O$ $Fe_5HO_8 \bullet 4H_2O$ Fe_3O_4	99,000	103,000	None Observed	Bacteria Archaea *Dehalococcoides* SRB
04	Insufficient Thickness for Modal Analysis	Al-Mg-Fe-O Fe-S	None observed	$CaCO_3$ $Fe_5HO_8 \bullet 4H_2O$ $FeOOH \bullet nH_2O$ $FeCO_3$	330,000	25,000	None Observed	Bacteria Archaea *Dehalococcoides* *Geobacteracea*
05	Insufficient Thickness for Modal Analysis	Si-Al-Fe-O Si-Fe-O Fe-S	Insufficient Surface Precipitate	$CaCO_3$ α-Fe_2O_3 α-FeOOH $FeCO_3$ $FeSO_4$ $KFe_3(OH)_6(SO_4)_2$	203,900	201,600	5,000	Bacteria Archaea *Dehalococcoides*
06	$CaCO_3$ $CaMg(CO_3)_2$ $(Fe,Mg)CO_3$	Ca-Mg-Fe-O Fe-O	$CaMg(CO_3)_2$ $Ca(Mn,Mg)(CO_3)_2$ $Ca(Fe,Mg)(CO_3)_2$	$CaCO_3$ $CaMg(CO_3)_2$ α-Fe_2O_3 α-FeOOH $Fe_5HO_8 \bullet 4H_2O$ $FeCO_3$	199,000	122,600	None Observed	Bacteria Archaea SRB
07	Insufficient Thickness for Modal Analysis	Si-Al-Fe-O	None	$CaCO_3$ $CaMg(CO_3)_2$ α-Fe_2O_3 α-FeOOH $FeOOH \bullet nH_2O$ $Fe_5HO_8 \bullet 4H_2O$ Fe_3O_4 $FeSO_4$	136,000	164,900	16,000	Bacteria Archaea *Dehalococcoides*

Based on the SEM-EDAX work, the spatial heterogeneity of minerals was quite high on the microfracture surface. Mineral grain sizes were on the order of tens of µm. While minerals may be common to all observed microfracture surfaces, their relative spacing and proximity to each other and to surface topography were quite varied. It may be that the biopatches that were observed with SEM reflected a more localized microbial community response to microfracture surface speciation. The proximity between microbes and mineral surfaces of metabolic value usually requires direct contact, frequently requiring cell membrane enzyme availability at the mineral surface to facilitate electron transfer between the mineral surface and electron transport proteins (See Rogers *et al*., 1999; 2001; Lower *et al*., 2001; Shelobolina *et al*., 2003.). The level of resolution of SEM, SEM-EDAX, and XPS was not high enough to discern such spatial relationships though such relations were likely. Hence, different areas on a microfracture surface may exhibit different terminal electron accepting processes depending on the minerals present with differences occurring over small distances (tens of µm).

3.17 Role of Microfracture Surfaces in TCE Transformation and Microbial Ecology

Biodegradation transformation products of TCE dechlorination were found in the packer water samples, including *cis*-1,2 DCE, *trans*-1,2 DCE, VC, and ethene. In each packer water sample, *cis*-1,2 DCE was most prevalent (37-480 µg/L), followed by *trans*-1,2 DCE (37-76 µg/L), VC (14 to 25 µg/L), and ethene (6-15 µg/L).

The presence of *Dehalococcoides* sp. was observed on five of seven microfractures from borehole BBC5 with primers aligned for the V3 region of the 16S rDNA of *Dehalococcoides ethenogenes* and *Dehalococcoides* sp. (strain FL2). This was indicative of the presence of a dehalorespirer that is capable of dechlorinating TCE to ethene (Löffler *et al*., 2000). *Dehalococcoides* sp. uses H_2 as an electron donor. There has been some work relating dehalorespiration and poised H_2 levels. Yang and McCarty (1998) found that a mixed culture growing at 28 °C on benzoate with *cis*-DCE as the terminal electron acceptor poised the H_2 concentration at 2 nM, suggesting a minimum concentration of H_2 that would support reductive dechlorination. Fennell and Gossett (1998) reported that the lowest H_2 concentration allowing dechlorination (at 35 °C) was 1.5 nM. In the case of the BBC site, H_2 was certainly present in the open fracture system of borehole BBC6 at Site 32 at concentrations that would support dechlorination. Concentrations of H_2 in the associated microfracture networks of borehole BBC6 are not known. The endpoint for complete dechlorination is ethene, also observed in the packer water samples.

The dominant terminal electron accepting process in the open fracture system appears to be Fe(III) reduction. The possible terminal electron accepting processes in the microfracture network could be methanogenesis, sulfate reduction, and ferric iron reduction. Dechlorination reactions can occur under all of these terminal electron accepting process conditions (Bouwer, 1994).

At this time, reductive dechlorination mediated by *Dehalococcoides* sp. appears to be one biodegradative pathway at the BBC site, at least in the microfracture networks. Other biotic and abiotic processes can not be discounted. *Dehalococcoides* sp. is widely distributed geospatially in soil and sediment samples at TCE contaminated sites (Hendrickson *et al*., 2002). *Dehalococcoides* sp. has also been observed in highly fractured and weathered dolomite contaminated with TCE (Hohnstock-Ashe *et al*., 2001; Hendrickson *et al*., 2002). The fact that *cis*-1,2 DCE was the predominant daughter product implied that *Dehalococcoides* sp. was perhaps rate limited in its dechlorination potential or not able to dechlorinate all of the available DCE. It is not clear if a dechlorinating consortium was involved (Flynn *et al*., 2000). Other means of TCE biodegradation, including aerobic and anaerobic respiratory and cometabolic processes, cannot be excluded.

4.0 Conclusions

The University of New Hampshire's Bedrock Bioremediation Center (BBC) uses a TCE contamination site at the former Pease Air Force Base in Portsmouth, NH, to study fundamental and applied geological, hydrological, microbial, and remedial processes in competent fractured bedrock. Eleven microfractures extracted from competent bedrock cores from boreholes BBC5 and BBC6 were characterized with a variety of surface spectroscopic and microbial techniques to determine if a relation exists between microfracture surface precipitates and the ecology and metabolic activity of attached microbial communities relative to terminal electron accepting processes or to chlorinated solvent biodegradation.

The microfracture surface precipitates showed various degrees of infilling, surface coverage, and precipitate thicknesses. These microfractures were all wetted when extracted and were various colors (white, yellow/green, slate blue, or black). Carbonate minerals (siderite, $FeCO_3$; calcite, $CaCO_3$; dolomite, $CaMg(CO_3)_2$) and quartz (SiO_2) were the dominant minerals in the surface precipitates. Other minerals, typical of the Kittery Formation metasandstones and metashales, were also observed. Limonite ($Fe_2O_3 \bullet nH_2O$) and pyrite (FeS_2) were present as accessory minerals.

The MIP data for this competent bedrock showed (with only one of 10 samples) three significant pore throat sizes of 131.1 µm, 1.136 µm, and 0.109 µm. The sample was found to have a porosity of 0.8%, a density of 2.65 g/cm^3, and a permeability of < 1 µDarcy. These data are similar to other competent deep bedrock sites where microbial biomass and metabolic activity have been observed in microfractures with similar pore throat widths.

XPS was particularly useful in identifying NOM functional groups and Fe mineral speciation on the microfracture surfaces. Ether, alcohol, ketone, aldehyde, amide, and carboxylic acid functional groups characteristic of a variety of humic substances and aquatic NOM were observed on the microfracture surfaces using the C1s photoelectron. NOM can form conditioning films on mineral surfaces. A number of candidate iron species were seen, including siderite, pyrrhotite (FeS), wüstite (FeO), goethite (α-FeOOH), hematite (Fe_2O_3), aged hydrous ferric oxide ($Fe_2O_3 \bullet 1.57\ H_2O$), limonite ($Fe_2O_3 \bullet nH_2O$)), and mixed ferrous and ferric minerals (e.g., magnetite (Fe_3O_4)). The Fe(III) minerals are capable of supporting microbial populations that reduce Fe(III).

Surface mass fragment fingerprints of chlorinated carbon fragments (1 and 2 carbons) obtained suggested that TCE, PCE, or VC was partitioned in the NOM conditioning layers on the microfracture surfaces. TCE is probably the species, given its hydrophobicity. More work is needed with this sensitive technique to confirm this observation.

Packer waters were alkaline (total alkalinity of 131-190 mg/L as $CaCO_3$, pH 8.8 to 9.6), dominated by the Fe^{3+}/Fe^{2+} couple at mildly reducing conditions (Eh of -208 to -160 mV, DO of 0.4 to 2.5 mg/L), and contained TCE, DCE, VC, H_2, methane, and ethene. H_2 was present in a number of the BBC boreholes at the site, including BBC6 (2.2 – 7.3 nM). *cis*-1,2-DCE was by far the most prevalent transformation product (up to 480 µg/L). NPDOC values were relatively low (0.8 to 1.7 mg/L). Sulfate was the dominant anion in the packer waters (110-120 mg/L). No sulfide was detected. The packer water chemistry was dominated by Ca, Si, Al, and Fe and was generally controlled by surface chemistry precipitation and dissolution reactions in a system at pseudo-equilibrium with the carbonates and quartz in the surface precipitates (e.g., $CaCO_3$, $CaMg(CO_3)_2$, $(Ca,Fe)CO_3$, SiO_2) and with simple Fe and Al oxy-hydroxides (e.g., $Fe(OH)_2$, FeOOH, $Al(OH)_3$, AlOOH).

SEM of microfracture surfaces revealed occasional biopatches of attached microbes. The biopatches were located in small depressions, cracks, or crevices on the microfracture surfaces. The microbes were predominantly rod-shaped and had dimensions of 1.0 µm (diameter) and 2.0 µm (length). In some instances, the bacteria had extracellular polymeric substances associated with them. In other cases, the microbes appeared to be encased in a film of organic material or surface precipitate-like material. Rod-shaped prokaryotes were the only morphology observed. TEM micrographs of calcite/quartz surface precipitates from microfracture MF11 revealed more diverse prokaryotic morphologies (e.g., spirilla, stalked bacteria, filaments). In some cases, flagella and possible cell division septa may have been present. There were many cells that contained large, clear organelles and small dark organelles. These may have been possible storage bodies.

All borehole BBC5 microfracture surfaces contained attached microbes that were extracted and characterized by denaturing gradient gel electrophoresis. Phylogenetic relationships were examined. In one case, gene sequencing and type identification were conducted. A large number of types (typically up to 20), as indicated by denaturing gradient gel electrophoresis banding, were present on the microfracture surfaces. Of the seven microfracture surfaces examined, only two had similar populations of microbes. The other five all significantly differed from each other and the two that were similar. This diversity is remarkable given the spatial proximity of microfracture samples. The unattached microbes from packer water samples differed from the attached populations. Three excised bands were sequenced and matched to DNA sequences in the DNA database. The matches were for an uncultured bacterium clone P39B-52 (98% sequence identity; #AF414577, a uranium mine sediment isolate), *Ultrabacterium* strain D-7, (99% sequence identity; #AB008505, a soil isolate), and an uncultured bacterium clone RA13C10 (99% sequence identity; #AF407400, a chlorobenzene-contaminated groundwater isolate).

Primers were used to identify the presence of bacteria, *Archaea* (including methanogens), sulfate-reducing bacteria, and dehalorespirers. Bacteria and *Archaea* were present on all seven microfractures tested. Sulfate-reducing bacteria were found on six of the seven microfractures tested. Dehalorespirers were found on six of the seven microfractures tested. These data at least suggest that dehalorespirers were present on the microfracture surfaces where TCE or its transformation product was co-located.

Although it could not be collected, microfracture porewater likely differed from packer water in chemical composition. The microfracture network may have been more reducing than the open fracture system based on the preponderance of primer data indicating the presence of sulfate-reducing bacteria and *Archaea*. The microfracture network in the Kittery Formation, by virtue of its smaller volume, reduced communication with the open fracture system, and likely mass transfer limitations probably did not significantly contribute to the contaminant or biogeochemical signatures seen in the packer waters collected under fairly transmissive conditions for fractured bedrock at the site. More work is needed to be able to better collect and analyze microfracture porewaters to see their relative pseudo-equilibria (or disequilibria) relative to the local mineralogical environment.

In terms of identification of a likely terminal electron accepting process in the open fracture system, the H_2 values observed for borehole BBC6 suggested sulfate reduction. However, high levels of sulfate, the absence of sulfide, and the low NPDOC values in the packer water samples suggested that sulfate reduction was not the dominant terminal electron accepting process, rather Fe(III) reduction might have been the dominant terminal electron accepting process. Observed H_2 levels in open samples from borehole BBC6 were also at levels supportive of reductive dechlorination.

Iron was a dominant microfracture surface element. Both Fe(II) and Fe(III) minerals were observed on the microfracture surfaces. The spatial prevalence of Fe, as well as its situation in the top few nm of the microfracture surfaces, suggested that Fe(III) was readily available for iron-reducing bacteria. The spectroscopic characterization of the microfracture surfaces pointed to Fe(III) reduction as perhaps a dominant terminal electron accepting process in the microfracture network.

There was generally good agreement between SEM-EDAX, XRD, and XPS about identification of biogeochemically-cycled C, S, and Fe within the microfracture surface precipitates and on their surfaces. However, the observed population diversity could not be related to the speciation of any of the three elements on the microfracture surfaces. The spatial heterogeneity of minerals was quite high on the microfracture surface. Mineral grain sizes were on the order of tens of μm. While minerals may have been common to all observed microfracture surfaces, their relative spacing and proximity to each other and to surface topography were quite varied. It may be that the biopatches that were observed with SEM reflect more localized microbial population response to surface mineral speciation and therefore explain how a number of terminal electron accepting processes could be occurring. Unfortunately, the level of spatial resolution of SEM, SEM-EDAX, and XPS was not high enough to discern such spatial relationships though such relations are likely.

The presence of transformation products of dehalorespiration, as well as H_2 concentrations, supported the role of *Dehalococcoides* sp. in dehalorespiration in the microfracture network. Dehalorespiration was strongly correlated to the presence of oxidized iron species on the microfracture. However, other means of TCE biodegradation, including aerobic and anaerobic respiratory and cometabolic processes, as well as abiotic degradation processes cannot be excluded.

A number of follow-on activities are suggested. Methods to collect and characterize microfracture porewaters may help to better describe terminal electron-accepting processes and may elaborate on real differences with packer water sample composition. The relative absence of NOM in the system, as well as the concentration of NOM on microfracture surfaces, deserve further examination. Understanding NOM bioavailability on microfracture surfaces may help to explain the phylogenetic and metabolic diversity seen on the microfracture surfaces. Studies looking at partitioning of TCE and transformation products to sorbed NOM under controlled isotherm conditions may help to better describe partitioning with respect to microfracture surface organic carbon fractions, particularly if more sensitive SIMS methods (such as

time of flight SIMS) are used. Understanding the spatial proximity of adhering microbes of terminal electron-accepting process activity to minerals necessary to that terminal electron accepting process may help describe the heterogeneous nature of terminal electron-accepting processes in the microfracture network and at the microscale within the formation. Determining the extent of the microfracture specific surface area relative to that of the open fracture network would help in determining the role of microfractures in terminal electron-accepting processes and biodegradative processes within contaminated bedrock aquifers. The role of mass transfer between the open fracture system and the microfracture network, as well as redox zonations that might develop relative to proximity to the open fractures, might be subjected to mass transfer and reaction path modeling exercises. Additional work defining the complex microbial communities, their metabolic interactions, and their possible syntrophy with respect to TCE degradation may help to explain observed accumulations of transformation products. Further, the expression of enzymatic activity relative to terminal electron-accepting processes and TCE biodegradation would help determine the metabolic activity on microfracture surfaces and why these might differ from those occurring in the open fracture groundwaters.

Acknowledgments

This work was supported by Cooperative Agreement CR 827878-01-0 from the U.S. EPA. Dr. Mary Gonsoulin of the U.S. EPA, Robert S. Kerr Environmental Research Center in Ada, OK, was the Project Officer. Special thanks to Dr. Frank Chapelle and Dr. Paul Bradley of the U.S. Geological Survey Stephenson Center in Columbia, SC, for their work on H_2 measurements at the BBC study site, to Mr. Dan Oblas at the University of Massachusetts at Lowell for assistance with SIMS, to Ms. Nancy Cherim of the UNH Instrumentation Center for assistance with SEM EDAX, and to Dr. John Wilson (U.S. EPA, Robert S. Kerr Environmental Research Center), Mr. Richard Willey and Mr. Steve Mangion (U.S. EPA Region 1), and three anonymous reviewers for their technical reviews. Particular thanks to Mr. Steve Vandegrift (U.S. EPA, Robert S. Kerr Environmental Research Center), Quality Assurance Officer. We also thank the BBC Advisory Board (from the U.S. EPA: Dr. Mary Gonsoulin, Dr. John Wilson, and Mr. Richard Willey; from the U.S. Geological Survey: Dr. Frank Chapelle, Dr. Ronald Harvey, Dr. Allen Shapiro, and Mr. Thomas Mack; from the U.S. Air Force: Maj. Darrin Curtis and Mr. A. Ditto; and from the N.H. Department of Environmental Services: Mr. John Regan). Also thanks to Ms. Kathy Tynsky of Computer Sciences Corporation for assisting in the preparation of this report.

References

Altschul, S.F., T.L. Madden, A.A. Schäffer, J. Zhang, Z. Zhang, W. Miller, and D.J. Lipman. 1997. Gapped BLAST and PSI-BLAST: a new generation of protein database search programs. *Nucleic Acids Research* 25: 3389-3402.

Amann R.I., B.J. Binder, R.J. Olson, S.W. Chisholm, R. Devereux, D.A. Stahl. 1990. Combination of 16S rRNA-targeted oligonucleotide probes with flow cytometry for analyzing mixed microbial populations. *Applied Environmental Microbiology* 56: 1919-1925.

Amann, R.I., W. Ludwig, and K.-H. Schleifer. 1995. Phylogenetic identification and *in situ* detection of individual microbial cells without cultivation. *Microbiological Reviews* 59: 143-169.

Amonette, J.E., D.J. Workman, D.W. Kennedy, J.S. Fruchter, and Y.A. Gorber. 2000. Dechlorination of carbon tetrachloride by Fe(II) associated with goethite. *Environmental Science & Technology* 34: 4606-4613.

Apul, D.S., M. Weimer, K.H. Gardner, T.T. Eighmy, A.-M. Fällman, and R. Comans. 2002. Application of surface complexation/precipitation modeling to contaminant leaching from weathered steel slag. Abstracts of Papers, 224th *ACS National Meeting*, Boston, MA, United States, August 18-22, 2002.

ATSDR. 1999. Agency for Toxic Substances and Disease Registry HazDat Database, vol. 2000. U.S. Department of Health and Human Services, Atlanta, GA.

Baer, D.R., A.M. Marmorstein, R.E. Williford, and D.L. Blanchard. 1992. Comparison spectra for calcite by XPS. *Surface Science Spectra* 1: 80-86.

Bancroft, G.M., J.B. Metson, and R.A. Kresovic. 1987. Leaching studies of natural and synthetic titanites using secondary ion mass spectrometry. *Geochimica Cosmochimica Acta* 51: 911-918.

Barr, T.L. 1983. An XPS study of Si as it occurs in adsorbents, catalysts, and thin films. *Applications of Surface Science* 15: 1-35.

Barrio-Lage, G.A., F.Z. Parsons, R.S. Nassar, and P.A. Lorenzo, P.A. 1987. Biotransformation of trichloroethene in a variety of subsurface materials. *Environmental Toxicology and Chemistry* 6: 571 – 578.

Barrio-Lage, G.A., F.Z. Parsons, R.M. Barbitz, P.L. Lorenzo, and H.E. Archer. 1990. Enhanced anaerobic biodegradation of vinyl chloride in ground water. *Environmental Toxicology and Chemistry* 9: 403 – 415.

Becker, M.W. and A.M. Shapiro. 2000. Tracer transport in crystalline fractured rock: evidence of non-diffusive breakthrough tailing. *Water Resources Research* 22, (9): 120S-134S.

Bekins, B. A., E.M. Godsy, and E. Warren. 1999. Distribution of microbial physiologic types in an aquifer contaminated by crude oil. *Microbial Ecology* 37: 263-275.

Bennett, P.C., F.K. Hiebert, and W.J. Choi. 1996. Microbial colonization and weathering of silicates in petroleum-contaminated groundwater. *Chemical Geology* 132: 45-53.

Bennett, P.C., J.R. Rogers, F.K. Hiebert, and W.J. Choi. 1999. Mineralogy and mineral weathering: fundamental components of subsurface microbial ecology. U.S. Geological Survey Toxic Substances Hydrology Program- Proceedings of the Technical Meeting, Charleston, S.C., March 8-12, 1999, Water-Resources Investigations Report 99-4018c, 169-176.

Bennett, P.C., F.K. Hiebert, and J.R. Rogers. 2000. Microbial control of mineral-groundwater equilibria: macroscale to microscale. *Hydrogeology Journal* 8: 47-62.

Bennett, P. C., J.R. Rogers, and W.J. Choi. 2001. Silicates, silicate weathering, and microbial ecology. *Geomicrobiology Journal* 18:3-19.

Bish, D.L., and J.E. Post. 1989. *Modern Powder Diffraction*, Mineralogical Society of America, Washington, DC.

Blake, D. 1990. Scanning electron microscopy. In *Instrumental Surface Analysis of Geologic Materials*, ed. D.L. Perry, 11-44. New York: VCH.

Boughriet, A., M. Wartel, and L. Gengembre. 1992. Solid-state ^{13}C NMR, X-ray photoelectron and electron spin resonance spectroscopies: a suggested approach to carbon analysis in aquatic solid phases. *Organic Geochemistry* 18: 457-467.

Bouwer, E.J. 1994. Bioremediation of chlorinated solvents using alternate electron acceptors. In *Handbook of Bioremediation*, eds. R.D. Norris, R.F. Hinchee, R. Brown, P.L. McCarty, L. Semprini, T.T. Wilson, D.H. Kampbell, M. Reinhard, E.J. Bouwer, R.C. Borden, T.M. Vogel, J.M. Thomas, C.H. Ward, 149-175. Boca Raton, Florida: Lewis Publishers.

Bradley, P.M., and F.H. Chapelle. 1996. Anaerobic mineralization of vinyl chloride in Fe(III)-reducing aquifer sediments. *Environmental Science & Technology* 30: 2084-2086.

Bradley, P.M., and F.H. Chapelle. 1997. Kinetics of DCE and VC mineralization under methanogenic and Fe(III)-reducing conditions. *Environmental Science & Technology* 31: 2692-2696.

Bradley, P.M., and F.H. Chapelle. 1998a. Effect of contaminant concentration on aerobic microbial mineralization of DCE and VC in stream-bed sediments. *Environmental Science & Technology* 32: 553-557.

Bradley, P.M., and F.H. Chapelle. 1998b. Microbial mineralization of VC and DCE under different terminal electron accepting conditions. *Anaerobe* 4: 81-87.

Bradley, P.M., and F.H. Chapelle. 2000. Aerobic microbial mineralization of dichloroethene as sole carbon substrate. *Environmental Science & Technology* 34: 221-223.

Bradley, P.M., F.H. Chapelle, and D.R. Lovley. 1998a. Humic acids as electron acceptors for anerobic microbial oxidation of vinyl chloride and dichloroethene. *Applied and Environmental Microbiology* 64: 3102-3105.

Bradley, P.M., F.H. Chapelle, and J.T. Wilson. 1998b. Field and laboratory evidence for intrinsic biodegradation of vinyl chloride contamination in a Fe(III)-reducing aquifer. *Journal of Contaminant Hydrology* 31: 111-127.

Bradley, P.M., J.E. Landmeyer, and R.S. Dinicola. 1998c. Anaerobic oxidation of [1,2-^{14}C] dichloroethene under Mn(IV)-reducing conditions. *Applied and Environmental Microbiology* 64: 1560-1562.

Brassant, O., M. Aragno, and E.P. Verrecchia. 2002. Calcium carbonate crystal morphology and mineralogy, why are bacteria in control? Abstract 225, p.61, Book of Abstracts, *2002 International Subsurface Microbiology Conference*, Copenhagen, Denmark, September 9-15, 2002.

Briggs, D., I.W. Fletcher, and N.M. Goncalves. 2002. High mass-resolution ToF-SIMS study of chlorine-containing polymers. *Surface and Interface Analysis* 33: 178-184.

Butler, E.C., and K.F. Hayes. 2000. Kinetics of the transformation of halogenated aliphatic compounds by iron sulfide. *Environmental Science & Technology* 33: 422-425.

Butler, E.C., and K.F. Hayes. 2001. Factors influencing rates and products in the transformation of trichloroethylene by iron sulfide and iron metal. *Environmental Science & Technology* 35: 3884-3891.

Calas, G., and F.C. Hawthorne. 1988. Introduction to spectroscopic methods, p. 1-10. In (F.C. Hawthorne, ed.) *Spectroscopic Methods in Mineralogy and Geology*, Mineralogical Society of America, Washington, DC.

Chandler, D. P., F. J Brockman, T. J. Bailey, and J.K. Fredrickson. 1998. Phylogenetic diversity of *Archaea* and bacteria in a deep subsurface. *Paleosols and Microbial Ecology* 36: 37-50.

Chang, Y. C., M. Hatsu, K. Jung, Y. S. Yoo, and K. Takamizawa. 2000. Isolation and characterization of a tetrachloroethylene dechlorinating bacterium, *Clostridium bifermentans* DPH-1. *Journal of Bioscience and Bioengineering* 89 489-491.

Chapelle, F.H. 1997. Identifying redox conditions that favor the natural attenuation of chlorinated ethenes in contaminated ground-water systems, p. 17-20. In *Symposium on Natural Attenuation of Chlorinated Organics in Ground Water*. U.S. Environmental Protection Agency, EPA/540/R-96/509.

Chapelle, F.H., J. E. Landmeyer, and P.M. Bradley. 2002. Identifying the Distribution of Terminal Electron-accepting Processes (TEAPS) in Ground- water Systems. In *Workshop on Monitoring Oxidation-Reduction Processes for Ground-water Restoration*, eds. R.T. Wilkin, R.D. Ludwig, and R.G. Ford, 3-17. Washington, DC.: U.S. EPA, EPA/600/R-02/002.

Chapelle, F.H., P.B. McMahon, N.M. Dubrovsky, R.F. Fujii, E.T. Oaksford, and D.A. Vroblesky. 1995. Deducing the distribution of terminal electron-accepting processes in hydrologically diverse groundwater systems. *Water Resources Research* 31: 359-371.

Chapelle, F.H., P.M. Bradley, D.R. Lovley, and D.A. Vroblesky. 1996a. Measuring rates of biodegradation in a contaminated aquifer using field and laboratory methods. *Ground Water* 34: 691-698.

Chapelle, F.H., S.K. Haack, P. Adriaens, M.A. Henry, and P.M. Bradley. 1996b. Comparison of Eh and H_2 measurements for delineating redox processes in a contaminated aquifer. *Environmental Science & Technology* 30: 3565-3569.

Chapelle, F.H., M.A. Widdowson , J. S. Brauner , E. Mendez III, and C.C. Casey. 2003. *Methodology for Estimating Times of Remediation Associated with Monitored Natural Attenuation*. Water-Resources Investigations Report 03-4057, Denver, Colorado: U.S. Geological Survey.

Chiou, C.T., and D.E. Kile. 1998. Deviations from sorption linearity on soils of polar and nonpolar organic compounds at low relative concentrations. *Environmental Science & Technology* 32: 338-343.

Christiansen, N., and B. K. Ahring. 1996. *Desulfitobacterium hafniense* sp. nov., an anaerobic reductively dechlorinating bacterium. *International Journal of Systematic Bacteriology* 46: 442-448.

Cole, J. R., B. Z. Fathepure, and J. M. Tiedje. 1995. Tetrachloroethene and 3-chlorobenzoate dechlorination activities are co-induced in *Desulfomonile tiedjei* DCB-1. *Biodegradation* 6: 167-172.

Coleman, N.V., T.E. Mattes, J.M. Gossett, and J.C. Spain. 2002. Phylogenetic and kinetic diversity of aerobic vinyl chloride-assimilating bacteria from contaminated sites. *Applied and Environmental Microbiology* 68: 6162-6171.

Colwell, F.S., T.C. Onstott, M.E. Delwiche, D. Chandler, J.K. Fredrickson, Q.J. Yao, J.P. McKinley, D.R. Boone, R. Griffiths, T.J. Phelps, D. Ringelberg, D.C. White, L. LaFreniere, D. Balkwill, R.M. Lehman, J. Konisky, and P.E. Long. 1997. Microorganisms from deep, high temperature sandstones: constraints on microbial colonization. *FEMS Microbiology Reviews* 20: 425-435.

Coyne, L.M., and S.W.S. McKeever. 1990. Spectroscopic characterization of minerals and their surfaces. In *Spectroscopic Characterization of Minerals and Their Surfaces*, eds. L.M. Coyne, S.W.S. McKeever, and D.F. Blake, 1-29. Washington, DC: American Chemical Society.

Davis, J.W., and C.L. Carpenter. 1990. Aerobic biodegradation of vinyl chloride in groundwater samples. *Applied and Environmental Microbiology* 56: 3870-3880.

deBruin, W.P., M. J. J. Kotterman, M. A. Posthumus, Gosse Schraa, and A. J. B. Zehnder. 1992. Complete biological reductive transformation of tetrachloroethene to ethane. *Applied Environmental Microbiology* 58: 1996-2000.

Devlin, J. F., and D. Muller. 1999. Field and laboratory studies of carbon tetrachloride transformation in a sandy aquifer under sulfate reducing conditions. *Environmental Science & Technology* 33: 1021-1027.

DiStefano, T. D., J. M. Gossett, and S. H. Zinder. 1991. Reductive dechlorination of high concentrations of tetrachloroethene to ethene by an anaerobic enrichment culture in the absence of methanogenesis. *Applied Environmental Microbiology* 57: 2287–2292.

Dong, H., R. Kukkadapu, J. K. Fredrickson, J.M. Zachara, D.W. Kennedy, and H.M. Kostandarithes. 2003. Microbial reduction of structural Fe(III) in illite and goethite. *Environmental Science & Technology* 37: 1268-1276.

Eggleston, C.M., J.-J. Ehrhardt, and W. Stumm. 1996. Surface structural controls on pyrite oxidation kinetics: an XPS-UPS, STM, and modeling study. *American Mineralogist* 81: 1036-1056.

Eighmy, T.T., A.E. Kinner, E.L. Shaw, J.D. Eusden Jr., and C.A. Francis. 1999. Hydroxylapatite ($Ca_5(PO_4)_3OH$) characterization by XPS: an environmentally important secondary mineral. *Surface Science Spectra* 6: 193-201.

Eighmy, T.T., J.C.M. Spear, W. Naser, J. Coulburn, L.S. Tisa, E. Sullivan, A. Mumford, W. Bothner, M. Mills, K. Newman, and N.E. Kinner. 2002a. Preliminary spectroscopic and microbial investigations on microfracture surfaces from TCE-contaminated Kittery formation bedrock from the Bedrock Bioremediation Center study site. Abstract 134, p.26, Book of Abstracts, *2002 International Subsurface Microbiology Conference*, Copenhagen, Denmark, September 9-15, 2002.

Eighmy, T.T., J.C.M. Spear, W. Naser, J. Coulburn, L.S. Tisa, E. Sullivan, A. Mumford, W. Bothner, M. Mills, K. Newman, and N.E. Kinner. 2002b. Mineral-microbial interactions on microfracture surfaces, *Northeast FOCUS Ground Water Conference*, National Groundwater Association, Burlington, Vermont, October 3-4, 2002.

Ekendahl, S., J. Arlinger, F. Stahl, and K. Pedersen. 1994. Characterization of attached bacterial populations in deep granitic groundwater from the Stripa research mine by 16S rRNA gene sequencing and scanning electron microscopy. *Microbiology* 140: 1575-1583.

Evanko, C., and D.A. Dzombak. 1998. Influence of structural features on sorption of NOM-analogue organic acids to goethite. *Environmental Science & Technology* 32: 2846-2855.

Fennell, D.E., and J.M.Gossett. 1998. Modeling the production of and competition for hydrogen in a dechlorinating culture. *Environmental Science & Technology* 32: 2450-2460.

Ferrey, M.L., R.T. Wilkin, R.G. Ford, and J.T. Wilson. 2004. Nonbiological removal of *cis*-Dichloroethylene and 1,1-Dichloroethylene in aquifer sediment containing magnetite. *Environmental Science & Technology* 38: 1746-1752.

Fisk, M.R., S.J. Giovanoni, and I.H. Thorseth. 1998. Alteration of oceanic volcanic glass: textural evidence of microbial activity. *Science* 281: 978-980.

Flynn, S. J., F. E. Loëffler, and J. M. Tiedje. 2000. Microbial community changes associated with a shift from reductive dechlorination of PCE to reductive dechlorination of *cis*-DCE and VC. *Environmental Science & Technology* 34: 1056–1061.

Forsythe, J.H., P.A. Maurice, and L.E. Hersman. 1998. Attachment of a *Pseudomonas* sp. to Fe(III)-(hydr)oxide surfaces. *Geomicrobiology Journal* 15:293-308.

Fox, B. G., J. G. Borneman, L. P. Wackett, and J. D. Lipscomb. 1990. Haloalkene oxidation by the soluble methane monooxygenase from *Methylosinus trichosporium* OB3b: mechanistic and environmental implications. *Biochemistry* 29: 6419-6427.

Fredrickson, J. K., and T.C. Onstott. 1996. Microbes deep inside the earth. *Scientific American* 275: 68-73.

Fredrickson, J.K., J.P. McKinley, B.N. Bjornstad, P.E. Long, D.B. Ringelberg, D.C. White, L.K. Krumholz, J.M. Sulflita, F.S. Colwell, R.M. Lehman, and T.J. Phelps. 1997. Pore-size constraints on the activity and survival of subsurface bacteria in a late cretaceous shale-sandstone sequence, northwestern New Mexico. *Geomicrobiology Journal* 14: 183-202.

Freedman, D.L., and J.M. Gossett. 1989. Biological reductive dechlorination of tetrachloroethylene and trichloroethylene to ethylene under methanogenic conditions. *Applied Environmental Microbiology* 55: 2144-2151.

Fry, N. K., J. K. Fredrickson, S. Fishbain, M. Wagner, and D. A. Stahl. 1997. Population structure of microbial communities associated with two deep, anaerobic, alkaline aquifers. *Applied Environmental Microbiology* 63:1498-504.

Garbarini, D.R., and L.W. Lion. 1986. Influence of the nature of soil organics on the sorption of toluene and trichloroethylene. *Environmental Science & Technology* 20: 1263-1269.

Geesey, G.G., A.L. Neal, P.A. Suci, and B.M. Peyton. 2002. A review of spectroscopic methods for characterizing microbial transformations of minerals. *Journal of Microbiological Methods* 51:125-139.

Gerritse, J., V. Renard, T. M. P. Gomes, P. A. Lawson, M. D. Collins, and J. C. Gottschal. 1996. *Desulfitobacterium* sp. strain PCE1, an anaerobic bacterium that can grow by reductive dechlorination of tetrachloroethene or *ortho*-chlorinated phenols. *Archives of Microbiology* 165: 132-140.

Giovannoni, S. J., E. F. DeLong, G. J. Oslen, and N. R. Pace. 1988. Phylogenetic group-specific oligonucleotide probes for identification of single microbial cells. *Journal of Bacteriology* 170: 720-726.

Gopinath, C.S., S.G. Hegde, A.V. Ramaswamy, and A. Mahapatra. 2002. Photoemission studies of polymorphic $CaCO_3$ minerals. *Material Research Bulletin* 37:1323-1332.

Gossett, J.M., and S.H. Zinder. 1997. Microbiological aspects relevant to natural attenuation of chlorinated ethenes, p. 1-13. In: *Symposium on Natural Attenuation of Chlorinated Organics in Ground Water*. U.S. Environmental Protection Agency, EPA/540/R-96/509.

Guillot, L., M. Siitari-Kauppi, K.-H. Hellmuth, C. Dubois, M. Rossy, and P. Gaviglio. 2000. Porosity changes in a granite close to quarry faces: quantification and distribution by 14C-MMA and Hg porosimetries. *European Physics Journal-Applied Physics* 9: 137-146.

Hartmans, S., and J.A.M. deBont. 1992, Aerobic vinyl chloride metabolism in *Mycobacterium aurum* L1. *Applied and Environmental Microbiology* 58: 1220-1226.

Hartmans, S., J.A.M. deBont, J. Tramper, and K.C. Luyben. 1985. Bacterial degradation of vinyl chloride. *Biotechnology Letter* 7: 383-388.

Harvey, D.T., and R.W. Linton. 1981. Chemical characterization of hydrous ferric oxides by x-ray photoelectron spectroscopy. *Analytical Chemistry* 53: 1684-1688.

Haveman, S.A., K. Pedersen, and P. Ruotsalainen. 1999. Distribution and metabolic diversity of microorganisms in deep igneous rock aquifers of Finland. *Geomicrobiology Journal* 16:277-294.

Hayes, M.H.B. 1997. Emerging concepts of the compositions and structures of humic substances, pp: 3-30. In: (M.H.B Hayes & W.S. Wilson, eds.) *Humic Substances in Soils, Peats and Waters: Health and Environmental Aspects*, The Royal Society of Chemistry, Cambridge, England.

He, J., K.M. Ritalahti, M.R. Aiello, and F.E. Loëffler. 2003. Complete detoxification of vinyl chloride by an anaerobic enrichment culture and identification of the reductively dechlorinating population as a *Dehalococcoides* species. *Applied and Environmental Microbiology* 69: 996-1003.

He, J., Y. Sung, M. E. Dollhopf, B. Z. Fathepure, J. M. Tiedje, and F. E. Loëffler. 2002. Acetate versus hydrogen as direct electron donors to stimulate the microbial reductive dechlorination process at chloroethene-contaminated sites. *Environmental Science & Technology* 36: 3945-3952.

Hendrickson, E. R., J. A. Payne, R. M. Young, M. G. Starr, M. P. Perry, S. Fahnestock, D. E. Ellis, and R. C. Ebersole. 2002. Molecular analysis of *Dehalococcoides* 16S ribosomal DNA from chloroethene-contaminated sites throughout North America and Europe. *Applied Environmental Microbiology* 68: 485-495.

Hiebert, F.K., and P.C. Bennett. 1992. Microbial control of silicate weathering in organic-rich ground water. *Science* 258:278-281.

Hochella, M. 1988. Auger and photoelectron spectroscopies. In *Spectroscopic Methods in Mineralogy and Geology*, ed. F.C. Hawthorne, 573-638. Washington, DC: Mineralogical Society of America.

Hohnstock-Ashe, A.M., S.M. Plummer, R.M. Yager, P. Baveye, and E.L. Madsen. 2001. Further biogeochemical characterization of a trichloroethene-contaminated fractured dolomite aquifer: electron source and microbial communities involved in reductive dechlorination. *Environmental Science & Technology* 35: 4449-4456.

Holliger, C., D. Hahn, H. Harmsen, W. Ludwig, W. Schumacher, B. Tindall, F. Vazquez, N. Weiss, and A. J. B. Zehnder. 1998. *Dehalobacter restrictus* gen. nov. and sp. nov., a strictly anaerobic bacterium that reductively dechlorinates tetra- and trichloroethene in an anaerobic respiration. *Archives of Microbiology* 169: 313-321.

Holliger, C., G. Wohlfarth, and G. Diekert. 1999. Reductive dechlorination in the energy metabolism of anaerobic bacteria. *FEMS Microbiological Reviews* 22: 383-398.

Horath, T., W. Von Sigler, T. Neu, and R. Bachofen. 2002. Endolithic microbial populations in dolomite rock. Abstract 207, p.53, Book of Abstracts, 2002 *International Subsurface Microbiology Conference*, Copenhagen, Denmark, September 9-15, 2002.

Hugenholtz, P., B. M. Goebel, and N. R. Pace. 1998. Impact of culture independent studies on the emerging phylogenetic view of bacterial diversity. *Journal of Bacteriology* 180: 4765–4774.

Hutchinson, C.S. 1974. *Laboratory Handbook of Petrographic Techniques*, New York: John Wiley & Sons.

Jakobsen, R., H-J. Albrechtsen, M. Rasmussen, H. Bay, P.L. Berg, and T.H. Christensen. 1998. H_2 concentrations in a landfill leachate plume (Grindsted, Denmark): *In situ* energetics of terminal electron acceptor processes. *Environmental Science & Technology* 32: 2142-2148.

Kalinowski, B. E., L.J. Liermann, S.L. Brantley, A. Barnes, and C.G. Pantano. 2000a. X-ray photoelectron evidence for bacteria-enhanced dissolution of hornblende. *Geochimica et Cosmochimica Acta* 64:1331-1343.

Kalinowski, B. E., L.J. Liermann, S. Givens, and S.L. Brantley. 2000b. Rates of bacteria-promoted solubilization of Fe from minerals: a review of problems and approaches. *Chemical Geology* 169: 357-370.

Kenneke, J.F. and E.J. Weber. 2003. Reductive Dehalogenation of halomethanes in iron- and sulfate reducing sediments. 1. Reactivity pattern analysis. *Environmental Science & Technology* 37: 713-720.

Kinner, N.E., C.L.M. Grout, M. Gonsoulin, and S.A. Vandegrift. 2001. Pease International Tradeport Site 32 Bedrock Bioremediation Research Quality Assurance Project Plan, December 21, 2001.

Kranz, R.L. 1983. Microcracks in rocks: a review. *Techtonophysics* 100: 449-480

Kruber, C., I.H. Thorseth, K. Lysnes, T. Torsvik, and R.B. Pedersen. 2002. Low-temperature hydrothermal mounds and chimneys formed by microbial mediated precipitation of Fe and Si. Abstract 320, Book of Abstracts Supplement, *2002 International Subsurface Microbiology Conference*, Copenhagen, Denmark, September 9-15, 2002.

Krumholz, L. R., R. Sharp, and S. Fishbain. 1996. A freshwater anaerobe coupling acetate oxidation to tetrachloroethene dehalogenation. *Applied Environmental Microbioliology* 62: 4108-4113.

Lane, D. J. 1991. 16S/23S r RNA sequencing. In *Nucleic Acid Techniques in Bacterial Sytematics*, ed. E. Stackebrandt and M. Goodfellow, 115-175. Chichester, UK: John Wiley & Sons Ltd.

Lane, D.J., B. Pace, G.J. Olson, D.A. Stahl, M.L. Sogin, and N.R. Pace. 1985. Rapid determination of 16S ribosomal RNA sequences for phylogenetic analyses. *Proceedings of the National Academy for Science USA* 82: 6955-6959.

Lee, W., and B. Batchelor. 2003. Reductive capacity of natural reductants. *Environmental Science & Technology* 37: 536-541.

Lehman, R. M., F.S. Colwell, and G. A. Bala. 2001a. Attached and unattached microbial communities in a simulated basalt aquifer under fracture- and porous-flow conditions. *Applied Environmental Microbiology* 67: 2799-2809.

Lehman, R. M., F.F. Roberto, D. Earley, D.F. Bruhun, S.E. Brink, S.P. O'Connell, M.E. Delwiche, and F.S. Colwell. 2001b. Attached and unattached bacterial communities in a 120-meter corehole in an acidic, crystalline rock aquifer. *Applied Environmental Microbiology* 67: 2095-2106.

Leis, A., R.N. Lamb, B. Gong, and R.P. Schneider. 2000. Evidence for the contribution of humic substances to conditioning films from natural waters. *Biofouling* 15: 207-220.

Lendvay, J.M., F.E. Loffler, M. Dollhope, M.R. Aiello, G. Daniels, B.Z. Fathepure, M.G. Ebhard, R. Heine, R. Helton, J. Shi, R. Krajmalnik-Brown, C.L. Major, Jr., M.J. Barcelona, E. Petrovskis, R. Hickey, J.M. Tiedje, and P. Adriaens. 2003. Bioreactive barriers: A comparison of bioaugmentation and biostimulation for chlorinated solvent remediation. *Environmental Science & Technology* 37, 1422-1431.

Li, S., and L. P. Wackett. 1992. Trichloroethylene oxidation by toluene dioxygenase. *Biochemical & Biophysical Research Communications* 185: 443-451.

Liermann, L. J., A.S. Barnes, B.E. Kalinowski, X. Zhou, and S.L. Brantley. 2000a. Microenvironments of pH in biofilms grown on dissolving silicate surfaces. *Chemical Geology* 171: 1-16.

Liermann, L. J., B. E. Kalinowski, S.L. Brantley, and J. G. Ferry. 2000b. Role of bacterial siderophores in dissolution of hornblende. *Geochimica et Cosmochimica Acta* 64: 587-602.

Löffler, F.E., R.A. Sanford, and J. M. Tiedje. 1996. Initial characterization of a reductive dehalogenase from *Desulfitobacterium chlororespirans* Co23. *Applied Environmental Microbiology* 62: 3809-3813.

Löffler, F.E., Q. Sun, J. Li, and J.M. Tiedje. 2000. 16S rRNA Gene- base detection of tetrachloroethene-dechlorinating *Desulfuromonas* and *Dehalococcoides* species. *Applied Environmental Microbiology* 66: 1369-1374.

Lovley, D.R., and F.H. Chapelle. 1995. Deep subsurface microbial processes. *Reviews in Geophysics* 33: 365-381.

Lovley, D.R., and S. Goodwin. 1988. Hydrogen concentrations as an indicator of the predominant terminal electron-accepting reactions in aquatic sediments. *Geochimica et Cosmochimica Acta* 52: 2993-3003.

Lovley, D.R., and E.J.P. Phillips. 1987. Competitive mechanisms for the inhibition of sulfate reduction and methane production in the zone of ferric iron reduction in sediments. *Applied and Environmental Microbiology* 53: 2636-2641.

Lower, S.K., M.F. Hochella, and T.J. Beveridge. 2001. Bacterial recognition of mineral surfaces: nanoscale interactions between *Shewanella* and α-FeOOH. *Science* 292: 1360-1363.

Magnuson, J. K., R. V. Stern, J. M. Gossett, S. H. Zinder, and D. R. Burris. 1998. Reductive dechlorination of tetrachloroethene to ethene by a two component enzyme pathway. *Applied Environmental Microbiology* 64: 1270-1275.

Maymó-Gatell, X., Y.-T. Chien, J. M. Gossett, and S. H. Zinder. 1997. Isolation of a bacterium that reductively dechlorinates tetrachloroethene to ethene. *Science* 276: 1568-1571.

Maymó-Gatell, X., T. Anguish, and S. H. Zinder. 1999. Reductive dechlorination of chlorinated ethenes and 1,2-dichloroethane by "*Dehalococcoides ethenogenes*" 195. *Applied Environmental Microbiology* 65: 3108-3113.

McCarty, P.L. 1997a. Breathing with chlorinated solvents. *Science* 276: 1521-1522.

McCarty, P.L. 1997b. Biotic and abiotic transformations of chlorinated solvents in ground water. In *Proceedings of the Symposium on Natural Attenuation of Chlorinated Organics in Ground Water*, 7-11. Washington, DC: U.S. EPA Office of Research and Development Report EPA/540/R-97/504.

McCarty, P.L., and L. Semprini. 1994. Ground-water treatment for chlorinated solvents. In *Handbook of Bioremediation*, eds. R.D. Norris, R.F. Hinchee, R. Brown, P.L. McCarty, L. Semprini, T.T. Wilson, D.H. Kampbell, M. Reinhard, E.J. Bouwer, R.C. Borden, T.M. Vogel, J.M. Thomas, C.H. Ward, 87-116. Boca Raton, Florida: Lewis Publishers.

McGuire, J.T., E.W. Smith , D.T. Long, D.W. Hyndman, S.K. Haack, M.J. Klug, and M.A. Velbel. 2000. Temporal variations in parameters reflecting terminal-electron-accepting processes in an aquifer contaminated with waste fuel and chlorinated solvents. *Chemical Geology* 169: 471-485.

Meima, J.A., R.D. van der Weijden, T.T. Eighmy, and R.N.J. Comans. 2002. Carbonation processes in municipal solid waste incinerator bottom ash and their effect on the leaching of copper and molybdenum. *Applied Geochemistry* 17: 1503-1513.

Metson, J.B. 1990. Secondary ion mass spectrometry. In *Instrumental Surface Analysis of Geologic Materials*, ed. D.L. Perry, 311-354. New York: VCH.

Miller, E., G. Wohlfarth, and G. Diekert. 1998. Purification and characterization of the tetrachloroethene reductive dehalogenase of strain PCE-S. *Archives of Microbiology* 169: 497-502.

Miller, E., G. Wohlfahrt, and G. Diekert. 1997. Comparative studies on tetrachloroethene reductive dechlorination by *Desulfitobacterium* sp. Strain PCE-S. *Archives of Microbiology* 168: 513-519.

Monteil-Rivera, F., E.B. Brouwer, S. Masset, Y. Deslandes, and J. Dumonceau. 2000. Combination of x-ray photoelectron spectroscopy and solid state ^{13}C nuclear magnetic resonance spectroscopy in the structural characterization of humic acids. *Analytica Chimica Acta* 424: 243-255.

Muyzer, G., S. Hottentrager, A. Teske, and C. Wawer. 1996. Denaturing gradient gel electrophoresis of PCR-amplified 16S rDNA-A new molecular approach to analyze the genetic diversity of mixed microbial communities. *Molecular and Microbial Ecology Manuscripts* 3.4.4:1-23.

Muyzer, G., and K. Smalla. 1998. Application of denaturing gradient gel electrophoresis (DGGE) and temperature gradient gel electrophoresis (TGGE) in microbial ecology. *Antonie Van Leeuwenhoek* 73, (1): 127-41.

Nesse, W.D. 2003. *Introduction to Optical Mineralogy*, Oxford University Press, New York.

Neumann, A., H. Scholz-Muramatsu, and G. Diekert. 1994. Tetrachloroethene metabolism of *Dehalospirillum multivorans*. *Archives of Microbiology* 162: 295-301.

Neumann, A., G. Wohlfarth, and G. Diekert. 1998. Tetrachloroethene dehalogenase from *Dehalospirillum multivorans*: cloning, sequencing of the encoding genes, and expression of the *pceA* gene in *Escherichia coli*. *Journal of Bacteriology* 180: 4140-4145.

Newman, L. M., and L. P. Wackett. 1997. Trichloroethylene oxidation by purified toluene 2-monooxygenase: products, kinetics, and turnover-dependent inactivation. *Journal of Bacteriology* 179: 90-96.

Ni, S., J.K. Fredrickson, and L. Xun. 1995. Purification and characterization of a novel 3-chlorobenzoate-reductive dehalogenase from the cytoplasmic membrane of *Desulfomonile tiedjei* DCB-1. *Journal of Bacteriology* 177: 5135-5139.

Odum, J.M., J. Tabinowski, M.D. Lee, and B.Z. Fathepure. 1995. Anaerobic biodegradation of chlorinated solvents — Comparative laboratory study of aquifer microcosms. In *Handbook of Bioremediation*, eds. R.D. Norris, R.F. Hinchee, R. Brown, P.L. McCarty, L. Semprini, T.T. Wilson, D.H. Kampbell, M. Reinhard, E.J. Bouwer, R.C. Borden, T.M. Vogel, J.M. Thomas, C.H. Ward, 17-24: Boca Raton, Florida: Lewis Publishers.

Onstott, T.C., T.J. Phelps, F.S. Colwell, D. Ringelberg, D.C. White, D.R. Boone, J.P. McKinley, T.O. Stevens, P.E. Long, D.L. Balkwill, W.T. Griffin, and T. Kieft. 1998. Observations pertaining to the origin and ecology of microorganisms recovered from the deep subsurface of Taylorsville Basin, Virginia. *Geomicrobiology Journal* 15: 353-385.

Onstott, T.C., D.P. Moser, S.M. Pfiffner, J.K. Fredrickson, F.J. Brockman, T.J. Phelps, D.C. White, A. Peacock, D. Balkwill, R. Hoover, L.R. Krumholz, M. Borscik, T.L. Kieft, and R. Wilson. 2003. Indigenous and contaminant microbes in ultradeep mines. *Environmental Microbiology* 5: 1168-1191.

Øvreas, L., L. Forney, F.L. Daae, and V. Torsvik. 1997. Distribution of bacterioplankton in Meromictic Lake Sælenvannet, as determined by denaturing gradient gel electrophoresis of PCR-amplified gene fragments coding for 16S rRNA. *Applied Environmental Microbiology* 33: 3367-3373.

Pedersen, K. 1997. Microbial life in granitic rock. *FEMS Microbiology Reviews* 20: 399-414.

Pedersen, K. 2000. Exploration of deep intraterrestrial microbial life: current perspectives. *FEMS Microbiology Letters* 185: 9-16.

Perry, D.L., J.H. Taylor, and C.D. Wagner. 1990. X-ray induced photoelectron and Auger Spectroscopy. In *Instrumental Surface Analysis of Geologic Materials*, ed. D.L. Perry, 45-86. New York: VCH.

Phelps, T.J., K. Malachowsky, R.M. Schram, and D.C. White. 1991. Aerobic mineralization of vinyl chloride by a bacterium of the order Actinomycetales. *Applied and Environmental Microbiology* 57: 1252-1254.

Robinson, N.I., J.M. Sharp, Jr., and I. Kreisel. 1998. Contaminant transport in sets of parallel finite fractures with fracture skins. *Journal of Contaminant Hydrology* 31: 83-109.

Rogers, J.R., and P.C. Bennett. 2001. Ferroan dolomite mineralization by iron-reducing bacteria. *EOS Transaction AGU 82(47), Fall Meeting Supplement*, Abstract B12C-0141.

Rogers, J.R., P.C. Bennett, and W.J. Choi. 1998. Feldspars as a source of nutrients for microorganisms. *American Mineralogist* 83: 1532-1540.

Rogers, J.R., P.C. Bennett, and W.J. Choi. 2001. Enhanced weathering of silicates by subsurface microorganisms: a strategy to release limiting inorganic nutrients? *Water-Rock Interaction: Proceedings of the Tenth International Symposium on Water-Rock Interaction*, Villasimus, Italy, July 10-15, 2001, A.A. Balkema, the Netherlands.

Rogers, J.R., P.C. Bennett, and F.K. Heibert. 1999. Patterns of microbial colonization on silicates. *U.S. Geological Survey Toxic Substances Hydrology Program--- Proceedings of the Technical Meeting*, Charleston, SC, March 8-12, 1999, Water-Resources Investigations Report 99-4018c, 237-242.

Röling, W.F.M., B.M. van Breukelen, M. Braster, B. Lin, and van H.W. Verseveld. 2001. Relationships between microbial community structure and hydrochemistry in a landfield leachate-polluted aquifer. *Applied Environmental Microbiology* 67: 4619-4629.

Sanford, R.A., J.R. Cole, F.E. Loëffler, and J.M. Tiedje. 1996. Characterization of *Desulfitobacterium chlororespirans* sp. nov., which grows by coupling the oxidation of lactate to the reductive dechlorination of 3-chloro-4-hydroxybenzoate. *Applied Environmental Microbiology* 62: 3800-3808.

Scholz-Muramatsu, H., A. Neumann, M. Meßmer, E. Moore, and G. Diekert. 1995. Isolation and characterization of *Dehalospirillum multivorans* gen. nov., sp. nov., a tetrachloroethene-utilizing, strictly anaerobic bacterium. *Archives of Microbiology* 163: 48-56.

Schwarzenbach, R.P., P.M. Gschwend, and D.M. Imboden. 1993. *Environmental Organic Chemistry*, Wiley-Interscience, N.Y.

Semprini, L. 1995. *In situ* bioremediation of chlorinated solvents. *Environmental Health Perspective* 103: 101-105.

Semprini, L., P.V. Roberts, G.D. Hopkins, and P.L. McCarty. 1990. A field evaluation of *in situ* biodegradation of chlorinated ethenes, Part 2 — Results of biostimulation and biotransformation experiments. *Ground Water* 28: 715-727.

Semprini, L., G.D. Hopkins, P.V. Roberts, D. Grbic-Galic, and P.L. McCarty. 1991. A field evaluation of *in situ* biodegradation of chlorinated ethenes, Part 3 — Studies of competitive inhibition. *Ground Water* 29: 239-250.

Shapiro, A.M. 2001. Effective matrix diffusion in kilometer-scale transport in fractured crystalline rock. *Water Resources Research*. 37: 507-522.

Sharma, P.K., and P.L. McCarty. 1996. Isolation and characterization of a facultatively aerobic bacterium that reductively dehalogenates tetrachloroethene to *cis*-1,2-dichloroethene. *Applied Environmental Microbiology* 62: 761-765.

Shelobolina, E.S., C.G. Vanpraagh, and D.R. Lovley. 2003. Use of ferric and ferrous iron containing minerals for respiration by *Desulfitobacterium frappieri*. *Geomicrobiology Journal* 20: 143-156.

Simmons, G., and D. Richter. 1976. Microcracks in rocks. In *The Physics and Chemistry of Minerals and Rocks*, ed. R.G. J. Strens, 105-137. New York: Wiley.

Smith, D.K. 1989. Computer analysis of diffraction data. In *Modern Powder Diffraction*, ed. D.L. Bish and J.E. Post, 83-100. Washington, DC: Mineralogical Society of America.

Snoeyenbos-West, O.L., K.P. Nevin, R.T. Anderson, and D.R. Lovley. 2000. Enrichment of *Geobacter* species in response to stimulation of Fe(III) reduction in sandy aquifer sediments *Microbial Ecology* 39: 153-167.

Snyder, R.L., and Bish, D.L. 1989. Quantitative analysis. In *Modern Powder Diffraction*, ed. D.L. Bish and J.E. Post, 101-136. Washington, DC: Mineralogical Society of America.

Stevenson, F.J. 1994. *Humus chemistry: Genesis, Composition, Reactions*. John Wiley & Sons, N.Y.

Stiber , N.A., M. Pantazidou, and M.J. Small. 1999. Expert system methodology for evaluating reductive dechlorination at TCE Sites. *Environmental Science & Technology* 33: 3012-3020

Stipp, S.L., and M.F. Hochella, Jr. 1991. Structure and bonding environments at the calcite surface as observed with X-ray photoelectron spectroscopy (XPS) and low energy electron diffraction (LEED). *Geochimica Cosmochimica Acta* 55: 1723-1736.

Suyama, A., M. Yamashita, S. Yoshino, and K. Furukawa. 2002. Molecular characterization of the PceA reductive dehalogenase of *Desulfitobacterium* sp. strain Y51. *Journal of Bacteriology* 184: 3419-3425.

Swanson, B.F. 1981. A simple correlation between permeabilities and mercury capillary pressures. *Journal of Petroleum Technology*, December, 2488-2504.

U.S. EPA. 1997. *Proceedings of the Symposium on Natural Attenuation of Chlorinated Organics in Ground Water.* U.S. EPA Office of Research and Development Report EPA/540/R-97/504, Washington, DC.

U.S. EPA. 1998. *The Technical Protocol for Evaluating Natural Attenuation of Chlorinated Solvents in Ground Water*. EPA/600/R-98/128, Washington, DC.

U.S. EPA. 2002. *Workshop on Monitoring Oxidation-Reduction Processes for Ground-water Restoration*. U.S. EPA Report EPA/600/R-02/002, Washington, DC.

Utkin, I., C. Woese, and J. Wiegel. 1994. Isolation and characterization of *Desulfitobacterium dehalogenans* gen. nov., sp. nov., an anaerobic bacterium which reductively dechlorinates chlorophenolic compounds. *International Journal of Systematic Bacteriology* 44: 612-619.

Vogel, T.M. 1994. Natural bioremediation of chlorinated solvents. In *Handbook of Bioremediation*, eds. R.D. Norris, R.F. Hinchee, R. Brown, P.L. McCarty, L. Semprini, J.T. Wilson, D.H. Kampbell, M. Reinhard, E.J. Bouwer, R.C. Borden, T.M. Vogel, J.M. Thomas, C.H. Ward, 201-225. Boca Raton, Florida: Lewis Publishers.

Vogel, T.M., and P.L. McCarty. 1985. Biotransformation of tetrachloroethylene to trichloroethylene, dichloroethylene, vinyl chloride and carbon dioxide under methanogenic conditions. *Applied Environmental Microbiology* 49: 1080-1083.

Vogel, T.M., C.S. Criddle, and P.L. McCarty. 1987. Transformation of halogenated aliphatic compounds. *Environmental Science & Technology* 21: 722-736.

Whan, R.E. 1986. *Metals Handbook, v. 10 - Materials Characterization*. American Society for Metals, Metals Park, Ohio.

Wiedemeier, T.H., M.A. Swanson, D.E. Moutoux, E.K. Gordon, J.T. Wilson, B.H. Wilson, D.H. Kampbell, P.E. Haas, R.N. Miller, J.E. Hansen, and F.H. Chapelle. 1998. *Technical protocol for evaluating natural attenuation of chlorinated solvents in ground water*. EPA/600/R-98/128. U.S. Environmental Protection Agency, Washington, DC.

Wiedemeier, T.H., J.T. Wilson, B.H. Wilson, and D.H. Kampbell. 1997. Natural attenuation of chlorinated aliphatic hydrocarbons at Plattsburgh Air Force Base, New York. In: *Symposium on Natural Attenuation of Chlorinated Organics in Ground Water*. U.S. Environmental Protection Agency, EPA/504/R-96/509; 1996, pp. 76-84.

Wild, A., R. Hermann, and T. Leisinger. 1996. Isolation of an anaerobic bacterium which reductively dechlorinates tetrachloroethene and trichloroethene. *Biodegradation* 7: 507-511.

Wilson, J.T. 2002. Current state of practice of oxidation reduction processes important to the biological and chemical destruction of chlorinated organic compounds in ground water. In *Workshop on Monitoring Oxidation-Reduction Processes for Ground-water Restoration*, eds. R.T. Wilkin, R.D. Ludwig, and R.G. Ford. 29-33 EPA/600/R-02/002. U.S. EPA Washington, D.C.

Wilson, J.T., and B.H. Wilson. 1985. Biotransformation of trichloroethylene in soil. *Applied and Environmental Microbiology* 49: 242-243.

Wu, W.-M., J. Nye, R.F. Hickey, M.K. Jain, and J.G. Zeikus. 1995. Dechlorination of PCE and TCE to ethene using an anaerobic microbial consortium, p.45-52. In (R.D. Norris, R.F. Hinchee, R. Brown, P.L. McCarty, L. Semprini, J.T. Wilson, D.H. Kampbell, M. Reinhard, E.J. Bouwer, R.C. Borden, T.M. Vogel, J.M. Thomas, C.H. Ward *et al.*, eds), *Handbook of Bioremediation*, Lewis Publishers, Boca Raton, Florida.

Xing, B., J.J. Pignatello, and B. Gigliotti. 1996. Competitive sorption between atrazine and other organic compounds in soils and model sorbents. *Environmental Science & Technology* 30: 2432-2440.

Yager, R.M., S.E. Bilotta, C.L. Mann, and E.L. Madsen. 1997. Metabolic adaption and *in situ* attenuation of chlorinated ethenes by naturally occurring microorganisms in a fractured dolomite aquifer near Niagara Falls, New York. *Environmental Science & Technology* 31: 3138-3147.

Yang, Y., and P.L. McCarty. 1998. Competition for hydrogen within a chlorinated solvent dehalogenating anaerobic mixed culture. *Environmental Science & Technology* 32: 3591-3597.

Zhu, L., B. Chen, S. Tao, and C.T. Chiou. 2003. Interactions of organic contaminants with mineral-adsorbed surfactants. *Environmental Science & Technology* 37: 4001-4006.

Zussman, J. 1976. *Physical Methods in Determinative Mineralogy*, Academic Press, London.

United States
Environmental Protection
Agency

National Risk Management
Research Laboratory
Cincinnati, OH 45268

Please make all necessary changes on the below label, detach or copy, and return to the address in the upper left-hand corner.

If you do not wish to receive these reports CHECK HERE ☐; detach, or copy this cover, and return to the address in the upper left-hand corner.

PRESORTED STANDARD
POSTAGE & FEES PAID
EPA
PERMIT No. G-35

Official Business
Penalty for Private Use
$300

EPA/600/R-05/121
June 2006